

INFORMATION TO USERS

This manuscript has been reproduced from the microfilm master. UMI films the text directly from the original or copy submitted. Thus, some thesis and dissertation copies are in typewriter face, while others may be from any type of computer printer.

The quality of this reproduction is dependent upon the quality of the copy submitted. Broken or indistinct print, colored or poor quality illustrations and photographs, print bleedthrough, substandard margins, and improper alignment can adversely affect reproduction.

In the unlikely event that the author did not send UMI a complete manuscript and there are missing pages, these will be noted. Also, if unauthorized copyright material had to be removed, a note will indicate the deletion.

Oversize materials (e.g., maps, drawings, charts) are reproduced by sectioning the original, beginning at the upper left-hand corner and continuing from left to right in equal sections with small overlaps.

Photographs included in the original manuscript have been reproduced xerographically in this copy. Higher quality 6" x 9" black and white photographic prints are available for any photographs or illustrations appearing in this copy for an additional charge. Contact UMI directly to order.

Bell & Howell Information and Learning
300 North Zeeb Road, Ann Arbor, MI 48106-1346 USA
800-521-0600

UMI[®]

University of Alberta

**Statistical Properties of Filtered Amplified Spontaneous Emission Noise
of Erbium-Doped Fiber Amplifiers**

by

Sik Heng Foo



A thesis submitted to the Faculty of Graduate Studies and Research in partial fulfillment
of the requirements for the degree of Master of Science

Department of Electrical and Computer Engineering

Edmonton, Alberta

Fall 1999



National Library
of Canada

Acquisitions and
Bibliographic Services

395 Wellington Street
Ottawa ON K1A 0N4
Canada

Bibliothèque nationale
du Canada

Acquisitions et
services bibliographiques

395, rue Wellington
Ottawa ON K1A 0N4
Canada

Your file Votre référence

Our file Notre référence

The author has granted a non-exclusive licence allowing the National Library of Canada to reproduce, loan, distribute or sell copies of this thesis in microform, paper or electronic formats.

The author retains ownership of the copyright in this thesis. Neither the thesis nor substantial extracts from it may be printed or otherwise reproduced without the author's permission.

L'auteur a accordé une licence non exclusive permettant à la Bibliothèque nationale du Canada de reproduire, prêter, distribuer ou vendre des copies de cette thèse sous la forme de microfiche/film, de reproduction sur papier ou sur format électronique.

L'auteur conserve la propriété du droit d'auteur qui protège cette thèse. Ni la thèse ni des extraits substantiels de celle-ci ne doivent être imprimés ou autrement reproduits sans son autorisation.

0-612-47029-6

University of Alberta

Library Release Form

Name of Author: **Sik Heng Foo**

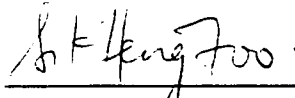
Title of Thesis: **Statistical Properties of Filtered Amplified Spontaneous
Emission Noise of Erbium-Doped Fiber Amplifiers**

Degree: **Master of Science**

Year this Degree Granted: **1999**

Permission is hereby granted to the University of Alberta Library to reproduce single copies of this thesis and to lend or sell such copies for private, scholarly, or scientific research purposes only.

The author reserves all other publication and other rights in association with the copyright in the thesis, and except as hereinbefore provided, neither the thesis nor any substantial portion thereof may be printed or otherwise reproduced in any material form whatever without the author's prior written permission.



8815, 182 Street

Edmonton, Alberta

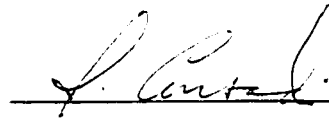
Canada T5T 0Y9

Date: September 17, 1999

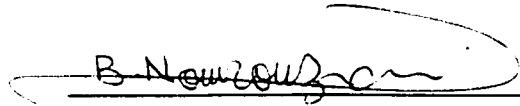
University of Alberta

Faculty of Graduate Studies and Research

The undersigned certify that they have read, and recommend to the Faculty of Graduate Studies and Research for acceptance, a thesis entitled **Statistical Properties of Filtered Amplified Spontaneous Emission Noise of Erbium-Doped Fiber Amplifiers** by **Sik Heng Foo** in partial fulfillment of the requirements for the degree of **Master of Science**.



Dr. Jan Conradi, Supervisor



Dr. Behrouz Nowrouzian, Internal Examiner



Dr. Walter Allegretto, External Examiner

Date: September 16, 1999

Dedicated to my parents for their love and support,

and

Kimberly Chan for her understanding and encouragement.

Abstract

This work is to investigate the statistical properties of the filtered amplified spontaneous emission (ASE) noise in an erbium-doped fiber amplifier (EDFA) pre-amplified receiver system, as the optical bandwidth approaches the electrical bandwidth. The theoretical derivation and analysis of a non-Gaussian noise theory is presented and compared to the widely used Gaussian approximation. The theoretical model includes both the ASE beat noises and the post detection Gaussian noises. Simulation of the probability density function (PDF), bit error ratio (BER), receiver sensitivity and optimum percentage threshold are done to study the differences between the Gaussian and non-Gaussian noise theory. Experiments are performed to measure the noise distribution, the optimum percentage threshold and BER. The experimental results are compared to the Gaussian and non-Gaussian noise theory. Optical filters with 3 dB bandwidth of 0.1, 0.2 and 0.4 nm are used in the experiments.

Acknowledgements

First and foremost, I wish to express my gratitude to my supervisor, Dr. Jan Conradi, for his guidance and expertise in erbium-doped fiber amplifiers and for establishing a good fiber optics transmission system laboratory in TRLabs. I wish to thank my co-supervisor, Dr. Jim McMullin, for the courtesy that he has shown me by taking me under his wing after the departure of Dr. Conradi from TRLabs, and his input in the completion of my thesis. I wish to thank Dr. Roger Pederson for his assistance in solving some of the challenges that I have encountered in TRLabs.

I wish to thank Sing Cheng and Gary Hassall for many stimulating and enlightening discussions on various topics in fiber optics systems and their assistance in the laboratory work. I wish to thank Mike Sieben for his tutorials in using the laboratory equipment. I thank Craig Unick for developing the new Labview vi for the FFP. I thank Clarence Kan for sharing his knowledge in nonlinear fiber optics.

I wish to thank David Clegg and Raymond Semeniuk for their contribution in the construction of the electronic equipment needed in the experimental work and keeping the laboratory in peak operating condition. I also wish to thank Luke Chong for his computer and network support.

I am grateful to all the staffs and students of TRLabs for making TRLabs a great environment for advance studies and research. I will cherish all the good friendships that have flourished.

Finally, I wish to thank TRLabs, the University of Alberta and the National Science and Engineering Research Council of Canada for their financial support in making this work possible.

Table of Contents

CHAPTER 1. INTRODUCTION.....	1
1.1. THESIS MOTIVATION AND OBJECTIVES.....	3
1.2. THESIS ORGANIZATION.....	5
CHAPTER 2. ERBIUM-DOPED FIBER AMPLIFIER.....	6
2.1. MODEL OF AN EDFA.....	7
2.2. EDFA SMALL SIGNAL GAIN.....	8
2.3. AMPLIFIED SPONTANEOUS EMISSION.....	9
2.4. NOISE FIGURE.....	10
2.5. EDFA STRUCTURE.....	11
2.6. RECENT DEVELOPMENT.....	13
CHAPTER 3. NOISE THEORY.....	15
3.1. THEORETICAL MODEL OF THE SYSTEM.....	16
3.2. PROBABILITY GENERATING FUNCTION.....	21
3.2.1 <i>Probability Generating Function of a Gaussian Random Variable</i>	22
3.3. THERMAL NOISE.....	22
3.4. SHOT NOISE.....	23
3.5. OVERALL PROBABILITY GENERATING FUNCTION.....	24
3.6. APPROXIMATE SOLUTION FOR THE PROBABILITY DENSITY FUNCTION.....	24
3.7. PROBABILITY OF ERROR.....	26
3.8. POLARIZATION STATES OF AMPLIFIED SPONTANEOUS EMISSION NOISE.....	27
3.9. MEAN AND VARIANCE.....	28
3.10. GAUSSIAN APPROXIMATION.....	29
3.11. BIT ERROR RATIO AND OPTIMUM DECISION THRESHOLD.....	30
3.12. CURRENT-TO-VOLTAGE CONVERSION.....	31
3.13. COUPLING AND TRANSMISSION EFFICIENCIES.....	32
3.14. DISCUSSION.....	32
CHAPTER 4. SIMULATION OF SYSTEM PERFORMANCE.....	34
4.1. NOISE IN THE RECEIVER.....	35
4.2. COMPARISON OF THE PROBABILITY DENSITY FUNCTIONS.....	38
4.2.1 <i>Optical Bandwidth Dependence of the PDFs</i>	38
4.2.2 <i>Electrical Bandwidth Dependence of the PDFs</i>	43
4.2.3 <i>EDFA Gain Dependence of the PDFs</i>	44

4.3. OPTIMUM DECISION THRESHOLD ANALYSIS.....	46
4.3.1 Bit Error Ratio as a Function of Percentage Decision Threshold.....	46
4.3.2 Optimum Percentage Threshold as a Function of Average Received Power	48
4.3.3 Optimum Percentage Threshold as a Function of Optical Bandwidth.....	50
4.3.4 Optimum Percentage Threshold as a Function of EDFA Gain.....	51
4.4. BIT ERROR RATIO ANALYSIS.....	52
4.4.1 Bit Error Ratio as a Function of Average Received Power.....	52
4.4.2 Bit Error Ratio as a Function of Optical Bandwidth.....	53
4.4.3 Bit Error Ratio as a Function of EDFA Gain.....	54
4.4.4 Bit Error Ratio as a Function of Extinction Ratio.....	55
4.5. RECEIVER SENSITIVITY ANALYSIS.....	55
4.5.1 Sensitivity as a Function of Optical Bandwidth.....	56
4.5.2 Sensitivity as a Function of EDFA Gain.....	56
4.6. DISCUSSION OF SIMULATION RESULTS	58
CHAPTER 5. EXPERIMENTAL RESULTS.....	61
5.1. PROBABILITY DENSITY MEASUREMENTS.....	61
5.2. THRESHOLD DETECTION OF NOISE	64
5.3. EXPERIMENTAL RESULTS OF PDF MEASUREMENTS	67
5.3.1 PDFs with 0.1 nm Fiber Bragg Gratings	67
5.3.2 PDFs with 0.2 nm Fiber Bragg Gratings	70
5.3.3 PDFs with 0.4 nm Fiber Bragg Gratings	73
5.4. OPTIMUM PERCENTAGE THRESHOLD MEASUREMENTS.....	76
5.4.1 BER as a Function of Received Power	79
5.4.2 Optimum Percentage Threshold	81
CHAPTER 6. CONCLUSION.....	88
6.1. FUTURE WORK.....	90
REFERENCES	91
APPENDIX A DERIVATION OF THE PROBABILITY GENERATING FUNCTION.....	94
APPENDIX B MATLAB PROGRAMS	96
B.1. POWER OF NOISE COMPONENTS.....	96
B.2. PROBABILITY DENSITY FUNCTIONS	97
B.3. NON-GAUSSIAN PROBABILITY DENSITY FUNCTION.....	98
B.4. GAUSSIAN PROBABILITY DENSITY FUNCTION.....	99
B.5. RECEIVER SENSITIVITY	99

B.6.	NON-GAUSSIAN OPTIMUM DECISION THRESHOLD.....	101
B.7.	GAUSSIAN OPTIMUM DECISION THRESHOLD	103
B.8.	NON-GAUSSIAN PROBABILITY OF ERROR	103
B.9.	GAUSSIAN PROBABILITY OF ERROR	104
B.10.	EDFA GAIN.....	105
B.11.	ASE POWER.....	105
B.12.	VARIANCE OF THERMAL NOISE.....	105
B.13.	MEAN AND VARIANCE OF SHOT NOISE	106
APPENDIX C CHARACTERISTICS OF OPTICAL COMPONENTS.....		107
C.1.	IONAS DFB FIBER LASER	107
C.2.	LUCENT MACH-ZEHNDER MODULATOR	107
C.3.	ERBIUM DOPED FIBER AMPLIFIERS.....	108
C.4.	FIBER BRAGG GRATINGS.....	110
C.5.	OPTICAL ISOLATORS	116
C.6.	OPTICAL CIRCULATORS	117
APPENDIX D CHARACTERISTICS OF ELECTRICAL COMPONENTS.....		119
D.1.	NORTEL 10 GB/S OPTICAL RECEIVER	119
D.2.	B&H ELECTRICAL AMPLIFIERS	120

List of Tables

Table 4.1: Simulation parameters.....	34
Table 5.1: Experimental parameters for the PDF measurements.....	67
Table 5.2: Experimental parameters for optimum percentage threshold measurements.	79
Table C.1: Specification of the IONAS DFB fiber laser.....	107
Table C.2: Specification of the Lucent Mach-Zehnder modulator.	107
Table C.3: Characteristics of the FBGs.....	112
Table C.4: Measured bandwidth of the FBGs.....	112
Table C.5: Insertion losses of optical isolators.	117
Table C.6: Characteristics of optical circulator #1.....	117
Table C.7: Characteristics of optical circulator #2.....	118
Table C.8: Characteristics of optical circulator #3.....	118
Table D.1: Specification of the B&H electrical amplifiers.....	120

List of Figures

Figure 2.1: Energy level of erbium ions.....	7
Figure 2.2: Erbium doped fiber amplifier with co-propagating pump.....	12
Figure 3.1: Optical receiver with an EDFA pre-amplifier.	16
Figure 3.2: Optical receiver with current-to-voltage conversion gain block.	31
Figure 4.1: Power of each noise component for $B_o = 20$ GHz.....	36
Figure 4.2: Power of each noise component for $B_o = 100$ GHz.....	37
Figure 4.3: PDF of logical ones for $B_o = 100$ GHz ($M = 10$).	39
Figure 4.4: PDF of logical ones for $B_o = 20$ GHz ($M = 2$).	39
Figure 4.5: PDF of logical zeros for $B_o = 100$ GHz ($M = 10$).	40
Figure 4.6: PDF of logical zeros for $B_o = 20$ GHz ($M = 2$).	41
Figure 4.7: PDFs of logical ones and zeros for $B_o = 100$ GHz ($M = 10$).....	42
Figure 4.8: PDFs of logical ones and zeros for $B_o = 20$ GHz ($M = 2$).....	42
Figure 4.9: PDF of logical ones for $B_{elec} = 5$ GHz ($M = 8$).....	43
Figure 4.10: PDF of logical zeros for $B_{elec} = 5$ GHz ($M = 8$).	44
Figure 4.11: PDF of logical ones for $G_o = 20$ dB.....	45
Figure 4.12: PDF of logical zeros for $G_o = 20$ dB.....	45
Figure 4.13: BER as a function of percentage threshold for $B_o = 100$ GHz.	47
Figure 4.14: BER as a function of percentage threshold for $B_o = 20$ GHz.	47
Figure 4.15: Optimum percentage threshold for $B_o = 100$ GHz.	49
Figure 4.16: Optimum percentage threshold for $B_o = 20$ GHz.	49
Figure 4.17: Optimum percentage threshold as a function of optical bandwidth.	50
Figure 4.18: Optimum percentage threshold as a function of EDFA gain.....	51
Figure 4.19: BER as a function of average received power.....	52
Figure 4.20: BER as a function of optical bandwidth.	53
Figure 4.21: BER as a function of EDFA small signal gain.	54
Figure 4.22: BER as a function of the extinction ratio.....	55
Figure 4.23: Sensitivity as a function of the optical bandwidth.....	56
Figure 4.24: Sensitivity as a function of the EDFA gain.	57
Figure 4.25: BER using only the non-Gaussian optimum decision threshold.	59

Figure 4.26: Sensitivity using only the non-Gaussian optimum decision threshold.....	59
Figure 5.1: Schematic of the optical components in the PDF measurement experiments.	61
Figure 5.2: Schematic of the electrical components in the PDF measurement experiments.	63
Figure 5.3: Components of the BERT.....	64
Figure 5.4: Threshold detection of noise.....	65
Figure 5.5: PDF of receiver noise for no signal power ($B_o = 16.41$ GHz).....	68
Figure 5.6: PDF of receiver noise for $P_{in} = -51.5$ dBm ($B_o = 16.41$ GHz).....	69
Figure 5.7: PDF of logical ones for $P_{in} = -36.5$ dBm ($B_o = 16.41$ GHz).....	70
Figure 5.8: PDF of receiver noise for no signal power ($B_o = 23.17$ GHz).....	71
Figure 5.9: PDF of receiver noise for $P_{in} = -50.0$ dBm ($B_o = 23.17$ GHz).....	72
Figure 5.10: PDF of logical ones for $P_{in} = -35.0$ dBm ($B_o = 23.17$ GHz).....	73
Figure 5.11: PDF of receiver noise for no signal power ($B_o = 51.08$ GHz).....	74
Figure 5.12: PDF of receiver noise for $P_{in} = -52.5$ dBm ($B_o = 51.08$ GHz).....	75
Figure 5.13: PDF of logical ones for $P_{in} = -37.5$ dBm ($B_o = 51.08$ GHz).....	76
Figure 5.14: Schematic of the optical components for percentage threshold measurements.	77
Figure 5.15: BER as a function of received power for $B_o = 16.41$ GHz.....	80
Figure 5.16: BER as a function of received power for $B_o = 23.17$ GHz.....	80
Figure 5.17: BER as a function of received power for $B_o = 51.08$ GHz.....	81
Figure 5.18: Optimum percentage threshold for $B_o = 16.41$ GHz.	82
Figure 5.19: Optimum percentage threshold for $B_o = 23.17$ GHz.	83
Figure 5.20: Optimum percentage threshold for $B_o = 51.08$ GHz.	84
Figure 5.21: BER for $B_o = 16.41$ GHz.	85
Figure 5.22: BER for $B_o = 23.17$ GHz.	86
Figure 5.23: BER for $B_o = 51.08$ GHz.	86
Figure C.1: Experimental setup for EDFA gain measurement.	108
Figure C.2: EDFA gain as a function of input power at 1550.92 nm.	109
Figure C.3: Experimental setup for measuring the reflection spectra of the FBGs.	111
Figure C.4: Reflection spectrum of FBG #1.	113

Figure C.5: Reflection spectrum of FBG #2.	113
Figure C.6: Reflection spectrum of FBG #3.	114
Figure C.7: Reflection spectrum of FBG #4.	114
Figure C.8: Reflection spectrum of cascaded FBG #1 and 2.	115
Figure C.9: Reflection spectrum of cascaded FBG #3 and 4.	115
Figure C.10: Reflection spectrum of cascaded FBG #5 and 6.	116
Figure D.1: Experimental setup for conversion gain measurement.	119
Figure D.2: Frequency response of amplifier with serial number 6235.	120
Figure D.3: Frequency response of amplifier with serial number 7693.	121

List of Abbreviations

ASE	Amplified Spontaneous Emission
ASK	Amplitude Shift Keying
BER	Bit Error Ratio
BERT	Bit Error Ratio Tester
BPF	Bandpass Filter
DC	Direct Current
DFB	Distributed Feedback
DSF	Dispersion-Shifted Fiber
DWDM	Dense Wavelength Division Multiplexing
EDF	Erbium-Doped Fiber
EDFA	Erbium-Doped Fiber Amplifier
FBG	Fiber Bragg Grating
FFP	Fiber Fabry-Perot
FWHM	Full Width Half Maximum
HP	Hewlett Packard
ISI	Inter-Symbol Interference
MZ	Mach-Zehnder
OPM	Optical Power Meter
PC	Personal Computer
PDF	Probability Density Function
PGF	Probability Generating Function
SNR	Signal-to-Noise Ratio
TRLabs	Telecommunications Research Laboratories

UV	Ultraviolet
VOA	Variable Optical Attenuator
WDM	Wavelength Division Multiplexer

Chapter 1. Introduction

The telecommunications industry has been in a constant state of growth and change in recent years, driven by wider competition and consumer demand. Innovations in information technology and governmental deregulation of the industry are largely responsible for much of the activity. Increased competition for global telecommunication markets has increased equipment sales and reduced consumer costs to the point that international call and internet communications are commonplace. At the same time, photonic technology has revolutionized long distance communications, and more recently, local access capabilities, thereby helping to sustain the growth in the information marketplace.

The first generation optical fiber telecommunication systems were made possible by the development of low loss, single-mode silica fiber and efficient single-mode injection lasers in the 1970's. With the development of fast detectors and auxiliary equipment necessary to connect these components, fiber optics became an alternative competitive technology to electrical systems for telecommunication. However, the optical amplifier was the essential missing link that now makes fiber optic systems so compelling. The fact that erbium ions (Er^{3+}) possess optical transitions in the 1550 nm window in a silica glass host has been known since 1965 [1]. However, this knowledge was not fully exploited until new techniques for the fabrication of low loss, rare-earth doped silica fibers were developed in 1985 and 1986 at the University of Southampton [1]. Erbium-doped fiber amplifier (EDFA) possesses a number of attractive features such as low cost, high gain, low noise, low cross talk, wide gain bandwidth, high output saturation power, polarization and bit-rate insensitivity. Given these characteristics, EDFAs are quickly deployed and became an essential element in modern optical fiber telecommunication systems.

Due to the attenuation of the optical signal in the fiber after travelling a long distance, amplification or regeneration of the optical signal is required. Prior to the advent of optical amplifiers, the standard way of coping with the attenuation of light

signals along a fiber span was to install electronic regenerators periodically along the fiber span. A regenerator consists of a photodetector to detect the weak incoming light, electronic amplifiers, timing circuitry to maintain the timing of the signals, and a laser along with its driver to launch the signal along the next fiber span. Back in the early 1980's, EDFAs were not available and regenerators were installed in regular intervals throughout the course of the optical link to compensate for optical attenuation. Such regenerators are limited by the speed of their electronic components. Therefore, even though optical fiber systems have inherently large transmission capacity and bandwidth, they are limited by electronic regenerators. This optical-electrical-optical regeneration scheme also introduces timing problem which leads to the undesired jittering effect. Furthermore, the cost of a regenerator is far more expensive than an EDFA. To put the economics into perspective, an EDFA cost an estimated US\$70,000 whereas a six fiber electronic regenerator cost about US\$800,000 [1]. Therefore, for long haul systems, the cost savings are enormous.

Optical amplifiers are purely optical in nature and require no high speed circuitry. The signal is simply amplified optically in strength by several orders of magnitude as it traverses the amplifier, without being limited by any electronic bandwidth. The shift from regenerators to optical amplifiers thus permits a dramatic increase in capacity of the transmission system. In addition, well-engineered amplified links can be upgraded in terms of bit-rate from the terminal end alone, reusing the fibers and amplifiers. The new generation of optical fiber telecommunication systems, with vastly improved capacity and cost, is based on the recent development of EDFA. Since the introduction of EDFA, rapid progress has been made in increasing the capacity and reach of optical fiber telecommunication systems. Transoceanic systems were the early beneficiaries, as EDFA repeaters replaced expensive and intrinsically unreliable electronic regenerators. Early EDFA technology was driven by the submarine system developers who were quick to recognize its advantages, soon after the first diode-pumped EDFA was demonstrated in 1989. Terrestrial telecommunication systems have also adopted EDFA technology in order to avoid electronic regeneration. Hybrid fiber/coax cable television networks also employ EDFAs to extend the number of homes served [2].

In conventional silica fiber, the chromatic dispersion is high in the 1550 nm communication window. However, for dispersion-shifted fiber (DSF), the dispersion minimum is shifted to the 1550 nm window. Systems using DSF will be primarily loss limited and EDFAs are ideal for compensating the fiber losses and extending the range of such systems. Another attractive feature of EDFA is its large gain bandwidth. The gain bandwidth is defined here as the effective bandwidth of the EDFA gain and not the conventional gain-bandwidth product. This definition will be used throughout the entire thesis. Along with providing gain at 1550 nm, in the low loss window of silica fiber, it can provide gain over a band that is more than 4 THz wide [2]. With available dense wavelength division multiplexing (DWDM), commercial systems currently transport more than 32 channels on a single fiber and the number is expected to approach 200 in the near future. Hence, installed systems can be upgraded many fold without adding new fiber, and new DWDM systems can be built inexpensively with much greater capacity.

Recent years have witnessed an explosive and exponential growth in worldwide fiber networks with the advent of EDFAs. At the end of 1997, the embedded fiber base was 69 million km in North America, 35 million km in Europe, 59 million km in Asia-Pacific, and 8 million km elsewhere, for a total of 171 million km, according to KMI Corporation, a company based in Newport, Rhode Island. In 1997 alone, 38 million km of fiber was installed worldwide. Additionally, over 366,000 cable-km of undersea fiber optic cable had been installed by 1997, an increase from 321,000 cable-km at the end of 1996. EDFAs are also key enablers for the development of all optical networks under study in the United States (MONET program) and Europe (ACTS program) [2].

1.1. Thesis Motivation and Objectives

In the modern optical fiber telecommunication system, higher transmission capacity is constantly in demand due to the increasing demand placed by multimedia applications of the internet and computer networks. The most promising scheme for increasing the data transmission rate is using DWDM, for which signals are transmitted in different channels using different wavelength that are separated by a fixed frequency

spacing. Broad and flat gain bandwidth of EDFAs is one of the essential elements for DWDM transmission systems.

In order to detect the signal of a particular channel without suffering from significant interference caused by neighboring channels, a narrow bandpass filter in the order of 100 GHz or less is employed to filter out all unwanted signals. One of the major issues of long haul DWDM systems such as transoceanic systems, is the limited optical amplifier bandwidth. In order to avoid complex optical gain equalization schemes, a solution would be to reduce the channel spacing so that many wavelengths can be transmitted through the limited EDFA gain bandwidth. The transmission of 64 channels of 5 Gb/s with 0.3 nm spacing over 7200 km has been demonstrated, and the transmission of 17 channels of 10 Gb/s with 0.7 nm has also been achieved. The latest development in this area is the transmission of 32 channels of 10 Gb/s with 0.4 nm (50 GHz) spacing over 6150 km [3]. This would require only a total EDFA gain bandwidth of 12.4 nm.

One drawback of EDFAs is the generation of spontaneous emission noise that travels through the system and is amplified together with the signal. As the signal level is kept constant by repeated amplification, the amplified spontaneous emission (ASE) grows proportionally with the number of amplifiers. Thus for long systems, the receiver noise becomes completely dominated by ASE noise. Other noise contributions such as shot noises in the detector and thermal noise in the electrical receiver circuit is negligible by comparison.

The statistical model accounting for the bandpass filtered ASE generated by the EDFA is well established for relatively wide bandwidth filtering. Traditionally, the Gaussian distribution is used in analysis of system performance such as bit error ratio (BER) and receiver sensitivity. However, there is some strong evidence indicating that for very narrowband filtering, the statistical properties of the ASE deviate significantly from the Gaussian distribution. Chan [4] had shown experimentally that for an optical bandwidth of 1.3 nm, the ASE noise distribution is non-Gaussian in nature, following closely with the theoretical non-Gaussian model presented by Marcuse [8] [9].

The objective of this research is to investigate the statistical properties of the noise at the receiver as the optical bandwidth approaches the two-sided electrical bandwidth. This will give us some insight into the noise distribution in the DWDM system of the future, where bandwidth for the individual channel approaches the electrical bandwidth of the receiver. The experimental work of this thesis involves optical filters with 3 dB bandwidths of 0.1, 0.2 and 0.4 nm.

1.2. Thesis Organization

In Chapter 2, an overview of EDFA and its model is presented. The generation of ASE noise is discussed. Chapter 3 presents the theoretical analysis of the non-Gaussian noise theory proposed by Marcuse [8] [9]. Chapter 4 presents the simulation results of the non-Gaussian noise theory and comparisons to the traditional Gaussian noise distribution. In Chapter 5, the experimental setups for measuring the PDFs and optimum decision thresholds are presented and the experimental results are compared to the theoretical Gaussian and non-Gaussian distributions. Similarities and differences between the experimental results and theoretical calculations are discussed. Chapter 6 is the conclusion of this thesis with some summary remarks, followed by references and supplemental appendices.

Chapter 2. Erbium-Doped Fiber Amplifier

One of the important factors leading to the rare-earth metal erbium being chosen to make the fiber amplifier, is that the gain spectrum of the erbium ion overlaps with the minimum attenuation 1550 nm optical communication window. In addition, the erbium ions has five well-defined absorption spectra located at around 380, 530, 800, 980 and 1480 nm [10]. Pump lasers at these absorption wavelengths are readily available.

Another critical factor for the success of EDFAs in optical communications is the long lifetime of the metastable state which permits the required high population inversion to be obtained under steady-state conditions using modest pump powers, typically in the range of 50 to 100 mW [10]. This is due to the confinement of pump and signal by the fiber guiding structure. An EDFA has high gain, which is typically in the range of 30 to 40 dB, and has low insertion loss. It has been shown that small signal gain efficiencies achieved are 10.2 dB/mW at a pump wavelength of 980 nm and 5.9 dB/mW at 1480 nm. EDFAs pumped at 980 nm have also achieved noise figures close to 3 dB, the quantum limit for optical amplifiers [10].

EDFAs are insensitive to the light polarization, signal modulation format and data transmission rate. So, multi-gigabit transmission rates are possible with no band limiting effect. Furthermore, the application of an EDFA is very versatile; it can be used as a transmitter post-amplifier, as an in-line amplifier or as a receiver pre-amplifier. EDFAs exhibit low signal crosstalk characteristics in DWDM systems, even under saturated operating conditions, due largely to the long fluorescence and stimulated lifetimes of the upper lasing level [1].

The following section will discuss the simplified model of an EDFA that governs the amplification mechanism, actual gain property and ASE.

2.1. Model of an EDFA

A three level laser system is shown in Figure 2.1. The three level system is chosen to illustrate the energy level of the erbium ions, which is the model for the 980 nm pump wavelength. Level E_1 is the ground level, level E_2 is the metastable level with a long lifetime τ , and level E_3 is the pump level.

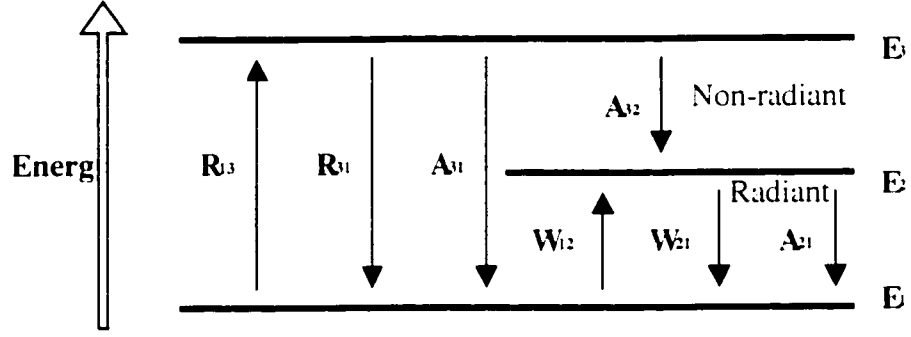


Figure 2.1: Energy level of erbium ions.

The pump absorption rate between levels 1 and 3 is R_{13} and the pump stimulated emission rate between levels 3 and 1 is R_{31} . From the excited state at level 3, there are two possibilities of decay: radiant and non-radiant. The spontaneous decay from level 3 is mainly non-radiant and will be referred to as A_{32} . The stimulated absorption and emission rates between levels 1 and 2 are W_{12} and W_{21} , respectively. The spontaneous decay from the excited state at level 2 is essentially radiant and is denoted by A_{21} , with $A_{21} = 1/\tau$, where τ is the fluorescence lifetime. The erbium ion density is given by

$$\rho = N_1 + N_2 + N_3 \quad (2.1)$$

where N_1 , N_2 and N_3 are the densities of ions in the energy states 1, 2 and 3, respectively. The generalized rate equations can be written as [11],

$$\frac{dN_1}{dt} = -R_{13}N_1 + R_{31}N_3 - W_{12}N_1 + W_{21}N_2 + A_{21}N_2 \quad (2.2)$$

$$\frac{dN_2}{dt} = W_{12}N_1 - W_{21}N_2 - A_{21}N_2 + A_{32}N_3 \quad (2.3)$$

$$\frac{dN_3}{dt} = R_{13}N_1 - R_{31}N_3 - A_{32}N_3 \quad (2.4)$$

In the steady-state regime, the ion populations are time-invariant and all the time derivatives are set to zero. Since the non-radiant decay rate A_{32} is large and the pump stimulated emission rate R_{31} is small, the following results are obtained [11]:

$$N_1 = \rho \frac{1 + W_{21}\tau}{1 + R_{13}\tau + W_{12}\tau + W_{21}\tau} \quad (2.5)$$

$$N_2 = \rho \frac{R_{13}\tau + W_{12}\tau}{1 + R_{13}\tau + W_{12}\tau + W_{21}\tau} \quad (2.6)$$

$$N_3 \approx 0 \quad (2.7)$$

The results show that the population in level 3 is negligible due to the dominant non-radiant decay to the metastable level 2.

2.2. EDFA Small Signal Gain

The signal gain of an EDFA decreases or its output power saturates with increasing input signal power. A quantity of practical interest is the output saturation power, P_{sat} , defined as the output power for which the amplifier gain is reduced by a factor of two from its unsaturated or small signal value. EDFAs are capable of high saturated output power and recent development has demonstrated that a gain-flattened broadband amplifier which provides up to 23 dBm output saturation power in the long wavelength region from 1575 to 1605 nm. This allows spans greater than 130 km and 64 densely spaced channels with 50 GHz spacing [12].

The EDFA gain can be calculated using the transcendental equation [13]

$$G = G_0 \exp\left(\frac{(1-G)P_{inave}}{P_{sat}}\right). \quad (2.8)$$

where G_0 is the unsaturated small signal gain and P_{inave} is the average optical power at the input of the EDFA given by

$$P_{inave} = Pr_0 P_{in0} + Pr_1 P_{in1}. \quad (2.9)$$

Pr_0 and Pr_1 are the probabilities of transmitting logical zeros and ones, whereas P_{in0} and P_{in1} are the average power required for logical zeros and ones, respectively. P_{inave} is used because EDFA cannot respond to fast varying power [14]. The relationship between P_{in0} and P_{in1} is given by

$$P_{in0} = \varepsilon P_{in1}, \quad (2.10)$$

where ε is the extinction ratio defined as the ratio of average optical power of logical zeros to logical ones. Equation (2.8) can be solved recursively using the Newton-Raphson method [22].

2.3. Amplified Spontaneous Emission

Noise generation in optical amplifiers is an effect of the spontaneous de-excitation of the laser ions. Since the ions have a finite excited state lifetime, $\tau \approx 10$ ms for Er^{3+} , some of the ions return to the ground state spontaneously and emit a photon. This photon is incoherent with respect to the incoming signal light, as opposed to a photon generated by stimulated emission. Spontaneous emission will result in randomly phased, incoherent radiation travelling in all direction. Therefore, those spontaneously generated photons which undergo gain in the fiber amplifier and travel in the same direction as the signal light, form a background noise that adds to the signal light. This background noise is referred to as amplified spontaneous emission. This is an inevitable phenomenon which degrade the signal-to-noise ratio (SNR) of the received signal.

The power of the ASE at the output of an EDFA is given by

$$P_{ase} = m_t N_{sp} (G - 1) h f_c B_o \quad (2.11)$$

where m_t is the number of polarization states, N_{sp} is the spontaneous emission factor, G is the EDFA gain, h is Planck's constant, f_c is the optical frequency and B_o is the noise equivalent optical bandwidth of the optical BPF following the EDFA. For an ideal amplifier, $N_{sp} = 1$. In single-mode fiber, ASE has two polarization states ($m_t = 2$). One of the polarization can be removed by inserting a polarizer ($m_t = 1$). The above equation shows that ASE noise is dependent on the gain and optical bandwidth of the system.

In optical digital transmission systems without optical amplifiers, the dominant source of noise is usually the thermal noise of the receiver. In an EDFA pre-amplified digital optical transmission system, an EDFA is used to amplify the signal power before detection to improve the SNR. The noise floor caused by the thermal noise of the receiver circuit is overcome by the ASE noise introduced by the EDFA.

At the optical detector, the electric field of the signal beats with the electric field of the ASE to produce two beat noise terms in the receiver, namely the signal-spontaneous and spontaneous-spontaneous beat noise. The expressions for the variance of the beat noise currents are shown in section 3.9. The beat noise power overwhelms the shot noise power at the amplifier output. The signal-spontaneous beat noise is proportional to the amplified signal level and it is the dominant noise component in the high signal power region. The dominant noise in the low signal power region is the spontaneous-spontaneous beat noise. Since the signal-spontaneous beat noise arises from the ASE photons associated with the amplified signal spectrum, this noise cannot be removed by a narrowband optical filter. In this sense, the signal-spontaneous beat noise is inherent to optical amplifiers. On the other hand, the spontaneous-spontaneous beat noise arises from the ASE photons in the gain bandwidth and can be effectively reduced by using a narrowband optical filter between the amplifier output and the photodetector.

2.4. Noise Figure

A common way to characterize the performance of an EDFA is through its noise figure. Noise figure is defined as the ratio of input SNR to output SNR of an amplifier [2]:

$$F_n = \frac{SNR_{in}}{SNR_{out}}. \quad (2.12)$$

F_n will always be greater than one since the amplifier adds noise during the amplification process and the output SNR is always lower than that of the input. The noise figure is usually given in dB. A high noise figure implies that the SNR has been impaired by the amplification process.

The noise figure at the input of the amplifier is computed assuming that the signal is shot noise limited. The electrical input SNR is thus expressed as [2],

$$SNR_{in} = \frac{I_{sig}^2}{qI_{sig}B_{elec}} = \frac{I_{sig}}{qB_{elec}}, \quad (2.13)$$

where I_{sig} is the signal photocurrent, q is the electronic charge and B_{elec} is the two-sided electrical bandwidth. The electrical output SNR of the amplifier is given by [2],

$$SNR_{out} = \frac{(GI_{sig})^2}{\sigma_{sig-sp}^2 + \sigma_{sp-sp}^2 + \sigma_{shot}^2}, \quad (2.14)$$

where G is the amplifier gain, σ_{sig-sp}^2 , σ_{sp-sp}^2 and σ_{shot}^2 are the variance of the signal-spontaneous beat noise, spontaneous-spontaneous beat noise and shot noise currents, respectively. Substituting equations (2.13) and (2.14) into equation (2.12), the EDFA noise figure can be expressed as the following after simplification [2]:

$$F_n = 2N_{sp} \frac{(G-1)}{G} \approx 2N_{sp}. \quad (2.15)$$

The above expression assumes that $G \gg 1$ and high input power. Therefore, the SNR is degraded by a factor of 2 (3 dB) even for an ideal amplifier with $N_{sp} = 1$. This is the quantum limit of noise figure for an ideal amplifier. Usually, F_n exceeds 3 dB and can be as large as 6 to 8 dB. Cases where the noise figure is below 3 dB can sometimes be encountered when the gain is low and N_{sp} is close to unity. This situation arises when the length of the erbium-doped fiber (EDF) is short. Since most practical systems operate with high gain, this situation is seldom encountered [2].

2.5. EDFA Structure

The simple model of an EDFA consists of a semiconductor pump laser usually at the wavelength of 980 or 1480 nm, a wavelength division multiplexer (WDM) to combine the signals and pump powers, a section of erbium doped fiber and another WDM to remove any residue pump power.

Three pumping configurations are possible for pumping a length of EDF: co-propagating pump and signal, counter-propagating pump and signal and bi-directional pumping.

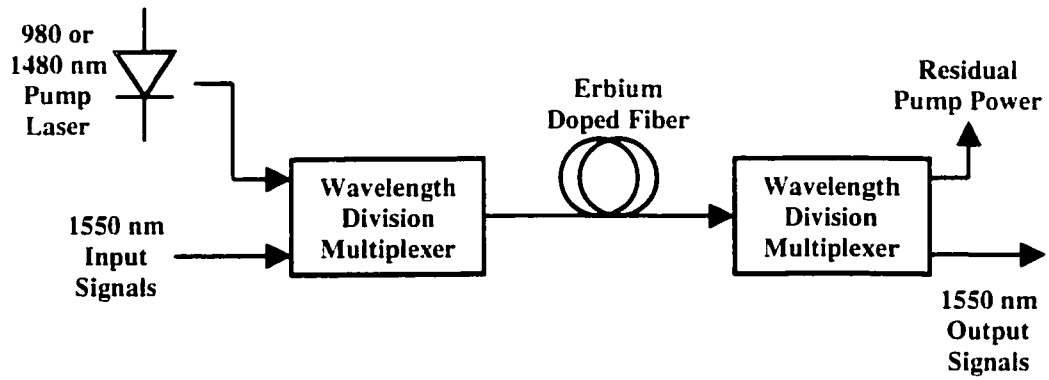


Figure 2.2: Erbium doped fiber amplifier with co-propagating pump.

The above figure shows a co-propagating pumped EDFA. The 980 or 1480 nm pump laser light and the 1550 nm input signals are multiplexed into the erbium-doped fiber. The pump laser light is absorbed by the erbium atoms in the fiber. The 1550 nm signal light passing through the erbium doped fiber is amplified by the process of stimulated emission. The WDM following the erbium-doped fiber separates the residual pump laser light from the 1550 nm signals. In an EDFA, complete inversion can only be achieved with 980 nm pump sources. Therefore, a 980 nm pumped EDFA can achieve a better noise figure than a 1480 nm pumped EDFA [2].

As far as small signal gain is concerned, co-propagating and counter-propagating pumps yield the same gain and only the total amount of pump power matters. This is because the ASE patterns generated by the two pumping schemes are identical and so the average upper state population is the same in both cases. The small signal power along the EDF is too weak to influence or change the ASE pattern and hence the energy transfer from pump to signal. Bi-directional pumping generates a different ASE pattern. When the EDF is sufficiently long, this can result in higher small signal gain at 1550 nm, for equal amount of pump power, than the co- and counter-propagating pumping schemes. This is because bi-directional pumping results in a more uniform inversion along the EDF and eliminates localized regions of high pump power [2].

For signal level in the range of -20 dBm, the counter-propagating pumping scheme yields higher output power than the co-propagating scheme when the EDF is long enough. This is due to the pump level evolution along the EDF being better tailored to the signal growth. The signal is strongest where the pump is strongest, allowing for an efficient transfer of energy between pump and signal without the ASE robbing too much of the pump power. However, bi-directional pumped EDFA yields the highest output power for input signal of -20 dBm for long EDF. For short EDF, the ASE power is low and the erbium ions are well inverted; therefore, the choice of pumping scheme does not matter [2].

The co-propagating scheme offers lower noise figure than the counter-propagating scheme. This is because for the co-propagating case, the portion of EDF that the signal enters into has higher ion population inversion than the section by which it exits. Therefore, the signal experiences more gain at near the input of the fiber than its output. For the counter-propagating scheme, the signal undergoes lower gain at the beginning of the EDF, which is equivalent to having a lower signal power at the input of the amplifier. Lower equivalent power at the input of the amplifier will degrade the noise figure [2].

2.6. Recent Development

In the pursuit of higher bandwidth in optical fiber communication systems, one solution would be to increase the gain bandwidth of EDFAs. The advantage of providing optical amplifiers with an ultra-wide bandwidth is the ability to carry more DWDM optical channels at a given spacing among the channels. This allows the transport capacity of a single fiber to be increased while managing both cost and performance. Intensive research has yielded a rapid growth in the flat-gain bandwidth available from optical amplifiers over the last several years. Gain flattening filters have made it possible to utilize larger fractions of the erbium gain spectrum. Recently, it has been shown that a low loss tellurite based EDFA with a gain flattening equalizer can achieve a 3 dB gain

bandwidth of 76 nm in the 1532 to 1608 nm wavelength region, thus increasing the transmission capacity of DWDM transmission networks [15].

Split band amplifier architectures have extended the gain bandwidth by permitting parallel use of the long wavelength portion of the erbium gain spectrum to wavelengths at which the emission cross section is roughly an order of magnitude below its peak value. Conventional EDFAs are well suited for wavelengths in the conventional band from 1530 to 1560 nm, called the C-band. Research in new material compositions and various structures have been used to obtain large gain bandwidth in the long wavelength range from 1570 to 1610 nm, called the L-band [16].

Novel host materials have further broadened the spectral width which can be achieved with EDFAs. Continued extension of the available optical amplifier bandwidth has been proposed through the use of combinations of different optical amplifier technologies, such as EDFAs in conjunction with Raman amplifiers and thulium-doped fiber amplifiers [17]. The simultaneous transmission of 10 channels from 1464 to 1478 nm, 12 channels from 1535 to 1558 nm, and 16 channels from 1574 to 1599 nm has recently been demonstrated. The 1464 to 1478 nm band is amplified using a thulium-doped fiber amplifier. The C-band is amplified using an EDFA and the L-band is amplified using a gain shifted EDFA [18].

Chapter 3. Noise Theory

Noise in a telecommunication system is any disturbance which distorts the received signal. In optical fiber communications, there are three main types of noise, namely thermal noise, shot noise and beat noise. EDFAs are widely deployed in the current optical fiber transmission systems to counter the attenuation of optical fiber. EDFAs are also used as a pre-amplifier to increase the sensitivity of the p-i-n photodetector. Without EDFA pre-amplifier, the dominant noise in the receiver is thermal noise, and signal shot noise if the signal power is large enough. However, in an EDFA pre-amplified optical receiver, signal-spontaneous beat noise and spontaneous-spontaneous beat noise are the dominant noise components.

The determination of receiver sensitivity and BER is essential in the design of high bit-rate digital optical fiber transmission systems at the 1550 nm communication window, where most sensitive receivers use optical pre-amplification. There are two categories of models for the analysis of ASE noise in the receiver. One category uses quantum mechanics to treat the spontaneous and stimulated emission processes in the optical amplifiers [28] [29] [30]. The advantage of the quantum mechanical model is its correctness in describing the physical process. The second category uses semi-classical square-law detection and the detected ASE beat noises was assumed to be Gaussian distributed in earlier studies [23] [24] [25]. However, it was shown later that the Gaussian distribution does not provide accurate analysis of BER performance as the ratio of the optical to electrical bandwidth decreases [8] [9] [26] [27]. The advantages of the semi-classical models are simplicity and they yield an analytical expression for the BER.

This work uses the model described by Marcuse [9] to investigate the statistical properties of the detected ASE noise as the ratio of optical to electrical bandwidth decreases.

3.1. Theoretical Model of the System

An intensity-modulated / direct detection optical transmission system using amplitude shift keying (ASK) is used as the model for this work. An optical amplifier is employed as a pre-amplifier before square-law detection, as shown in Figure 3.1, such that the beat noises arising from the ASE are the dominant noise components. The ASE noise at the EDFA output is assumed to be white Gaussian.

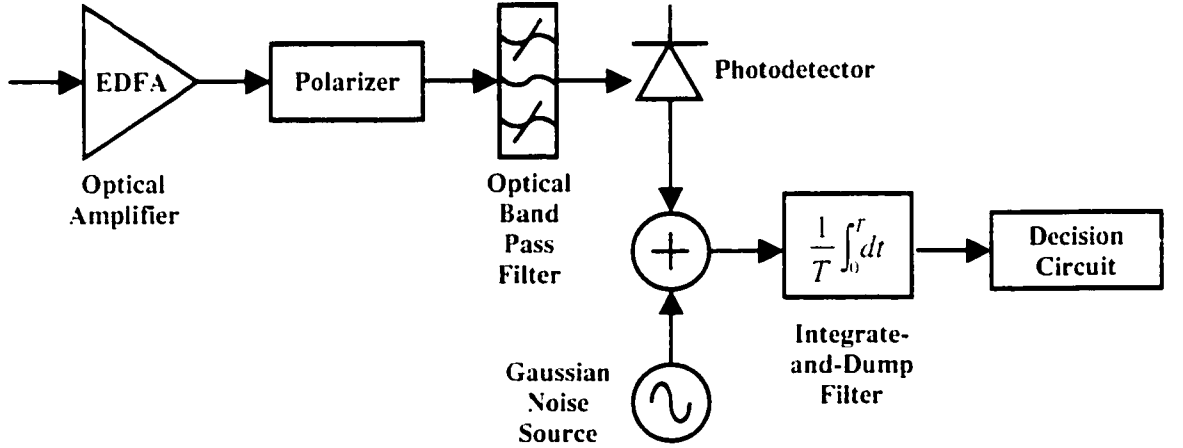


Figure 3.1: Optical receiver with an EDFA pre-amplifier.

ASE noise has two polarization states in single-mode fiber and a polarizer is used to align one of the ASE polarization states with the signal and remove the other. The advantage of an optical pre-amplifier receiver is a significant improvement of the receiver sensitivity, which is defined as the received optical power required to achieve a certain BER. The optical pre-amplifier is treated as part of the receiver and the received power is defined as the power at the input of the optical pre-amplifier. The light passes through an optical bandpass filter (BPF) of bandwidth B_0 prior to photodetection to remove part of the ASE generated by the EDFA. The BPF is modeled as an ideal device with a transfer function of unit magnitude inside the passband and zero otherwise.

The photodetector is modeled as a square-law device. After square-law detection, the on-off keyed signal is recovered by removing the optical carrier. The non-Gaussian distribution of the spontaneous-spontaneous beat noise originates from the square-law

characteristic of the p-i-n photodiode. The detected photocurrent is directly proportional to the optical power as shown in the following relation:

$$I_{ph}(t) = \mathfrak{R} P_{opt}(t). \quad (3.1)$$

$I_{ph}(t)$ is the photocurrent, $P_{opt}(t)$ is the optical power and \mathfrak{R} is the responsivity of the p-i-n diode given by

$$\mathfrak{R} = \frac{\eta q \lambda}{hc}, \quad (3.2)$$

where η is the quantum efficiency of the p-i-n diode, q is the electronic charge, λ is the wavelength of light, h is the Planck's constant and c is the speed of light in free space. The above equation shows that the responsivity is linearly proportional to the wavelength. However, in reality, equation (3.2) is only an approximation for a small window of wavelength. Zemel and Gallant [19] have shown that the responsivity of a p-i-n diode is a weak function of the wavelength in a narrow range of wavelengths.

The Gaussian noise source models the Gaussian distributed thermal and shot noises. The integrate-and-dump filter has the following impulse response:

$$h(t) = \int_0^T \delta(t) dt = \begin{cases} 1, & 0 \leq t \leq T \\ 0, & \text{otherwise} \end{cases}, \quad (3.3)$$

where $\delta(t)$ is the delta function in time-domain. The normalized power magnitude response of the integrate-and-dump filter is

$$|H(f)|_{normalized}^2 = |\text{sinc}(\pi fT)|^2. \quad (3.4)$$

The one-sided full-width-half-maximum (FWHM) is the electrical bandwidth, B_e , where the power is half its maximum value. Therefore,

$$|\text{sinc}(\pi B_e T)| = \sqrt{0.5}. \quad (3.5)$$

From the above expression, the one-sided electrical bandwidth is approximately [4]

$$B_e = \frac{1}{2T}. \quad (3.6)$$

Therefore, the two-sided electrical bandwidth is denoted as

$$B_{elec} = 2B_e = \frac{1}{T}. \quad (3.7)$$

The decision circuit is used to decode the noise-corrupted signal based on the amplitude of the received pulses.

The signal and ASE noise are expressed as Fourier series with a time base extending over the interval of one bit. This ensures that the sine and cosine function used for series expansions of the signal and noise are orthogonal over one bit period, simplifying the analysis of the integrate-and-dump filter that consists of temporal integration of the signal and noise over the bit interval T . The optical electric fields of the signal and ASE noise in the time domain are expressed as,

$$E_s(t) = \sum_{\nu=-\infty}^{\infty} E_{\nu} \exp(j\omega_{\nu}t) \quad (3.8)$$

and

$$e_{sp}(t) = \sum_{\nu=-\infty}^{\infty} c_{\nu} \exp(j\omega_{\nu}t), \quad (3.9)$$

respectively, where

$$E_{\nu} = |E_{\nu}| \exp(j\theta_{\nu}), \quad (3.10)$$

$$c_{\nu} = |c_{\nu}| \exp(j\phi_{\nu}) = c_{r\nu} + jc_{i\nu} \quad (3.11)$$

and

$$\omega_{\nu} = \frac{2\pi\nu}{T}. \quad (3.12)$$

In the Fourier series representation, the optical filter covers the range from $\nu = \nu_1$ to $\nu = \nu_2$ with

$$\nu_2 = \nu_1 + M. \quad (3.13)$$

Therefore, the optical bandwidth can be written as

$$B_o = \frac{M}{T}. \quad (3.14)$$

Using the above equation and (3.7), M can be expressed as the ratio of optical and two-sided electrical bandwidth:

$$M = \frac{B_o}{B_{elec}}. \quad (3.15)$$

The filtered electric fields of the optical signal and noise are given by,

$$\hat{E}_s(t) = \sum_{\nu=-\nu_2}^{-\nu_1} |E_\nu| \exp[j(\omega_\nu t + \theta_\nu)] + \sum_{\nu=\nu_1}^{\nu_2} |E_\nu| \exp[j(\omega_\nu t + \theta_\nu)] \quad (3.16)$$

and

$$\hat{e}_{sp}(t) = \sum_{\nu=-\nu_2}^{-\nu_1} |c_\nu| \exp[j(\omega_\nu t + \phi_\nu)] + \sum_{\nu=\nu_1}^{\nu_2} |c_\nu| \exp[j(\omega_\nu t + \phi_\nu)]. \quad (3.17)$$

After simplification, the above equations can be expressed as

$$\hat{E}_s(t) = 2 \sum_{\nu=\nu_1}^{\nu_2} |E_\nu| \cos(\omega_\nu t + \theta_\nu) \quad (3.18)$$

and

$$\hat{e}_{sp}(t) = 2 \sum_{\nu=\nu_1}^{\nu_2} |c_\nu| \cos(\omega_\nu t + \phi_\nu). \quad (3.19)$$

The square-law detector produces an electrical current that is proportional to the absolute square value of the sum of the signal and noise as given by,

$$I_{ph}(t) = K \left| \hat{E}_s(t) + \hat{e}_{sp}(t) \right|^2 \quad (3.20)$$

where K is a proportionality constant. The phase information is eliminated by the squaring operation and is ignored in the analysis. At a fixed instant in time, the above equation can be expanded as

$$I_{ph} = K \left[\left| \hat{E}_s \right|^2 + \hat{E}_s \hat{e}_{sp}^* + \hat{E}_s^* \hat{e}_{sp} + \left| \hat{e}_{sp} \right|^2 \right]. \quad (3.21)$$

The first term is the signal. The second and third terms are the signal-spontaneous beat noise, which is the dominant noise for logical one due to the presence of large signal power. The fourth term is the spontaneous-spontaneous beat noise, which is the dominant noise for logical zero provided that the ASE power is sufficiently high and the signal power level is low. The time average signal current over a bit period T is

$$I_{sig} = 2K \sum_{\nu=\nu_1}^{\nu_2} |E_\nu|^2 = \mathcal{R}P_{sig}, \quad (3.22)$$

where P_{sig} is the time average signal power. The time average ASE noise current is

$$I_{sp} = 2K \sum_{v=v_1}^{v_2} |c_v|^2 = 2K \sum_{v=v_1}^{v_2} (c_{rv}^2 + c_{iv}^2). \quad (3.23)$$

The expansion coefficients, c_v , are assumed to be zero mean independent Gaussian random variables. Since the ASE noise represents a broad spectrum of random noise, the squares of the real and imaginary parts of c_v are assumed to be identical and independent of the label v in the interval $v_1 < v < v_2$:

$$\langle c_{rv}^2 \rangle = \langle c_{iv}^2 \rangle = \sigma_c^2, \quad (3.24)$$

with σ_c^2 indicating the variance of the real and imaginary parts of c_v . Therefore, I_{sp} can be written as,

$$I_{sp} = 4KM\sigma_c^2 = \mathcal{R}P_{ase} \quad (3.25)$$

which represent a temporal as well as an ensemble average.

The decision of whether a logical one or zero has been received is based on the decision random variable at the output of the integrate-and-dump filter,

$$y = y_{ph} + y_{th} + y_{shot}, \quad (3.26)$$

with

$$y_{ph} = \frac{1}{T} \int_0^T I_{ph}(t) dt = \frac{K}{T} \int_0^T [\hat{E}_s(t) + \hat{e}_{sp}(t)]^2 dt, \quad (3.27)$$

$$y_{th} = \frac{1}{T} \int_0^T I_{th}(t) dt, \quad (3.28)$$

and

$$y_{shot} = \frac{1}{T} \int_0^T I_{shot}(t) dt. \quad (3.29)$$

I_{th} is the thermal noise current of the electrical circuit and I_{shot} is the shot noise current contribution of the photodiode. Since the thermal noise and shot noise currents are both Gaussian random variables, their contributions to the output of the integrate-and-dump circuit, y_{th} and y_{shot} , are also zero mean Gaussian random variables. The decision random variable due to the photocurrent can be expanded as

$$y_{ph} = 2K \sum_{v_1}^{v_2} \left[|E_v|^2 + c_{rv}^2 + c_{iv}^2 + 2|E_v|(c_{rv} \cos \theta_v + c_{iv} \sin \theta_v) \right]. \quad (3.30)$$

The probability density function (PDF) of the decision variable y is required to calculate the bit error ratio (BER). However, it is more convenient to calculate the probability generating function (PGF), which is the Laplace transform of the PDF.

3.2. Probability Generating Function

The probability generating function (PGF) for a random variable y with PDF $f_Y(y)$ is defined as the following [5]

$$G(s) = \int_{-\infty}^{\infty} f_Y(y) \exp(-sy) dy, \quad (3.31)$$

which is the bilateral Laplace transform of $f_Y(y)$.

The advantage of using the PGF for computing the PDF is that the generating function can be viewed as the mean of the function $\exp(-sy)$. The mean of $\exp(-sy)$ can be computed by using the known probability distributions, such as the Gaussian distribution, for the coefficients c_{rv} and c_{iv} , and random variables y_{th} and y_{shot} . The probability distribution of a Gaussian random variable is completely determined by its mean and variance, which is the case for c_{rv} , c_{iv} , y_{th} and y_{shot} . All c_{rv} and c_{iv} have the same probability distribution since they have identical means and variances. Since c_{rv} , c_{iv} , and y_{th} are all statistically independent, the total probability distribution is the product of all the individual probability distribution. y_{shot} is not an independent random variable due to the ASE noise component. However, y_{shot} can be made unconditional as described in section 3.4.

The PGF of the decision random variable y_{ph} , neglecting thermal and shot noises, is given by

$$G_{ph}(s) = \frac{1}{(4K\sigma_c^2 s + 1)^M} \exp \left(\frac{-2Ks \sum_{v=v_1}^{v_2} |E_v|^2}{4K\sigma_c^2 s + 1} \right). \quad (3.32)$$

The derivation of the above equation is shown in Appendix A. If the signal is perfectly extinct and there is no optical power for logical zeros, the above expression will yield a central chi-square distribution with $2M$ degrees of freedom. For non-zero signal power, the expression will give a non-central chi-square distribution with $2M$ degrees of freedom [4] [6]. By using equations (3.22) and (3.25), the PGF can be expressed in terms of experimentally measurable physical quantities:

$$G_{ph}(s) = \frac{1}{\left(\frac{\Re P_{ase}}{M} s + 1\right)^M} \exp\left(\frac{-\Re P_{sig} s}{\frac{\Re P_{ase}}{M} s + 1}\right). \quad (3.33)$$

3.2.1 Probability Generating Function of a Gaussian Random Variable

If $f_Y(y)$ is a Gaussian PDF with zero mean and variance σ_g^2 , then the PGF is given by

$$G_g(s) = \frac{1}{\sqrt{2\pi\sigma_g^2}} \int_{-\infty}^{\infty} \exp\left(-\frac{y^2}{2\sigma_g^2} - sy\right) dy. \quad (3.34)$$

By completing the square in the exponential term and using Gauss' integral for complex argument [7], the PGF can be expressed as

$$G_g(s) = \exp\left(\frac{\sigma_g^2}{2} s^2\right), \quad (3.35)$$

where σ_g^2 is the variance of the Gaussian random variable.

3.3. Thermal Noise

Thermal noise is a temperature dependent spontaneous fluctuation caused by thermally excited random motion of free electrons in the equivalent load resistance, R_L , of the receiver. This randomly varying current in the circuit has a zero mean Gaussian PDF and its two sided electrical power spectral density is flat with frequency as given by

$$S_{th} = \frac{2kT_k}{R_L}, \quad (3.36)$$

where k is the Boltzmann's constant, T_k is the absolute temperature. The variance of the thermal noise current is given by

$$\sigma_{th}^2 = \langle i_{th}^2 \rangle = \frac{2kT_k B_{elec}}{R_L}. \quad (3.37)$$

Therefore, high impedance reduces the thermal noise current as shown in the above equation. However, high impedance will result in a larger time constant, which will integrate the received signal and requires equalization. A good compromise would be using a transimpedance receiver, where it has higher impedance than a 50 ohm receiver but not as high as to cause signal distortion. Using equation (3.35), the PGF of the thermal noise can be expressed as

$$G_{th}(s) = \exp\left(\frac{\sigma_{th}^2}{2} s^2\right). \quad (3.38)$$

3.4. Shot Noise

Shot noise arises as a result of the statistical nature of the electron generation when an optical signal is incident on the photodiode. Due to the ASE noise, the PDF of the shot noise is a conditional PDF which depends on the photocurrent random variable. However, shot noise is not a dominant noise component and thus the analysis can be simplified by using the mean photocurrent. The two-sided power spectral density of the combined signal and spontaneous shot noise is expressed as

$$S_{shot} = q(I_{sig} + I_{sp}). \quad (3.39)$$

Note that these noise components extend over an infinite bandwidth due to the assumption of infinite photodetector bandwidth. However, the shot noise is passed through the receiver circuit which has a two-sided bandwidth of B_{elec} . Therefore, the variance of the shot noise current is written as

$$\sigma_{shot}^2 = q(I_{sig} + I_{sp})B_{elec} = q\Re(P_{sig} + P_{ase})B_{elec}. \quad (3.40)$$

The shot noises are Gaussian distributed and by using equation (3.35), the PGF of the shot noise can be expressed as

$$G_{shot}(s) = \exp\left(\frac{\sigma_{shot}^2}{2} s^2\right). \quad (3.41)$$

3.5. Overall Probability Generating Function

Since the thermal noise is independent of the signal and beat noises, and the PDF of the shot noise has been made unconditional, the overall PGF is a product of the individual PGFs in equations (3.33), (3.38) and (3.41). The overall PGF can be shown as,

$$G(s) = \frac{1}{\left(\frac{\Re P_{ase}}{M} s + 1\right)^M} \exp\left(\frac{-\Re P_{sig} s}{\frac{\Re P_{ase}}{M} s + 1}\right) \exp\left(\frac{\sigma_{th}^2}{2} s^2\right) \exp\left(\frac{\sigma_{shot}^2}{2} s^2\right). \quad (3.42)$$

By using the following substitutions,

$$A = \Re P_{sig}, \quad (3.43)$$

$$B = \frac{\Re P_{ase}}{M}, \quad (3.44)$$

$$C = \frac{\sigma_{th}^2 + \sigma_{shot}^2}{2}, \quad (3.45)$$

the expression of the PGF can be simplified to

$$G(s) = \frac{1}{(Bs + 1)^M} \exp\left(\frac{-As}{Bs + 1}\right) \exp(Cs^2). \quad (3.46)$$

3.6. Approximate Solution for the Probability Density Function

The PDF is obtained from the inverse Laplace transform of the generating function,

$$f(y) = \frac{1}{j2\pi} \int_{\alpha-j\infty}^{\alpha+j\infty} \frac{1}{(Bs + 1)^M} \exp\left(\frac{-As}{Bs + 1}\right) \exp(Cs^2) \exp(ys) ds. \quad (3.47)$$

The first term can be rewritten as

$$\frac{1}{(Bs + 1)^M} = \exp[-M \ln(Bs + 1)], \quad (3.48)$$

and by using the transformation

$$u = Bs + 1, \quad (3.49)$$

the PDF can be written in the form of

$$f(y) = \frac{1}{j2\pi B} \int_{1+B\alpha-j\infty}^{1+B\alpha+j\infty} \exp \left[\frac{C(u-1)^2}{B^2} + \frac{y(u-1)}{B} - \frac{A(u-1)}{Bu} - M \ln u \right] du. \quad (3.50)$$

By letting

$$F(u) = \frac{C(u-1)^2}{B^2} + \frac{y(u-1)}{B} - \frac{A(u-1)}{Bu} - M \ln u, \quad (3.51)$$

the PDF can be expressed as

$$f(y) = \frac{1}{j2\pi B} \int_{1+B\alpha-j\infty}^{1+B\alpha+j\infty} \exp[F(u)] du. \quad (3.52)$$

An exact solution of this integral is hard to obtain. However, a very good approximation can be worked out by using the well known method of steepest descent [7], which requires the stationary point u_0 of $F(u)$ to be found. Therefore, the equation of

$$F'(u_0) = 0 \quad (3.53)$$

must be solved to find the stationary point, u_0 . By differentiating $F(u)$ and equating it to zero, we have

$$u_0^3 + \left(\frac{yB}{2C} - 1 \right) u_0^2 - \frac{MB^2}{2C} u_0 - \frac{AB}{2C} = 0. \quad (3.54)$$

Chan [4] had shown in detail the derivation of the PDF using the method of steepest descent. The closed form expression of the PDF is found to be

$$f(y) = \frac{\exp[(F(u_0))]}{B\sqrt{2\pi F''(u_0)}}, \quad (3.55)$$

where

$$F(u_0) = \exp \left[\frac{C(u_0-1)^2}{B^2} + \frac{y(u_0-1)}{B} - \frac{A(u_0-1)}{Bu_0} - M \ln u_0 \right] \quad (3.56)$$

and

$$F''(u_0) = \frac{2A}{Bu_0^3} + \frac{M}{u_0^2} + \frac{2C}{B^2}. \quad (3.57)$$

Marcuse [9] reported that the steepest descend approximation is very accurate and the percentage error is less than 1% as confirmed by Chan [4]. For the special case that all random fluctuations are caused by thermal noise with no ASE noise, the steepest descend approximation yields the exact Gaussian distribution [9].

3.7. Probability of Error

The probability of detecting a logical zero when a logical one is being transmitted is given by

$$P_1 = \int_{-\infty}^{I_d} f_1(y) dy = \int_{u_{d1}}^{\infty} \left(-\frac{dy}{du_0} \right) f_1(u_0) du_0, \quad (3.58)$$

where $u_{d1} = u_0(I_d)$ is the saddle point at the decision threshold I_d for logical one. Similarly, the probability of detecting a logical one when a logical zero has been transmitted is,

$$P_0 = \int_{I_d}^{\infty} f_0(y) dy = \int_0^{u_{d0}} \left(-\frac{dy}{du_0} \right) f_0(u_0) du_0, \quad (3.59)$$

where $u_{d0} = u_0(I_d)$ is the saddle point at the decision threshold I_d for logical zero. The values of u_{d0} and u_{d1} are different from each other due to the different signal power of logical ones and zeros.

Rearranging equation (3.54), the decision random variable can be expressed as

$$y = \frac{A}{u_0^2} + \frac{MB}{u_0} - \frac{2Cu_0}{B} + \frac{2C}{B}, \quad (3.60)$$

and its first derivative with respect to the saddle point is

$$\frac{dy}{du_0} = -\frac{2A}{u_0^3} - \frac{MB}{u_0^2} - \frac{2C}{B}. \quad (3.61)$$

Using equation (3.57), the above equation can be written as

$$\frac{dy}{du_0} = -BF_s''(u_0), \quad (3.62)$$

where the subscript s denotes logical ones or zeros. Therefore, the probability of error can be expressed as

$$P_s = \int_{u_{n1}}^{u_{n2}} \frac{\exp[F_s(u_0)]}{B\sqrt{2\pi F_s''(u_0)}} \left(-\frac{dy}{du_0} \right) du_0 \quad (3.63)$$

$$= \frac{1}{\sqrt{2\pi}} \int_{u_{n1}}^{u_{n2}} \exp \left[F_s(u_0) + \frac{1}{2} \ln \left(\frac{2A}{Bu_0^3} + \frac{M}{u_0^2} + \frac{2C}{B^2} \right) \right] du_0. \quad (3.64)$$

The integration limits depend on the label s in accordance with (3.58) and (3.59). For $s = 0$, $u_{n1} = 0$ and $u_{n2} = u_{d0}$; for $s = 1$, $u_{n1} = u_{d1}$ and $u_{n2} = \infty$. The integral can be written as

$$P_s = \frac{1}{\sqrt{2\pi}} \int_{u_{n1}}^{u_{n2}} \exp[H_s(u_0)] du_0, \quad (3.65)$$

where

$$H_s(u_0) = F_s(u_0) + \frac{1}{2} \ln \left(\frac{2A}{Bu_0^3} + \frac{M}{u_0^2} + \frac{2C}{B^2} \right). \quad (3.66)$$

A satisfactory approximation of the integral can be computed using Taylor series expansion. Expanding $H(u_0)$ as Taylor series at u_{ds} and ignoring higher order terms, the following can be obtained:

$$H_s(u_0) \cong H_s(u_{ds}) + (u_0 - u_{ds})H'_s(u_{ds}). \quad (3.67)$$

By substituting (3.67) into (3.65), the probability of error can be approximated by

$$P_s \cong \frac{\exp[H_s(u_{ds})]}{\sqrt{2\pi}} \int_{u_{n1}}^{u_{n2}} \exp[(u_0 - u_{ds})H'_s(u_{ds})] du_0. \quad (3.68)$$

Using the above equation, P_1 can be solved as

$$P_1 \cong \frac{\exp[H_1(u_{d1})]}{\sqrt{2\pi}} \int_{u_{d1}}^{\infty} \exp[(u_0 - u_{d1})H'_1(u_{d1})] du_0 \quad (3.69)$$

$$\cong \frac{\exp[H_1(u_{d1})]}{\sqrt{2\pi}} \left[-\frac{1}{H'_1(u_{d1})} \right], \quad (3.70)$$

where $H'_1(u_{d1})$ is assumed to be negative. Similarly, P_0 can be approximated by,

$$P_0 \cong \frac{\exp[H_0(u_{d0})]}{\sqrt{2\pi}} \int_0^{u_{d0}} \exp[(u_0 - u_{d0})H'_0(u_{d0})] du_0 \quad (3.71)$$

$$\cong \frac{\exp[H_0(u_{d0})]}{\sqrt{2\pi}} \left\{ \frac{1 - \exp[-u_{d0}H'_0(u_{d0})]}{H'_0(u_{d0})} \right\}. \quad (3.72)$$

3.8. Polarization States of Amplified Spontaneous Emission Noise

In the preceding analysis, it has been assumed that the ASE noise is polarized in the same direction as the signal. However, for unpolarized noise in a single-mode fiber, the ASE noise has two polarization states. Each polarization state contributes an equal amount of statistically independent noise, which double the number of terms in the Fourier series expansion of the ASE noise. This doubling of noise has no effect on the

Fourier expansion of the signal and signal-noise beats since the signal beats only with noise in its own polarization state [8], [9]. Therefore, the expression for M is modified as,

$$M = \frac{m_t B_o}{B_{elec}}, \quad (3.73)$$

where m_t is the number of polarization states of the ASE noise. It is equal to 1 for polarized light and 2 for unpolarized light. In equation (3.42), M is only connected with the noise-noise beat term $\Re P_{ase}/M$. This ratio stays constant even when the ASE noise has two polarization states since P_{ase} also doubles.

3.9. Mean and Variance

The mean and variance of the random variable y can be obtained from the derivatives of the PGF [20]. From (3.46), the mean is found to be

$$\bar{I}_s = - \left. \frac{dG(s)}{ds} \right|_{s=0} = \Re(P_{sig} + P_{ase}), \quad (3.74)$$

and the variance is

$$\sigma_s^2 = (-1)^2 \left. \frac{d^2 G}{ds^2} \right|_{s=0} - \bar{I}_s^2 = \frac{(\Re P_{ase})^2 + 2\Re^2 P_{sig} P_{ase}}{M} + \sigma_{th}^2 + \sigma_{shot}^2, \quad (3.75)$$

where the subscript s denotes logical ones or zeros. The first term in (3.75) represents the spontaneous-spontaneous beat noise and the second term represents the signal-spontaneous beat noise. Using equations (3.73) and (2.11) for M and P_{ase} , the spontaneous-spontaneous and signal-spontaneous beat noises can be expressed as

$$\sigma_{sp-sp}^2 = [\Re N_{sp} (G-1) h f_c]^2 m_t B_o B_{elec} \quad (3.76)$$

and

$$\sigma_{sig-sp}^2 = 2\Re^2 G P_{in} N_{sp} (G-1) h f_c B_{elec}, \quad (3.77)$$

respectively. P_{sig} has been replaced by $G P_{in}$, where P_{in} is the optical power incident at the input of the EDFA.

The electrical signal-to-noise ratio (SNR) is then

$$SNR = \frac{(\Re P_{sig})^2}{\sigma_{sp-sp}^2 + \sigma_{sig-sp}^2 + \sigma_{th}^2 + \sigma_{shot}^2} \quad (3.78)$$

$$= \frac{(\Re GP_{in})^2}{[\Re N_{sp}(G-1)hf_c]^2 m_t B_o B_{elec} + 2\Re^2 GP_{in} N_{sp}(G-1)hf_c B_{elec} + \sigma_{th}^2 + \sigma_{shot}^2} \quad (3.79)$$

For large values of G, G-1 can be approximated as G and the SNR can be written as

$$SNR \cong \frac{P_{in}^2}{(N_{sp} hf_c)^2 m_t B_o B_{elec} + 2P_{in} N_{sp} hf_c B_{elec} + \frac{\sigma_{th}^2 + \sigma_{shot}^2}{(\Re G)^2}} \quad (3.80)$$

3.10. Gaussian Approximation

The Gaussian random variable is widely used in the field of telecommunications due to its simplicity since the Gaussian PDF is completely characterized by its mean and variance. Using the mean and variance in (3.74) and (3.75), the PDF of the Gaussian approximation can be written as

$$f_{y_i}(y) = \frac{1}{\sqrt{2\pi\sigma_i^2}} \exp\left[-\frac{(y - \bar{I}_i)^2}{2\sigma_i^2}\right] \quad (3.81)$$

The probability of error for logical zero can be expressed as

$$P_{s0}(I_d) = \frac{1}{\sqrt{2\pi\sigma_0^2}} \int_{I_d}^{\infty} \exp\left[-\frac{(y - \bar{I}_0)^2}{2\sigma_0^2}\right] dy \quad (3.82)$$

$$= \frac{1}{\sqrt{2\pi\sigma_0^2}} \int_{\frac{I_d - \bar{I}_0}{\sqrt{2\sigma_0^2}}}^{\infty} \exp(-t^2) dt \quad (3.83)$$

$$= \frac{1}{2} \operatorname{erfc}\left(\frac{I_d - \bar{I}_0}{\sqrt{2\sigma_0^2}}\right), \quad (3.84)$$

where $\operatorname{erfc}(x)$ is the complementary error function defined as [21]

$$\operatorname{erfc}(x) = \frac{2}{\sqrt{\pi}} \int_x^{\infty} \exp(-t^2) dt. \quad (3.85)$$

Similarly, the probability of error for logical one can be expressed as

$$P_{s1}(I_d) = \frac{1}{\sqrt{2\pi\sigma_1^2}} \int_{-\infty}^{I_d} \exp\left[-\frac{(y - \bar{I}_1)^2}{2\sigma_1^2}\right] dy \quad (3.86)$$

$$= 1 - \frac{1}{\sqrt{2\pi\sigma_1^2}} \int_{\frac{I_d - \bar{I}_1}{\sqrt{2\sigma_1^2}}}^{\infty} \exp(-t^2) dt \quad (3.87)$$

$$= 1 - \frac{1}{2} \operatorname{erfc} \left(\frac{I_d - \bar{I}_1}{\sqrt{2\sigma_1^2}} \right). \quad (3.88)$$

3.11. Bit Error Ratio and Optimum Decision Threshold

The probabilities of transmitting zeros and ones are given by \Pr_0 and \Pr_1 respectively, and the BER can be expressed as

$$BER = \Pr_0 P_0(I_d) + \Pr_1 P_1(I_d). \quad (3.89)$$

If the logical ones and zeros are equally probable, the BER can be written as

$$BER = \frac{1}{2} [P_0(I_d) + P_1(I_d)]. \quad (3.90)$$

The optimum decision threshold is obtained when BER assumes a minimum value. This can be found by differentiating BER with respect to y and setting the derivative to zero,

$$\frac{dBER}{dy} = \frac{d(\Pr_0 P_0 + \Pr_1 P_1)}{dy} = 0. \quad (3.91)$$

Since the derivatives of P_0 and P_1 with respect to y are the PDFs $f_0(y)$ and $f_1(y)$, the optimum decision threshold, I_{dopt} , can be determined as the solution of the following relation:

$$\Pr_0 f_0(I_{dopt}) = \Pr_1 f_1(I_{dopt}). \quad (3.92)$$

The above equation can be solved numerically using the bisection method [22].

For the Gaussian distribution, the optimum decision threshold, I_{gdopt} , can be found by solving for the roots of the following polynomial:

$$(\sigma_1^2 - \sigma_0^2) I_{gdopt}^2 + 2(I_1 \sigma_0^2 - I_0 \sigma_1^2) I_{gdopt} + I_0^2 \sigma_0^2 - I_1^2 \sigma_0^2 + \sigma_1^2 \sigma_0^2 \ln \left(\frac{\Pr_1^2 \sigma_0^2}{\Pr_0^2 \sigma_1^2} \right) = 0. \quad (3.93)$$

I_{gdopt} can also be approximated by [9]

$$I_{\text{adapt}} \equiv \frac{\bar{I}_1 \sigma_0^2 + \bar{I}_0 \sigma_1^2}{\sigma_0^2 + \sigma_1^2}. \quad (3.94)$$

3.12. Current-to-Voltage Conversion

In an experimental setup, the photocurrent is usually too small to be measured accurately due to the precision and resolution of the measurement equipment. However, the photocurrent can be converted to voltage and amplified by a transimpedance receiver and electrical amplifiers. The amplified signal voltage is easier to measure.

The random variable y of the time-averaged current is then converted to a random variable representing voltage. By performing the current-to-voltage conversion, the calculated theoretical PDF can be used to compare to the experimental result. The conversion is done by including an additional gain block, $R_L G_e$, to the theoretical model as shown in the following figure.

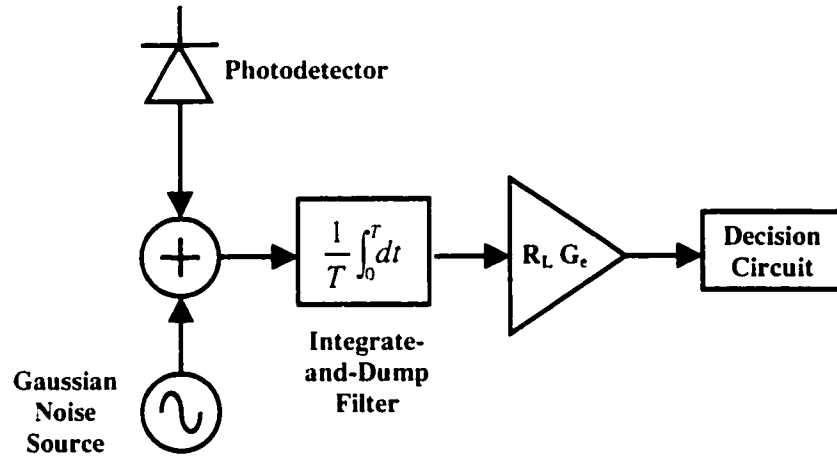


Figure 3.2: Optical receiver with current-to-voltage conversion gain block.

The current-to-voltage conversion is performed by R_L , which is the load resistance or the transimpedance of the receiver circuit. G_e is the electrical gain provided by the electrical amplifiers. The new equation of the PDF can be obtained by multiplying the photocurrents produced by the signal and ASE with $R_L G_e$. The variances of the thermal and shot noise are multiplied by $(R_L G_e)^2$ since they have a unit of A^2 . The time average current random variable y is converted to a voltage random variable by

multiplying with $R_L G_e$. When the noise associated with the electrical amplifier is referred to the load resistor R_L , the noise of the electrical amplifier can be expressed as a noise figure F . Therefore, the thermal noise equation (3.37) is modified as

$$\sigma_{th}^2 = \langle i_{th}^2 \rangle = \frac{2kTB_{elec}F}{R_L}. \quad (3.95)$$

3.13. Coupling and Transmission Efficiencies

In a real system, there are insertion losses introduced by optical components such as isolators, circulators, filters, etc. The coupling efficiencies at the input and output of the EDFA are denoted by μ_{in} and μ_{out} , respectively. The transmission efficiency from the output of the EDFA to the input of the receiver is denoted by L , which accounts for all the insertion losses of the optical components. Therefore, the detected signal and ASE power should be denoted as

$$P_{sig} = \mu_{in} G \mu_{out} L P_{in} \quad (3.96)$$

and

$$P_{ase} = \mu_{out} L P'_{ase}. \quad (3.97)$$

where P_{in} is the signal power incident at the input of the EDFA and P'_{ase} is the actual ASE noise power generated by the EDFA.

3.14. Discussion

A careful examination of equations (3.42) reveals that the non-Gaussian PDF converges to the Gaussian distribution as M increases [8] [9] [6]. This is the case when the optical bandwidth is much larger than the two-sided electrical bandwidth. The Gaussian approximation will only yield acceptable results when M is in the order of 30 [6]. However, the new generations of optical transmission system have M less than 10. In this case, the Gaussian approximation behaves poorly and the non-Gaussian distribution should be used.

A more general model was developed by Ribeiro et al. [27] which included intersymbol interference (ISI) and unrestricted electrical filter response. If the receiver is

modeled as an integrate-and-dump filter, the result obtained by Ribeiro et al. agrees with equation (3.32).

Chapter 4. Simulation of System Performance

The effects of the ASE noise and various system parameters on the performance of an EDFA pre-amplified receiver, such as the optimum decision threshold, BER and receiver sensitivity, are evaluated in this chapter.

Symbol	Description	Value	Unit
h	Planck's constant	6.63×10^{-34}	Js
k	Boltzmann's constant	1.38×10^{-23}	J/K
q	Electronic charge	1.60×10^{-19}	C
c	Speed of light in free space	2.998×10^8	m/s
λ	Wavelength of light carrier	1550.92	nm
T_k	Temperature	298	K
Pr_1	Probability of logical one	0.5	-
Pr_0	Probability of logical zero	0.5	-
N_{sp}	Spontaneous emission factor	2	-
P_{sat}	Output saturation power of EDFA	30	mW
μ_{in}	EDFA input coupling efficiency	1	-
μ_{out}	EDFA output coupling efficiency	1	-
L	Transmission efficiency between EDFA and receiver	1	-
\mathcal{R}	Responsivity of p-i-n diode	0.83	A/W
R_L	Transimpedance of receiver	500	Ω
F	Noise figure of electrical amplifier	7	dB
m_t	Number of polarization mode	2	-
ϵ	Extinction ratio	variable	dB
P_{inave}	Average received power	variable	dBm
G_o	EDFA small signal gain	variable	dB
B_o	Optical bandwidth	variable	GHz
B_{elec}	Two-sided electrical bandwidth	variable	GHz

Table 4.1: Simulation parameters.

Table 4.1 shows a list of simulation parameters. Some of the parameters are kept constant throughout the analysis and their values are shown in the table. The coupling and the transmission loss are neglected in the simulations. Therefore, μ_{in} , μ_{out} and L are set to unity. The optical receiver modeled in the simulations is based on parameters from the datasheet of Nortel 10 Gb/s optical receiver, which has a responsivity of 0.83 A/W and a transimpedance of 500 Ω .

4.1. Noise in the Receiver

The various noise components in the receiver are plotted as a function of the average received power to show the significance of each component. The received power is defined as the optical power at the input of the EDFA pre-amplifier. The influence of the optical bandwidth on the receiver noise is shown and discussed. The simulation parameters are $\epsilon = -20$ dB, $G_o = 35$ dB, $B_o = 20$ GHz and $B_{elec} = 20$ GHz.

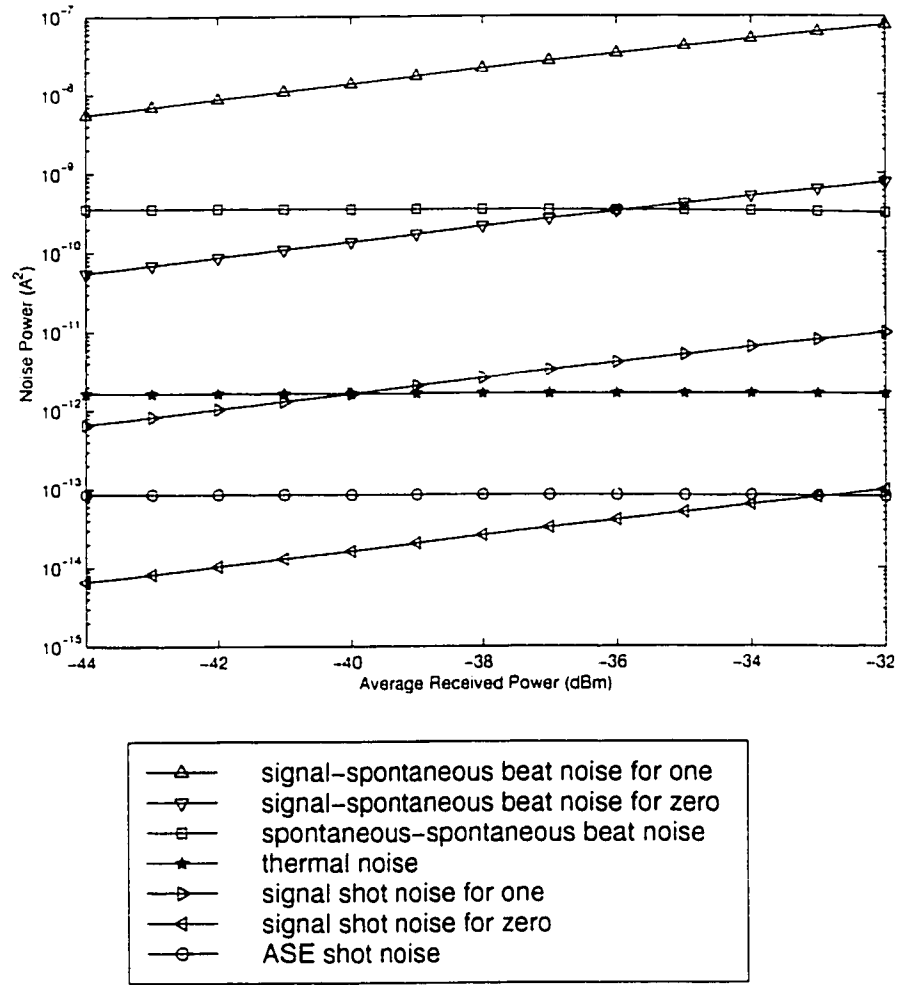


Figure 4.1: Power of each noise component for $B_o = 20$ GHz.

The spontaneous-spontaneous and the signal-spontaneous beat noises are calculated using equations (3.76) and (3.77), respectively. The dominant noise component for logical ones is the signal dependent signal-spontaneous beat noise. When the average received power is relatively high, in this case above -36 dBm, the dominant noise for logical zeros is signal-spontaneous beat noise. Otherwise, the spontaneous-spontaneous beat noise is dominant. The signal-spontaneous beat noise for logical zeros can be reduced if better extinction ratio, ϵ , is achieved.

Thermal noise is inversely proportional to the equivalent resistance of the optical receiver and directly proportional to the electrical bandwidth, as shown in equation

(3.95). This noise will be dominant if the EDFA gain is low. Since the equivalent resistance of a $500\ \Omega$ transimpedance amplifier is used in the simulation, the thermal noise is much lower than the case where a $50\ \Omega$ low impedance receiver is used. The shot noises expressed in equation (3.40) are negligible at low received power. However, if the received power is high and the EDFA gain is low, the signal shot noise for logical ones can become dominant. All of the signal dependent noise components increase with increasing received power and EDFA gain.

The simulation parameters used to generate the following plot are the same as before except that an optical bandwidth of 100 GHz is used to show the impact of optical bandwidth on the noise components.

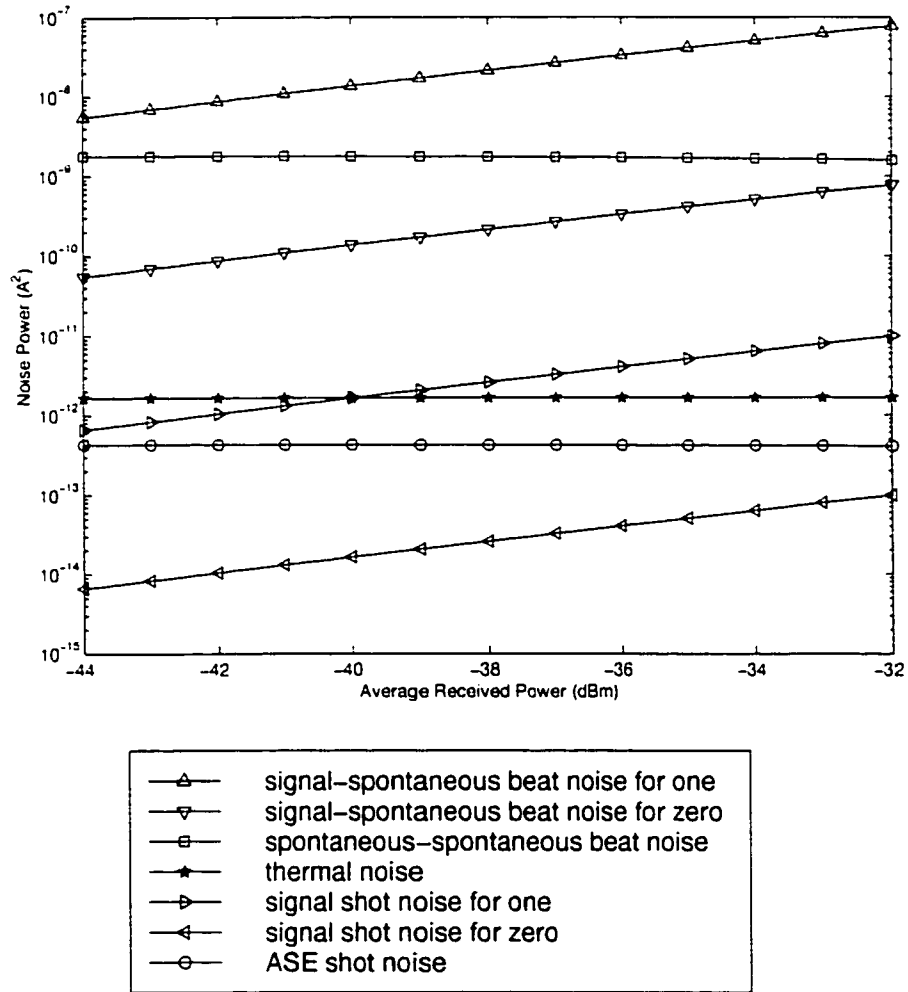


Figure 4.2: Power of each noise component for $B_o = 100$ GHz.

The spontaneous-spontaneous beat noise is dependent on the optical bandwidth as shown in equation (3.76). For larger optical bandwidth, more ASE noise will be incident on the photodetector; as a result, the spontaneous-spontaneous beat noise and ASE shot noise will increase. Figure 4.2 shows that the spontaneous-spontaneous beat noise power and ASE shot noise power are higher than those in Figure 4.1. All other noise components remain the same since they do not depend on the optical bandwidth. Therefore, narrowband optical filter is crucial in reducing electrical noise components originating purely from ASE noise.

4.2. Comparison of the Probability Density Functions

In this section, the Gaussian and non-Gaussian PDFs are compared and their dependence on the optical bandwidth and EDFA gain is investigated. The Gaussian and non-Gaussian distributions are calculated using expressions (3.81) and (3.55), respectively.

4.2.1 Optical Bandwidth Dependence of the PDFs

The Gaussian and non-Gaussian PDFs are compared to investigate the influence of the optical bandwidth. The simulation parameters are $\epsilon = -20$ dB, $G_o = 30$ dB, $B_{elec} = 20$ GHz and $P_{inave} = -35$ dBm. The comparisons are made between the optical bandwidths of 20 and 100 GHz, for M being equal to 2 and 10, respectively.

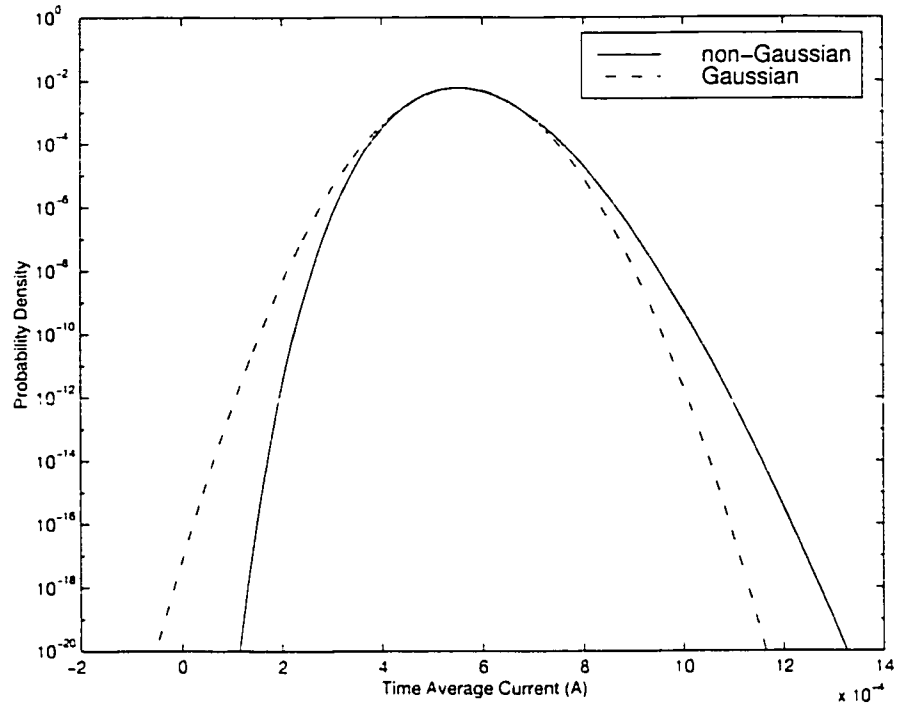


Figure 4.3: PDF of logical ones for $B_0 = 100$ GHz ($M = 10$).

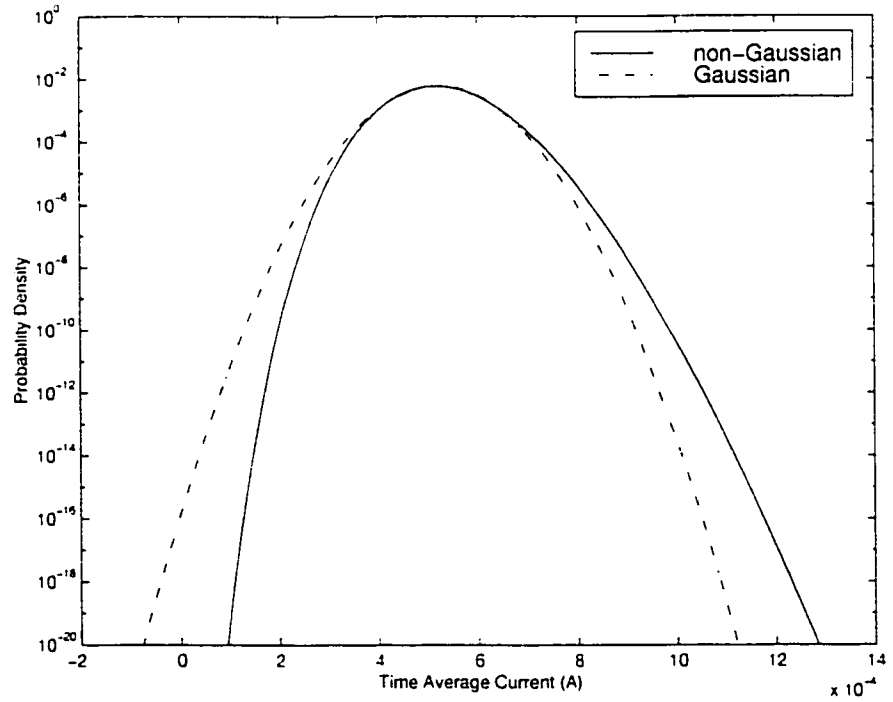


Figure 4.4: PDF of logical ones for $B_0 = 20$ GHz ($M = 2$).

From Figure 4.3 and Figure 4.4, it is evident that even for logical ones, the Gaussian PDFs differ very much from the non-Gaussian PDFs. The difference between the Gaussian and non-Gaussian distribution barely changes when M decreases from 10 to 2. This is because reduction of the optical filter bandwidth does not decrease the signal-spontaneous beat noise provided that all frequency components of the signal spectrum pass through the optical filter. The signal beats only with the ASE noise with the same frequency components as the signal. Therefore, decreasing the optical filter bandwidth does not change the signal-spontaneous beat noise.

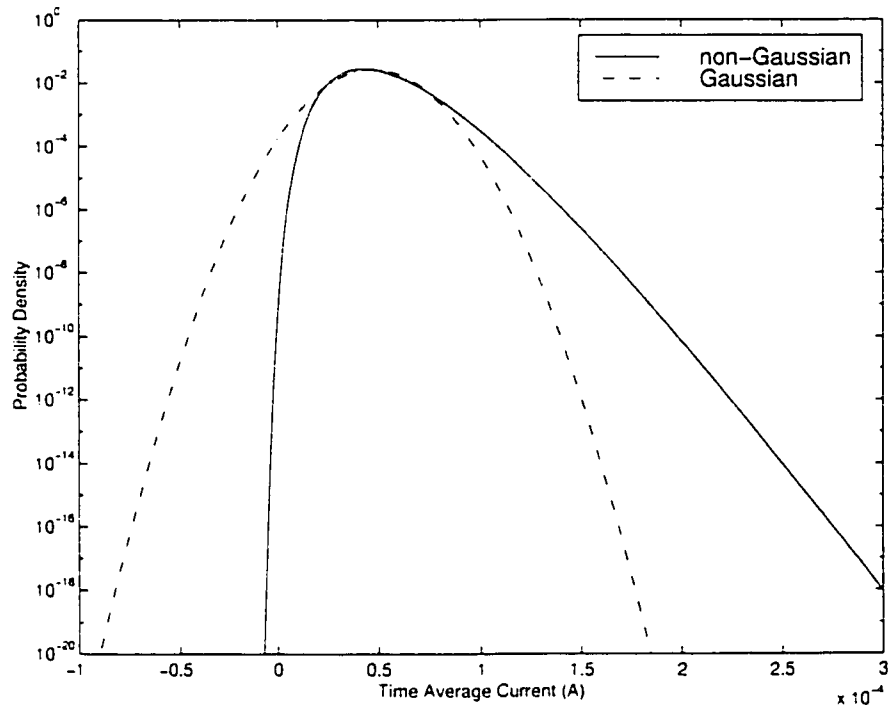


Figure 4.5: PDF of logical zeros for $B_o = 100$ GHz ($M = 10$).

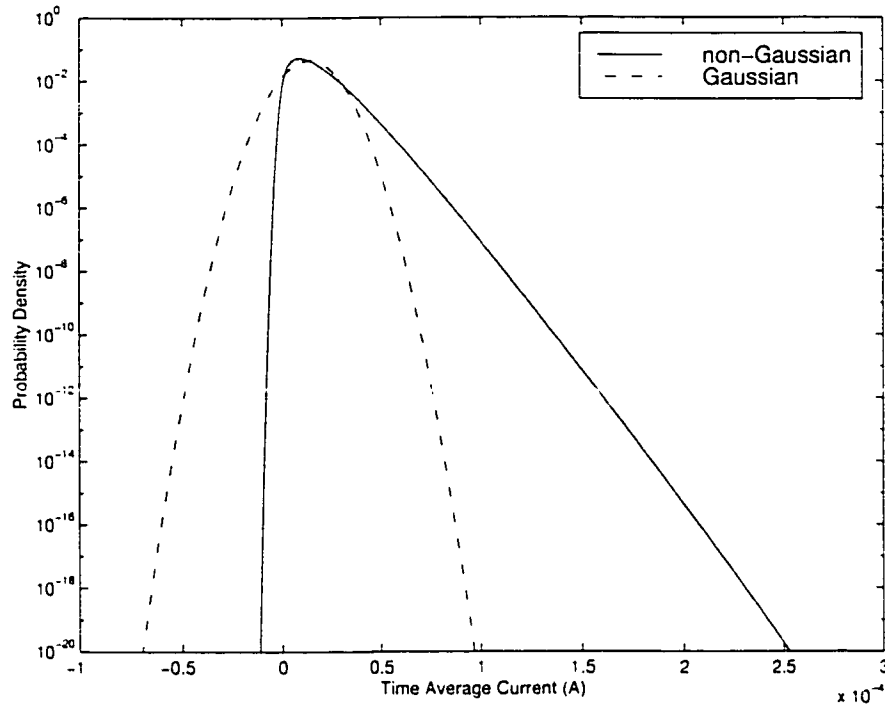


Figure 4.6: PDF of logical zeros for $B_o = 20$ GHz ($M = 2$).

A comparison of Figure 4.5 and Figure 4.6 shows that the PDF of the logical zeros shifts away from the Gaussian distribution as M decreases. It is evident that the PDF of logical zeros is highly non-Gaussian and it tends towards the chi-square distribution even at an M of 10. The means and variances of the PDFs are directly proportional to the optical bandwidth as shown in equations (3.74) and (3.75), since P_{ase} and M are directly proportional to B_o . Decreasing the optical bandwidth decreases the spontaneous-spontaneous beat noise, resulting in narrower PDFs and their peaks shifted to the left. Notice that the tails on the left side of the PDFs extend slightly into the negative current region. This is due to the contributions of the Gaussian thermal and shot noises.

The following plots show the optimum decision thresholds for the Gaussian and non-Gaussian distributions. All simulation parameters remained the same as before.

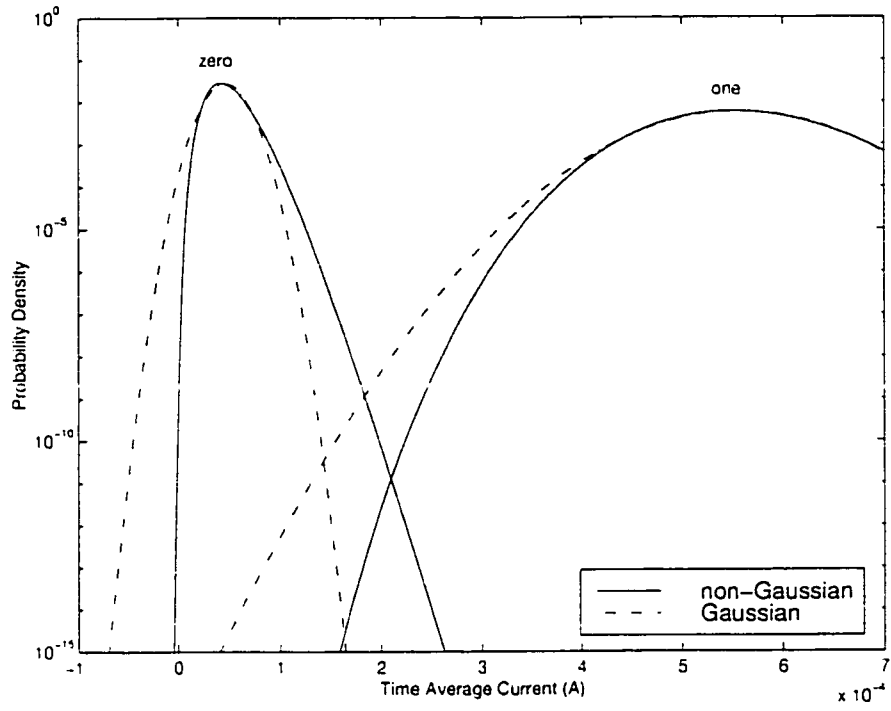


Figure 4.7: PDFs of logical ones and zeros for $B_0 = 100$ GHz ($M = 10$).

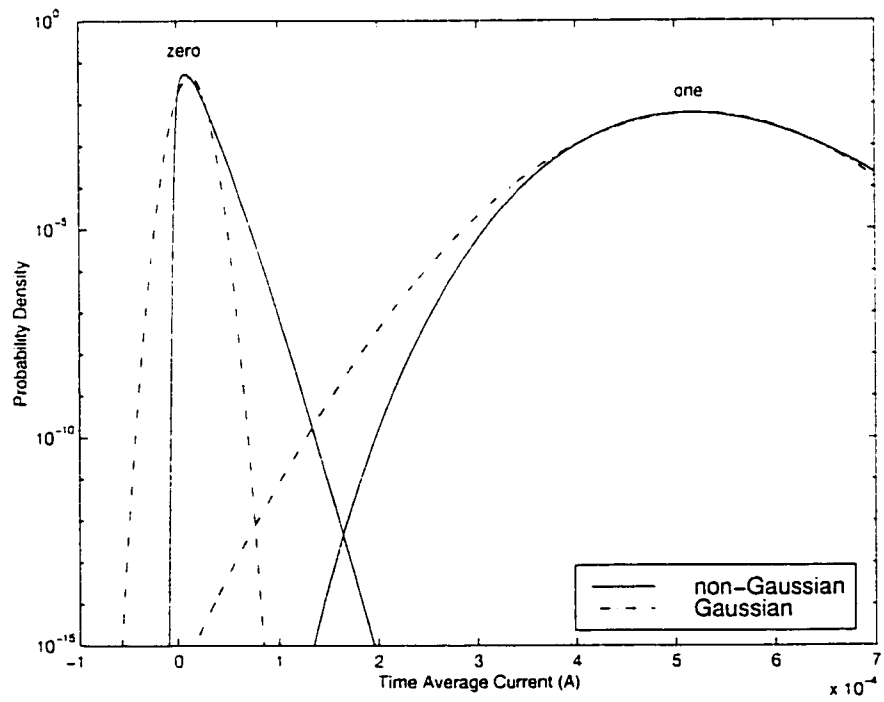


Figure 4.8: PDFs of logical ones and zeros for $B_0 = 20$ GHz ($M = 2$).

It is evident that the optimum decision thresholds predicted by the Gaussian PDFs differ a lot from those predicted by the non-Gaussian PDFs. The difference is greater for a lower value of M . Therefore, the Gaussian approximation is not adequate in providing accurate results in analysis involving the optimum decision threshold.

4.2.2 Electrical Bandwidth Dependence of the PDFs

All of the noise components are directly proportional to the electrical bandwidth and its effect on the PDF is investigated. The electrical bandwidth is reduced to 5 GHz and the optical bandwidth is 20 GHz, which yields an M of 8. All other simulation parameters remained the same as before.

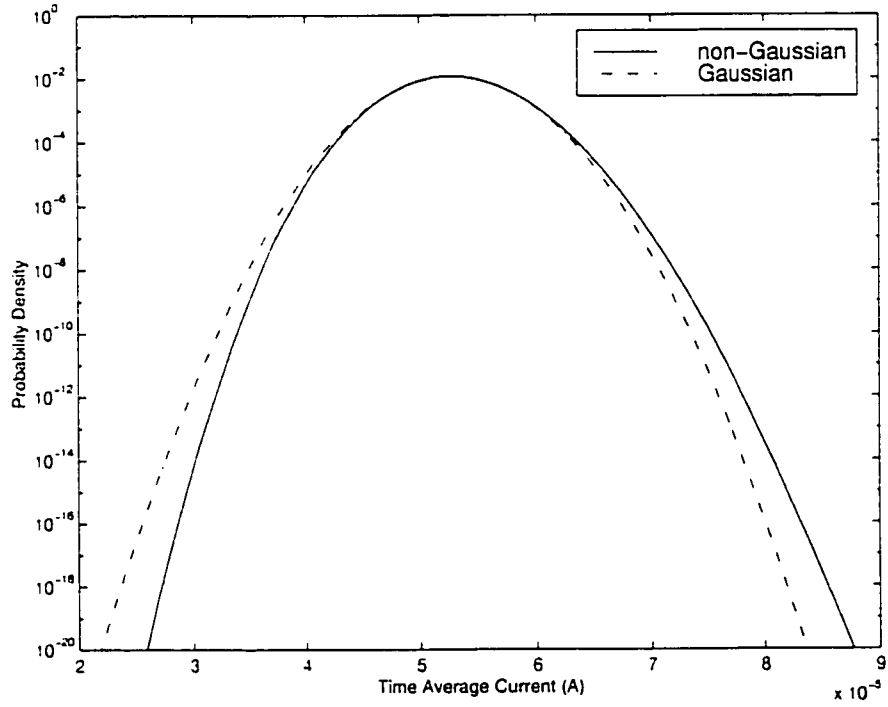


Figure 4.9: PDF of logical ones for $B_{\text{elec}} = 5$ GHz ($M = 8$).

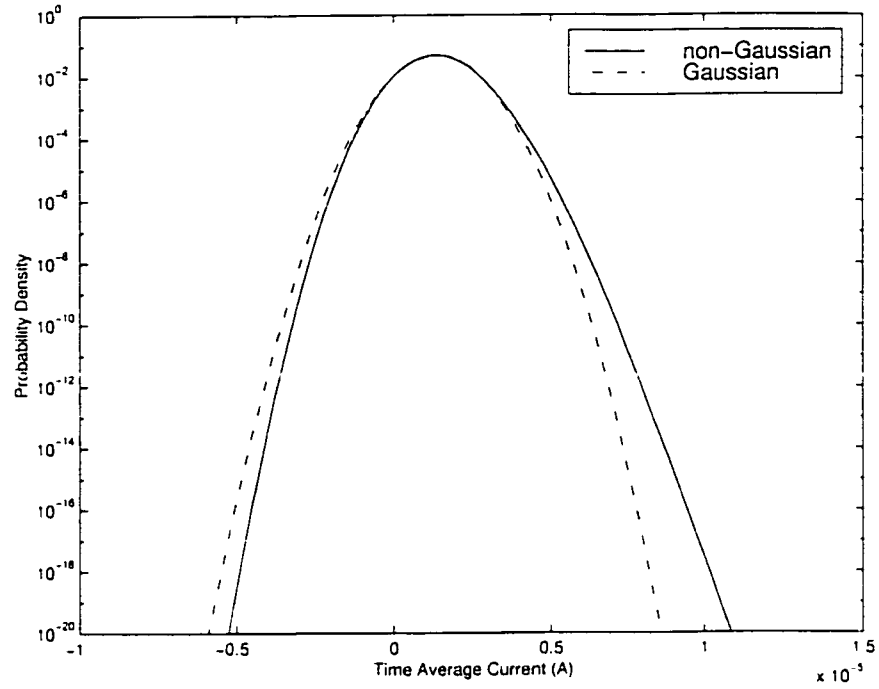


Figure 4.10: PDF of logical zeros for $B_{\text{elec}} = 5 \text{ GHz}$ ($M = 8$).

Comparing Figure 4.9 to Figure 4.4 and Figure 4.10 to Figure 4.6, it is evident that when the electrical bandwidth is reduced, the PDFs become narrower. This is due to lower noise current in the receiver since the variance of the PDFs are directly proportional to the electrical bandwidth, as shown by equation (3.75). Notice that as the electrical bandwidth is reduced, M increases and the shape of the non-Gaussian PDF approaches the Gaussian distribution.

4.2.3 EDFA Gain Dependence of the PDFs

The EDFA small signal gain is reduced to 20 dB to investigate the gain dependence of the PDFs. The simulation parameters are $\epsilon = -20 \text{ dB}$, $B_o = 20 \text{ GHz}$, $B_{\text{elec}} = 20 \text{ GHz}$ and $P_{\text{inave}} = -35 \text{ dBm}$.

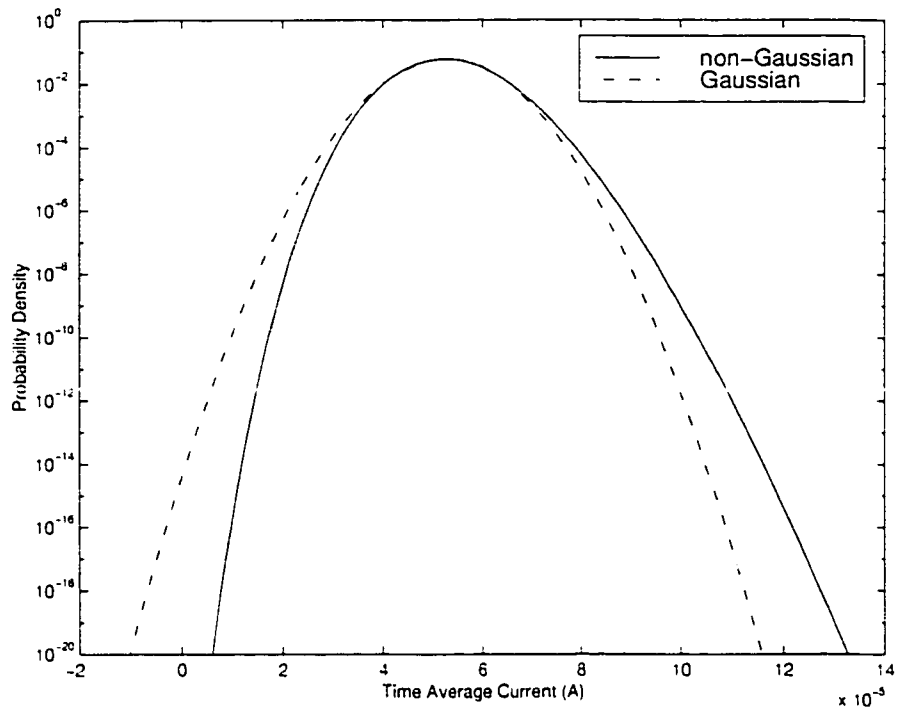


Figure 4.11: PDF of logical ones for $G_o = 20$ dB.

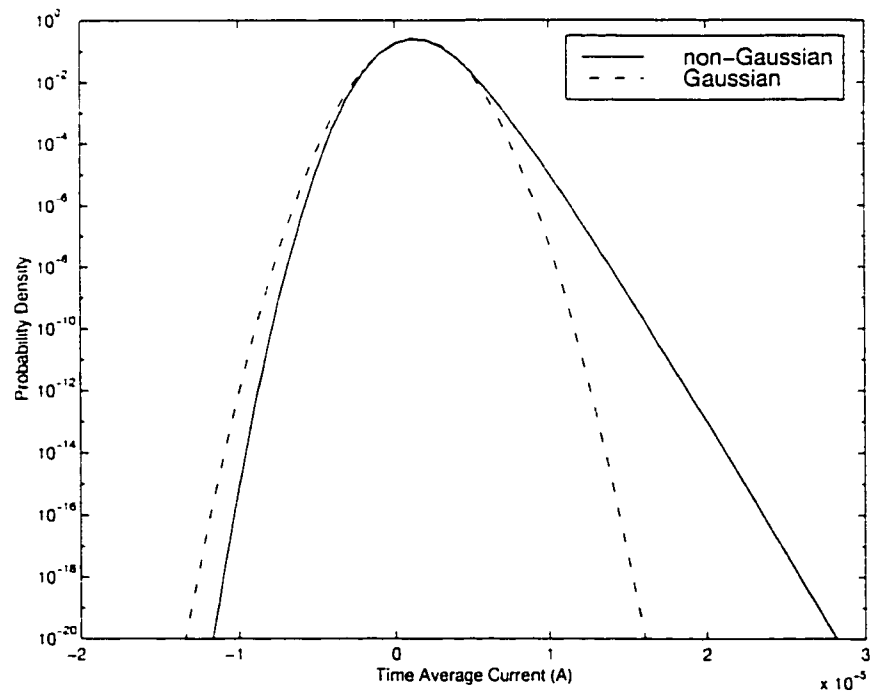


Figure 4.12: PDF of logical zeros for $G_o = 20$ dB.

Comparing Figure 4.11 to Figure 4.4 and Figure 4.12 to Figure 4.6, it is evident that when the EDFA gain is reduced, the peaks of the PDFs shift to the less positive side. This is due to the lower optical power incident on the photodiode. The variances of the PDFs are directly proportional to the square of the EDFA gain, as shown in equations (3.76) and (3.77). Therefore, the PDFs will be narrower for lower EDFA gain. Also, if Figure 4.11 and Figure 4.12 are plotted on the same scale as Figure 4.4 and Figure 4.6, it can be seen that as the EDFA gain is reduced, the non-Gaussian PDF approaches the Gaussian distribution. This is due to the reduction in ASE noise and hence a reduction in spontaneous-spontaneous and signal-spontaneous beat noises. Therefore, the thermal noise will become more dominant in the receiver.

4.3. Optimum Decision Threshold Analysis

Section 4.2 has shown that as the ratio of optical to electrical bandwidth decreases, the PDFs of the logical ones and zeros tend towards the non-Gaussian distribution, which is in fact the chi-square distribution if the Gaussian thermal and shot noises are negligible [6] [8]. A change in the noise distribution will impact the optimum decision threshold in the decision circuit.

4.3.1 Bit Error Ratio as a Function of Percentage Decision Threshold

The BER is plotted as a function of the percentage threshold at different received power levels. The percentage threshold is defined as

$$PercentageThreshold = \frac{I_d - \bar{I}_0}{\bar{I}_1 - \bar{I}_0} \times 100\% . \quad (4.1)$$

I_d is obtained by solving expression (3.92). The simulation parameters are $\epsilon = -20$ dB, $G_o = 30$ dB, $B_{elec} = 20$ GHz, $B_o = 20$ and 100 GHz.

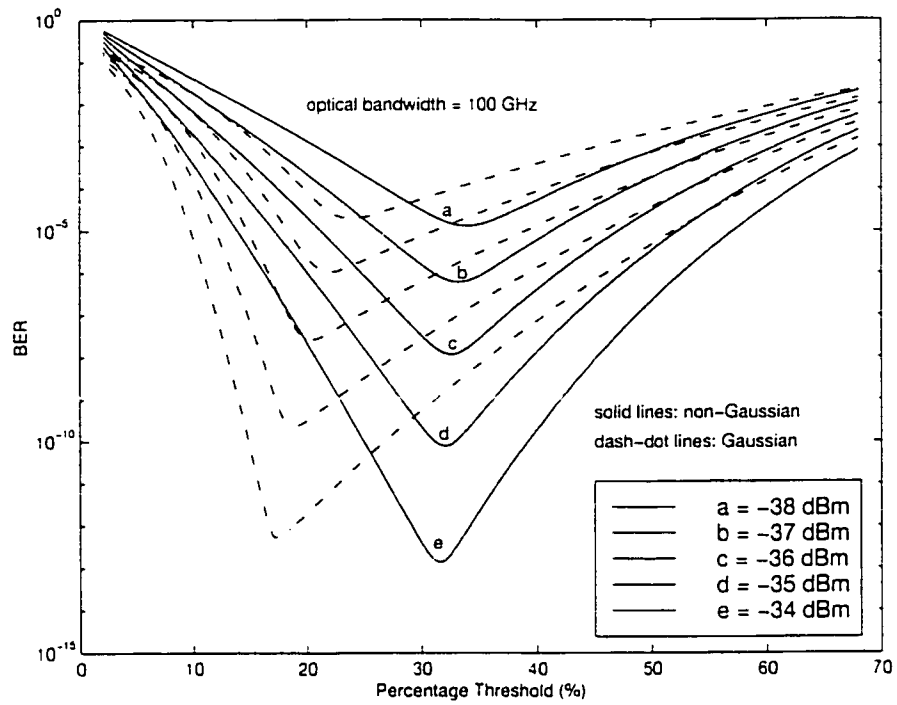


Figure 4.13: BER as a function of percentage threshold for $B_o = 100$ GHz.

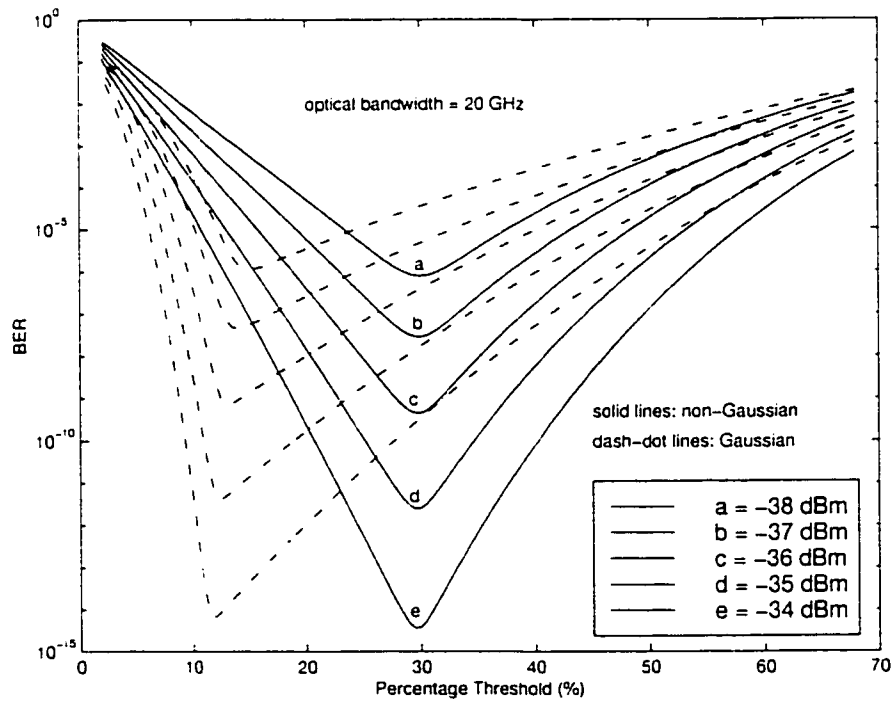


Figure 4.14: BER as a function of percentage threshold for $B_o = 20$ GHz.

For an optical bandwidth of 100 GHz, the difference between the Gaussian and non-Gaussian optimum percentage thresholds shown in Figure 4.13, which are the minimum points on the curves, is about 14.2% for an average received power of -34 dBm.

For an optical bandwidth of 20 GHz, the difference between the Gaussian and non-Gaussian optimum percentage thresholds is 17.8% for an average received power of -34 dBm, as shown in Figure 4.14. If the voltage difference between logical ones and zeros at the input of the decision circuit is 1 V, then the 17.8% difference in optimum threshold will translate into 178 mV difference in actual voltage, which is very significant.

By comparing the preceding two figures, it is evident that the difference between the Gaussian and non-Gaussian optimum decision threshold increases as the optical bandwidth decreases.

4.3.2 Optimum Percentage Threshold as a Function of Average Received Power

The optimum percentage threshold is plotted as a function of average received power in the following two figures. The simulation parameters are $\epsilon = -20$ dB, $G_o = 30$ dB, $B_{elec} = 20$ GHz, $B_o = 20$ and 100 GHz.

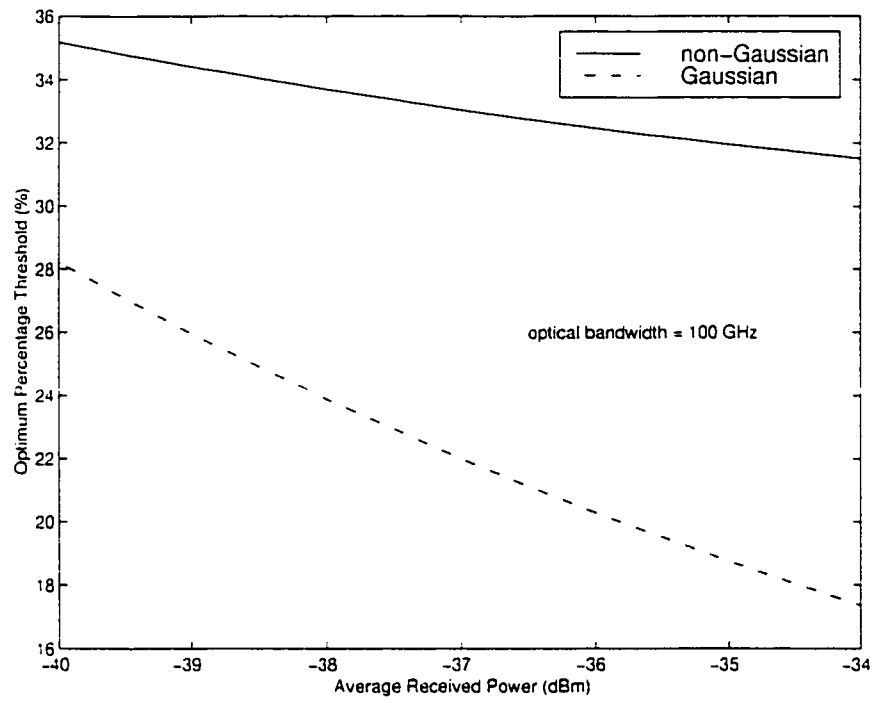


Figure 4.15: Optimum percentage threshold for $B_o = 100$ GHz.

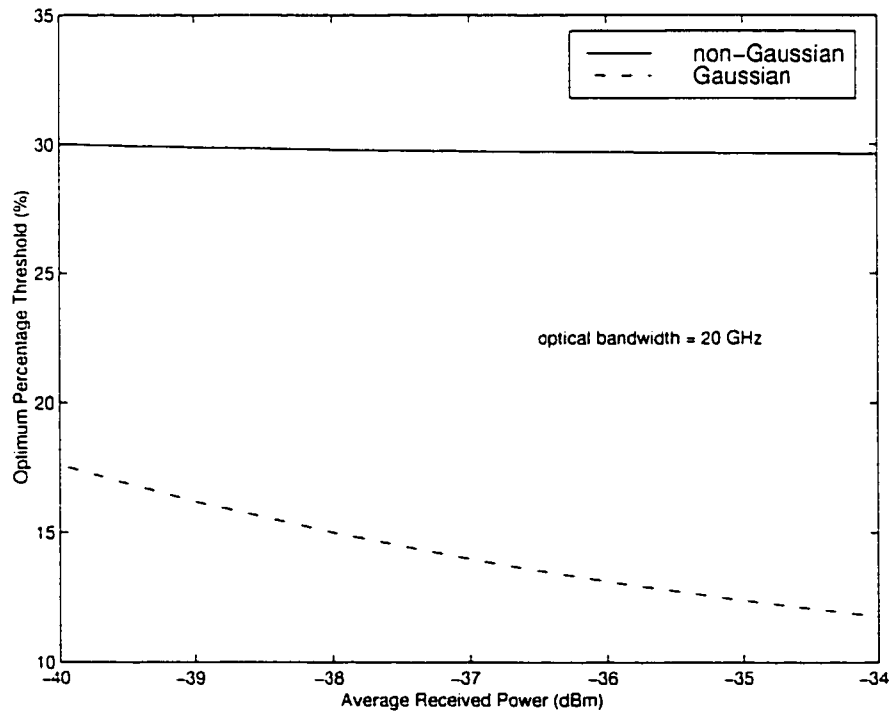


Figure 4.16: Optimum percentage threshold for $B_o = 20$ GHz.

Figure 4.15 shows that for an optical bandwidth of 100 GHz, the optimum percentage threshold for the non-Gaussian distribution varies by 3.7% when the average received power changes from -34 to -40 dBm. For the Gaussian distribution, the optimum percentage threshold varies by 10.9% over the same range of received power. Figure 4.16 shows that when the optical bandwidth is reduced to 20 GHz, the optimum percentage threshold for the non-Gaussian distribution varies by 0.4% while for the Gaussian distribution, the change is 5.8%.

The result shows that the optimum percentage threshold predicted by the non-Gaussian distribution stays fairly constant over the range of received power, while the Gaussian case varies over a larger range.

4.3.3 Optimum Percentage Threshold as a Function of Optical Bandwidth

The influence of the optical bandwidth on the optimum threshold is shown in the following figure. The simulation parameters are $\varepsilon = -20$ dB, $G_o = 30$ dB, $P_{inave} = -35$ dBm and $B_{elec} = 20$ GHz.

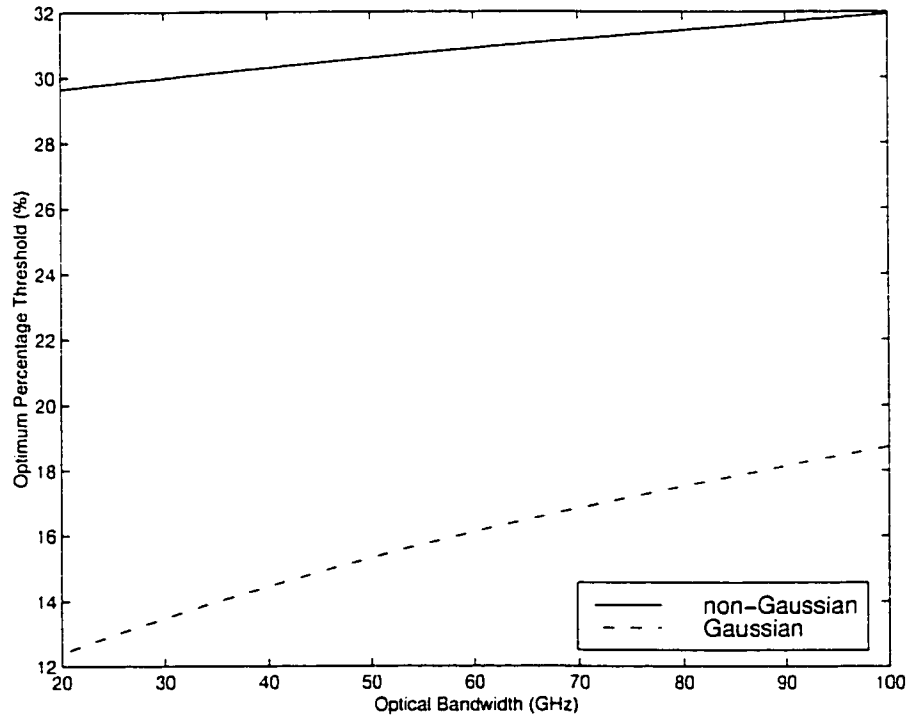


Figure 4.17: Optimum percentage threshold as a function of optical bandwidth.

Figure 4.17 shows that as the optical bandwidth decreases, the difference between the Gaussian and non-Gaussian optimum thresholds increases. The optimum percentage threshold of the non-Gaussian distribution only varies by 2.3% for the range of optical bandwidth from 20 to 100 GHz. The optimum percentage threshold predicted by the Gaussian distribution changes by 6.3% over the same range of optical bandwidth.

4.3.4 Optimum Percentage Threshold as a Function of EDFA Gain

Figure 4.18 shows the relationship between the optimum percentage threshold and the EDFA gain. The simulation parameters are $\epsilon = -20$ dB, $P_{\text{inave}} = -35$ dBm, $B_o = 20$ GHz and $B_{\text{elec}} = 20$ GHz.

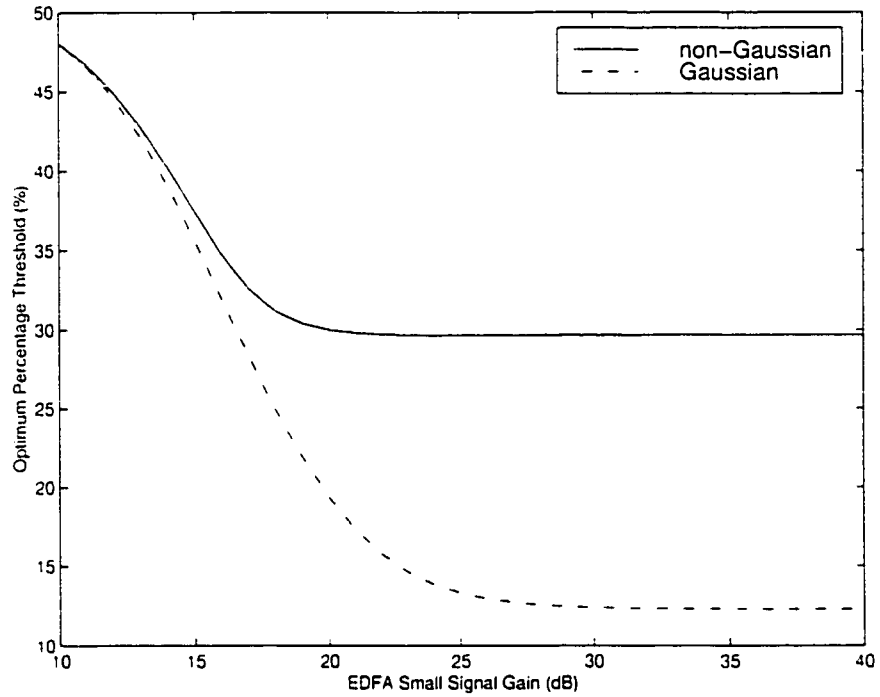


Figure 4.18: Optimum percentage threshold as a function of EDFA gain.

When the EDFA gain is small, the thermal noise is dominant; hence the non-Gaussian PDFs tend towards the Gaussian distribution. Therefore, the optimum thresholds predicted by both distributions do not differ much from each other. However, as the EDFA gain is increased, the ASE noise increases and the difference between the Gaussian and non-Gaussian distribution becomes prominent. When the gain is sufficiently large, in this case greater than 25 dB for Gaussian and 20 dB for the non-

Gaussian distribution, increasing the gain has negligible effect on the optimum percentage threshold. This is because the SNR is almost independent of the gain as shown in equation (3.80).

4.4. Bit Error Ratio Analysis

The effects of the various parameters such as the received optical power, optical bandwidth, EDFA gain and extinction ratio on the BER are investigated in this section. BER is calculated using equation (3.89).

4.4.1 Bit Error Ratio as a Function of Average Received Power

The BER of the system is evaluated over a range of received power. The simulation parameters are $\epsilon = -20$ dB, $G_o = 30$ dB, $B_{elec} = 20$ GHz, $B_o = 20$ and 100 GHz.

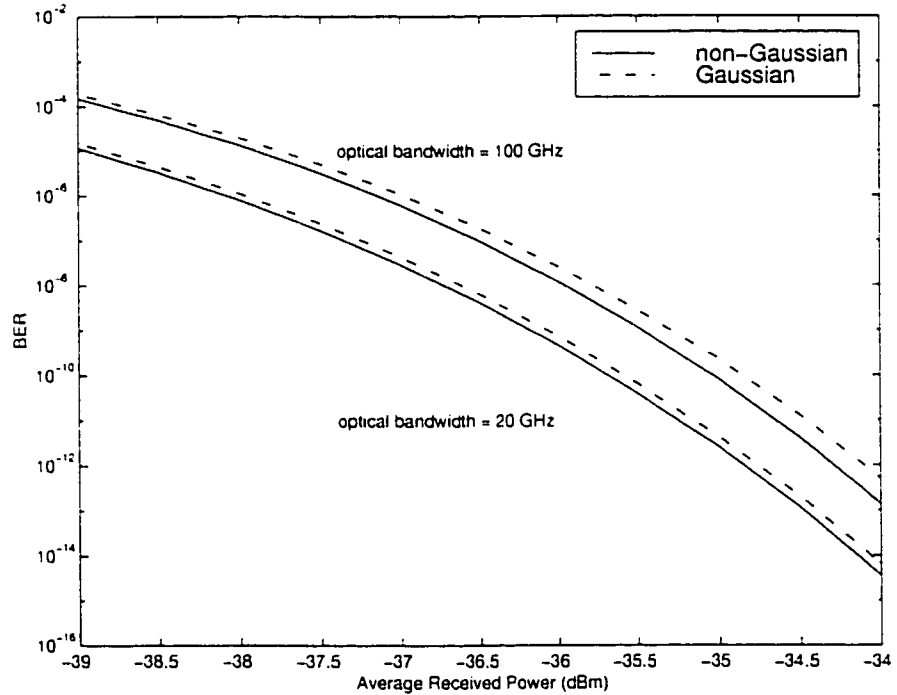


Figure 4.19: BER as a function of average received power.

The signal shot noise and the signal-spontaneous beat noise are both signal-dependent noises with the signal-spontaneous beat noise being the dominant component. The signal-spontaneous beat noise power is directly proportional to the optical signal power as shown in equation (3.77). However, the electrical signal power is directly

proportional to the square of the optical signal power. Therefore, the electrical SNR improves with increasing optical signal power. As a result, the data eye diagram has a wider eye opening and hence better BER is achieved.

When the optical bandwidth is increased, the spontaneous-spontaneous beat noise increases, which resulted in an increase in BER. Figure 4.19 shows that the Gaussian distribution overestimates the BER compared to the non-Gaussian distribution. However, the difference in BER performance between the two distributions is not very significant. When the optical bandwidth is increased, the signal power requires to be increased to maintain the same BER. For a BER of 10^{-12} , the incurred power penalty by increasing the optical bandwidth from 20 to 100 GHz is about 0.6 dB for the non-Gaussian distribution.

4.4.2 Bit Error Ratio as a Function of Optical Bandwidth

BER is plotted as a function of optical bandwidth in Figure 4.20. The simulation parameters are $\epsilon = -20$ dB, $G_o = 30$ dB, $P_{\text{inave}} = -35$ dBm and $B_{\text{elec}} = 20$ GHz. The optical bandwidth ranges from 20 to 100 GHz, giving values of M from 2 to 10.

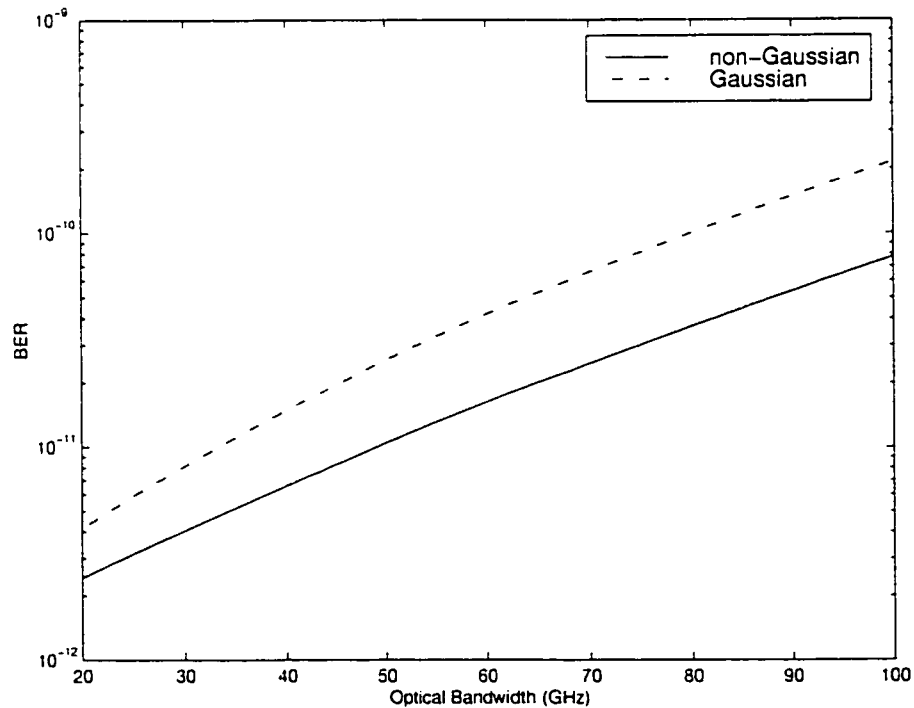


Figure 4.20: BER as a function of optical bandwidth.

Improvement of the BER when the optical bandwidth decreases is due to a reduction of spontaneous-spontaneous beat noise, which is directly proportional to the optical bandwidth. The Gaussian distribution overestimates the BER as compared to the non-Gaussian distribution. However, the BER difference between the two cases is not very significant.

4.4.3 Bit Error Ratio as a Function of EDFA Gain

The BER is plotted as a function of the EDFA small signal gain. The simulation parameters are $\epsilon = -20$ dB, $P_{\text{inave}} = -35$ dBm, $B_{\text{elec}} = 20$ GHz, $B_o = 20$ and 100 GHz.

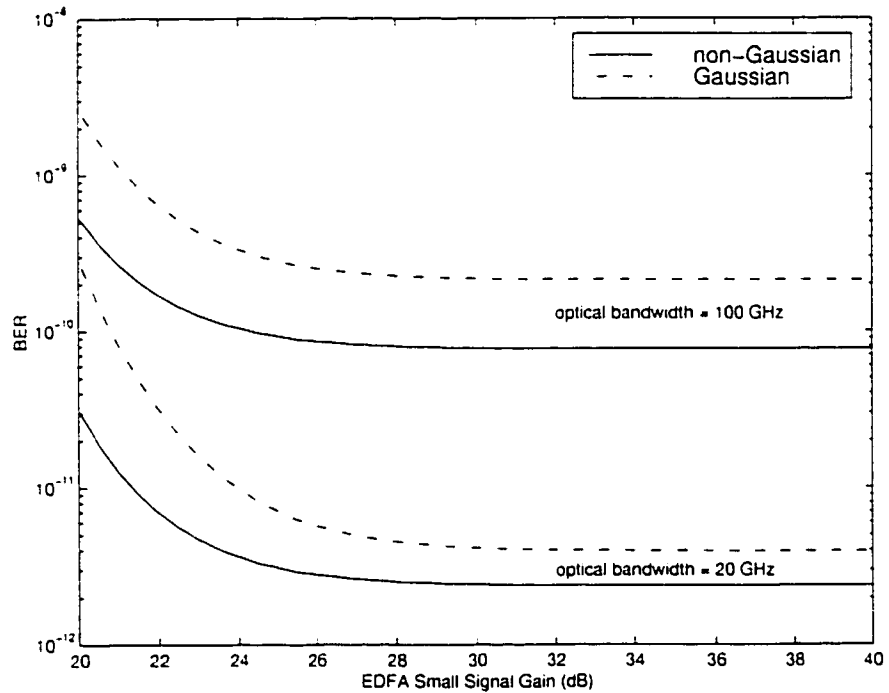


Figure 4.21: BER as a function of EDFA small signal gain.

Figure 4.21 shows that the BER approaches a minimum asymptotically. This is due to the fact that the electrical SNR approaches a constant when the EDFA gain is sufficiently large, which can be seen from equation (3.80). The difference in BER between the Gaussian and non-Gaussian distributions is less than half a decade for $B_o = 100$ GHz. This difference becomes smaller as the optical bandwidth decreases.

4.4.4 Bit Error Ratio as a Function of Extinction Ratio

The relationship between the BER and the extinction ratio is investigated. The simulation parameters are $G_o = 30$ dB, $P_{\text{inave}} = -35$ dBm, $B_{\text{elec}} = 20$ GHz, $B_o = 20$ and 100 GHz.

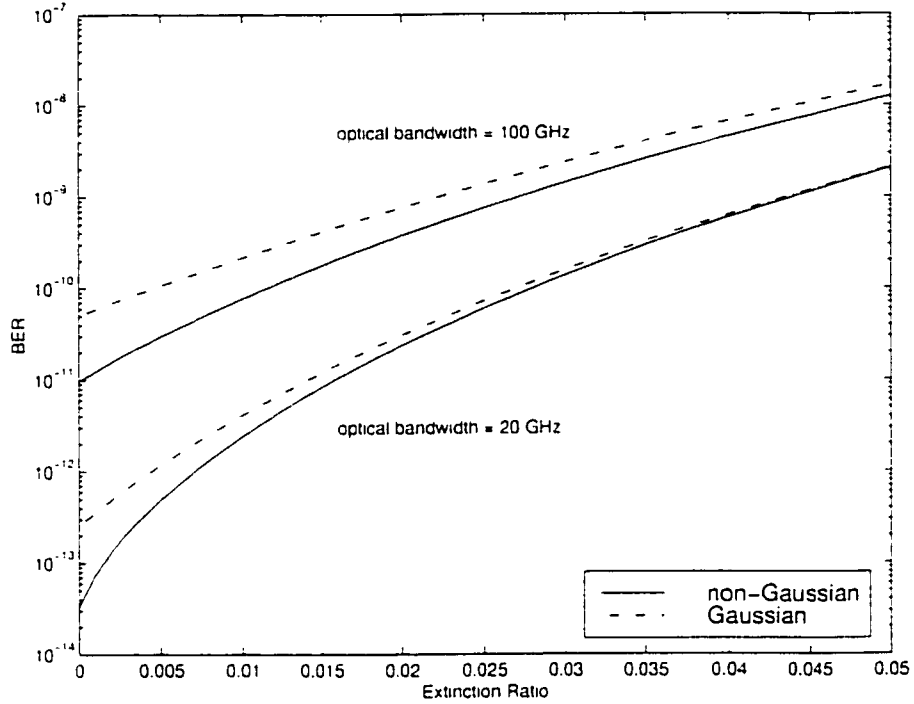


Figure 4.22: BER as a function of the extinction ratio.

Figure 4.22 shows the BER increases with the extinction ratio. This is because when the extinction ratio is increased, the mean power level of logical zeros is increased which increases the signal-spontaneous beat noise for logical zeros. This reduces the data eye opening which increases the BER. The maximum difference between the Gaussian and non-Gaussian distributions occurs when logical zeros are perfectly extinct. However, the difference in BER is less than a decade.

4.5. Receiver Sensitivity Analysis

The sensitivity of an optical receiver is the required received optical power to achieve a certain BER. For an EDFA pre-amplified receiver, the received power is defined as the power at the input of the EDFA.

4.5.1 Sensitivity as a Function of Optical Bandwidth

Spontaneous-spontaneous beat noise is the only noise component that is dependent on the optical bandwidth, as shown in equation (3.77), and its influence on the receiver sensitivity is investigated. The simulation parameters are $\epsilon = -20$ dB, $G_o = 30$ dB, $B_{elec} = 20$ GHz and the optical bandwidth is varied from 20 to 100 GHz.

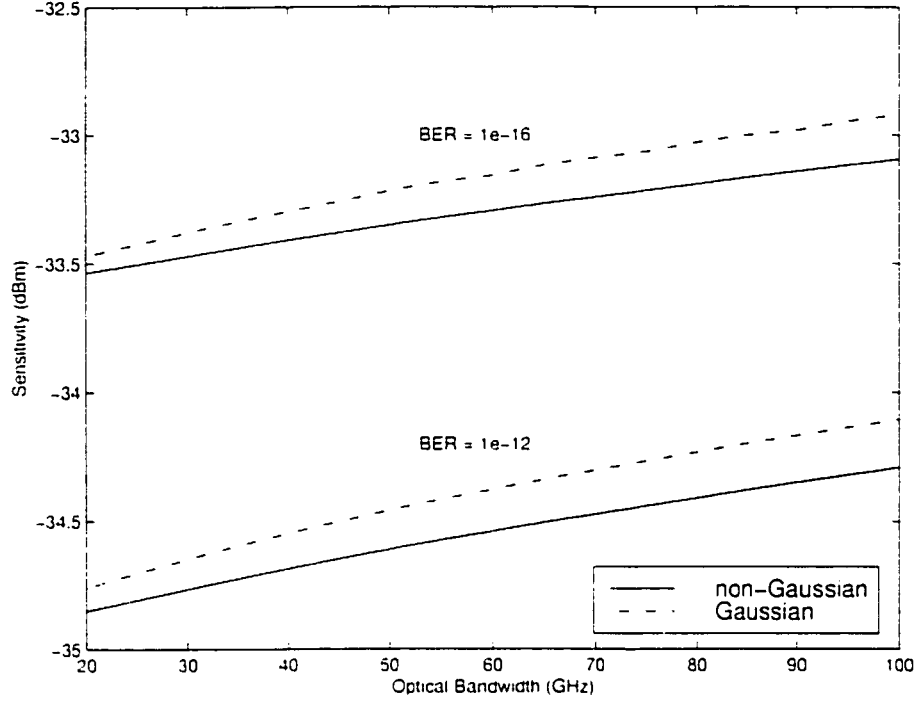


Figure 4.23: Sensitivity as a function of the optical bandwidth.

As the optical bandwidth decreases, the spontaneous-spontaneous beat noise is reduced, which improves the electrical SNR and BER. Therefore, for a constant BER, the receiver sensitivity will improve as the optical bandwidth decreases, as shown in Figure 4.23. The non-Gaussian distribution yields slightly better performance than the Gaussian distribution but the difference is insignificant.

4.5.2 Sensitivity as a Function of EDFA Gain

The influence of the EDFA gain on the receiver sensitivity is investigated in this section. The simulation parameters are $\epsilon = -20$ dB, $B_o = 20$ GHz and $B_{elec} = 20$ GHz. The EDFA small signal gain is varied from 10 to 40 dB.

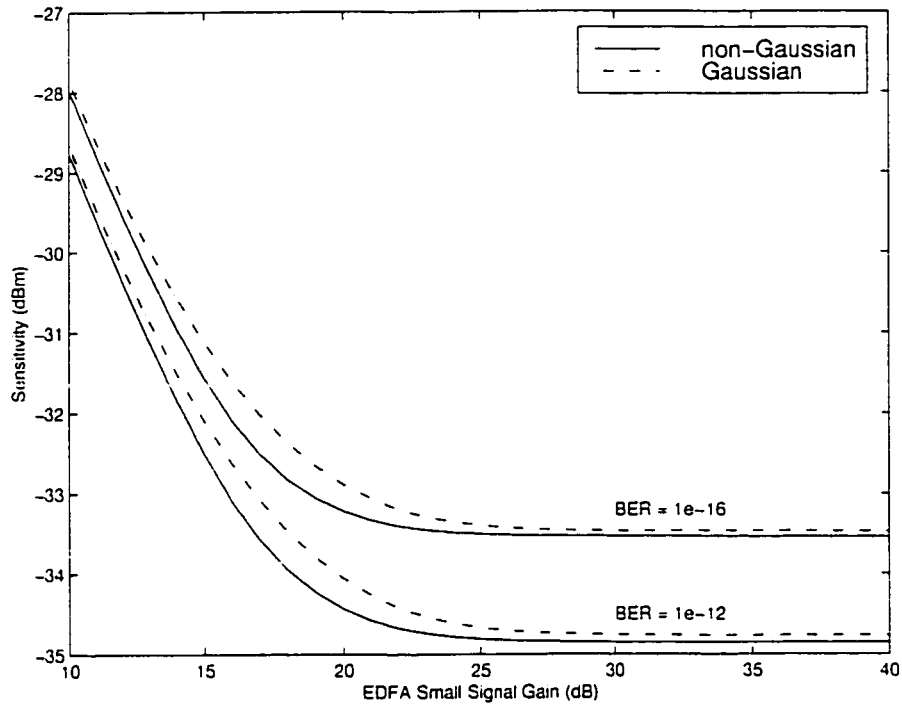


Figure 4.24: Sensitivity as a function of the EDFA gain.

The EDFA gain independent thermal noise is the dominant noise component when the gain is small. Equation (3.79) shows that for small EDFA gain, as the gain increases, there is a larger increase in the signal photocurrent relative to the total noise current, which results in a higher electrical SNR and a lower BER. For a constant BER, increasing the EDFA gain will yield better receiver sensitivity. Figure 4.24 shows that when the gain is increased from 10 to 20 dB, the receiver sensitivity improves significantly.

When the gain is sufficiently large, the signal-spontaneous and the spontaneous-spontaneous beat noises become the dominant noise components and are directly proportional to the square of the gain. Therefore, the electrical SNR approaches a constant since the last term of the denominator in equation (3.80) approaches zero. As a result, the sensitivity does not improve any further with increasing gain, which is shown in Figure 4.24 for gain greater than 25 dB.

The Gaussian and non-Gaussian distributions provide similar sensitivity performance with insignificant difference.

4.6. Discussion of Simulation Results

When the EDFA small signal gain is sufficiently large, the PDFs of logical ones and zeros will tend towards the chi-square distribution as the ratio of the optical to electrical bandwidth decreases. As a result, the optimum decision threshold deviates away from the Gaussian prediction.

The simulation results show that the Gaussian distribution is a good approximation to the non-Gaussian distribution in the BER and receiver sensitivity analysis with negligible error. This is because the optimum decision threshold has been considered separately for both distributions.

The impact of the non-Gaussian distribution on the system shows up in the optimum decision threshold analysis. The optimum decision threshold predicted by the Gaussian distribution is significantly different from that of the non-Gaussian distribution. If the BER and receiver sensitivity were computed using the Gaussian distribution with the optimum decision threshold predicted by the non-Gaussian PDFs, a large error will be generated.

In the following figures, both distributions use the same optimum decision threshold predicted by the non-Gaussian distribution. All simulation parameters used in Figure 4.25 are the same as Figure 4.20. In this case, the Gaussian distribution produced a significantly higher BER: almost three decades for $B_o = 100$ GHz and close to four decades for $B_o = 20$ GHz.

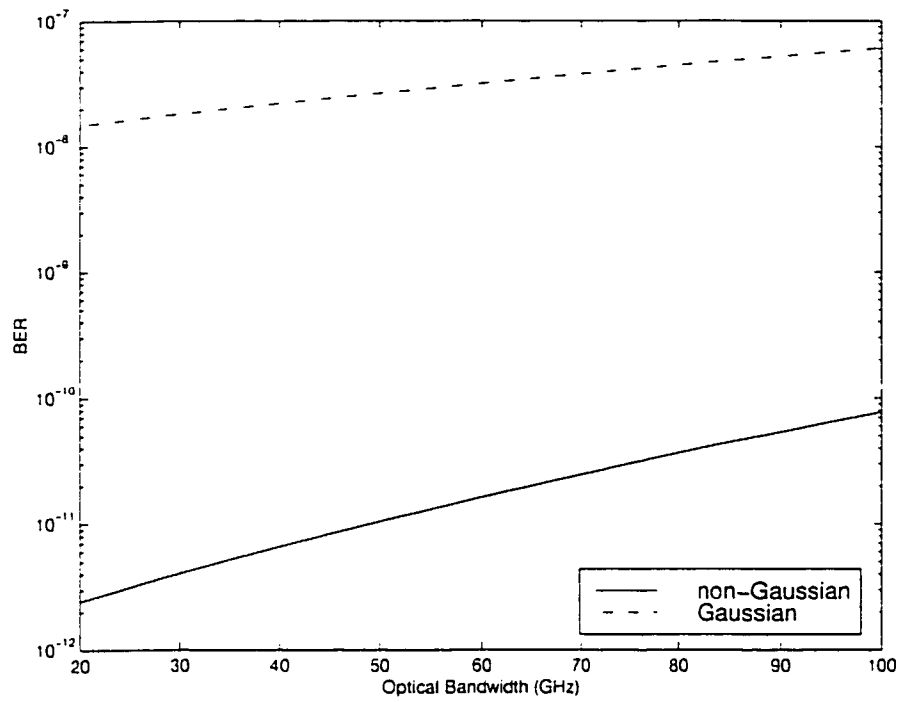


Figure 4.25: BER using only the non-Gaussian optimum decision threshold.

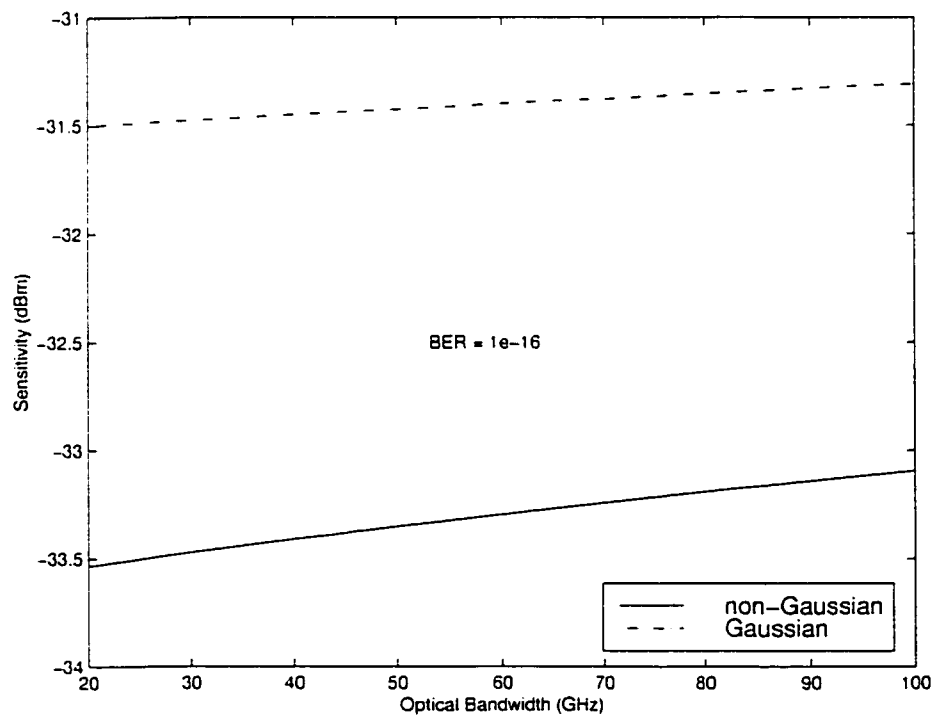


Figure 4.26: Sensitivity using only the non-Gaussian optimum decision threshold.

All simulation parameters used in the sensitivity analysis in Figure 4.26 are the same as Figure 4.23. In this case, the Gaussian distribution yielded power penalties of 1.8 dB for $B_o = 100$ GHz and 2 dB for $B_o = 20$ GHz relative to the receiver sensitivity predicted by the non-Gaussian distribution.

Therefore, when the optimum decision threshold of a system is known, the Gaussian distribution should not be used in analysis involving BER and receiver sensitivity.

Chapter 5. Experimental Results

The noise distributions for the logical ones and zeros for an EDFA pre-amplified receiver are measured experimentally to investigate the behavior of the PDFs as the optical bandwidth approaches the electrical bandwidth. The experimental optimum decision thresholds are compared to the Gaussian and non-Gaussian theories and its effect on the BER is investigated.

5.1. Probability Density Measurements

A pre-amplified optical receiver is used in the experiment to measure the probability distributions of logical ones and zeros. Since the theoretical analysis does not include ISI, the experiment is setup to eliminate the effect of ISI.

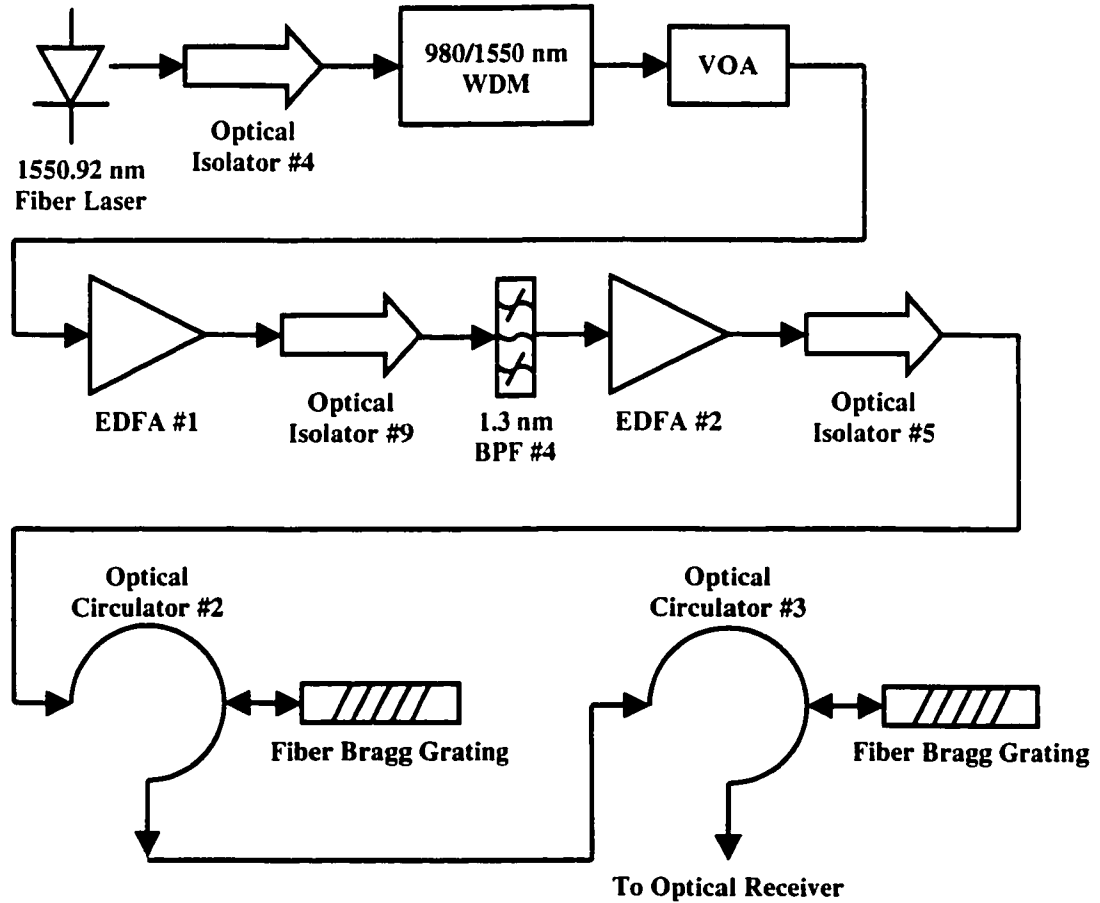


Figure 5.1: Schematic of the optical components in the PDF measurement experiments.

The experimental setup shown in Figure 5.1 consists of an optical source, EDFAs, optical filters and a direct detection receiver. The light source is an IONAS DFB fiber laser operating at a wavelength of 1550.92 nm. The wavelength of the laser conforms to channel 33 of the ITU Standard Fiber Optic Telecommunication Channel. The fiber laser is chosen for its narrow linewidth of less than 20 kHz and center wavelength temperature coefficient of 0.0028 nm/K. The specification of the fiber laser is documented in Appendix A.14. An optical isolator is placed at the output of the laser to protect the laser from reflected light. Since the fiber laser uses a 980 nm pump laser to generate laser emission at 1550.92 nm using erbium doped fiber, a wavelength division multiplexer (WDM) is used to remove the residue 980 nm pump power. A variable optical attenuator (VOA) is used to control the output power of the laser source. The laser power is constant and not modulated so that ISI will not be present. The laser power is very stable, with fluctuation less than ± 0.2 dB. This stability is required for the PDF measurements. Different level of laser power is used to represent either logical ones or zeros and their PDFs are measured individually.

The EDFAs are built in TRLabs and they are treated as a single entity in the experiments. At 1550.92 nm, the combined small signal gain of the two EDFAs including the losses introduced by the 1.3 nm bandpass filter (BPF) and two optical isolators is 41.1 dB. The EDFA gain curve is shown in Figure C.2. The purpose for having such high gain is to compensate for the high insertion loss introduced by the optical circulators and FBGs, so that electrical noise currents originating from the ASE are dominant in the receiver. An optical isolator is placed at the output of each EDFA to eliminate any backscattering of the signal and backward propagating ASE. Signal and ASE travelling through the EDFA in the backward direction will decrease the EDFA forward gain. The 1.3 nm BPF placed between the EDFAs is to reject the out of band ASE generated by the first EDFA to prevent saturation of the second EDFA.

Fiber Bragg gratings (FBGs) are chosen as BPFs for this experiment because of their narrow bandwidths. FBG operates by reflecting a narrowband of light centered around the Bragg wavelength. Therefore, optical circulators are needed to extract the

reflected signal from the gratings. Two FBGs with similar bandwidth are used to achieve better sideband rejection. The FBGs have full width half maximum (FWHM) bandwidths of 0.1, 0.2 and 0.4 nm. A general overview of FBGs and their characteristics are documented in Appendix A.17.

From equation (2.11), it can be seen that the ASE power is time independent. In reality, the ASE power does vary in time, which may be due to slight power fluctuation in the pump lasers. However, the variation is small and does not affect the PDF measurements of the spontaneous-spontaneous beat noise.

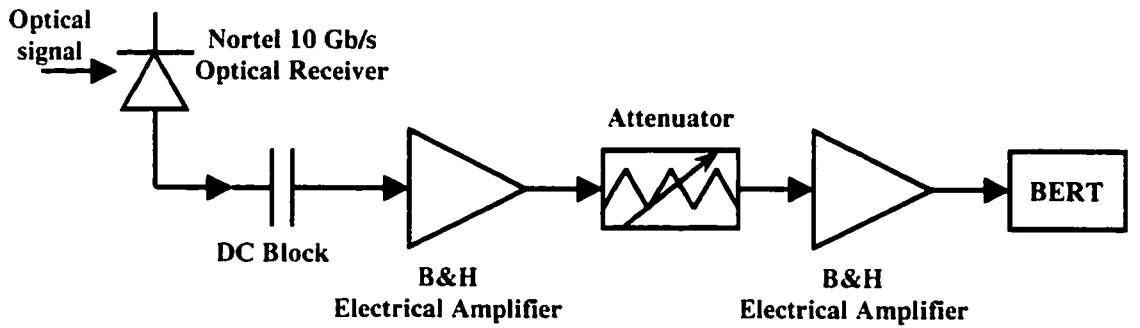


Figure 5.2: Schematic of the electrical components in the PDF measurement experiments.

The optical receiver used in the experiment is a prototype Nortel 10 Gb/s transimpedance receiver which has a responsivity of 0.7 A/W [32] and transimpedance gain of 392 Ω , as shown in Appendix A.20. The one-sided noise equivalent bandwidth of the receiver is 8 GHz. A DC block is connected at the output of the receiver to remove the DC signal level of the light carrier such that only the fluctuation caused by the noise is passed through. Two B&H electrical amplifiers are used to amplify the noise level and their frequency response is documented in Appendix A.21. The amplifiers have a bandwidth of 26 GHz, 23 dB gain and 7 dB noise figure. An attenuator is placed between the electrical amplifiers to prevent saturation of the second amplifier and to remain within the limits of the allowable input voltage of the bit error ratio tester (BERT) to prevent any damage.

The BERT consists of an error detector Hewlett Packard (HP) 70842, a pattern generator HP 70841A and a synthesized signal generator HP 70322A, as shown in Figure 5.3.

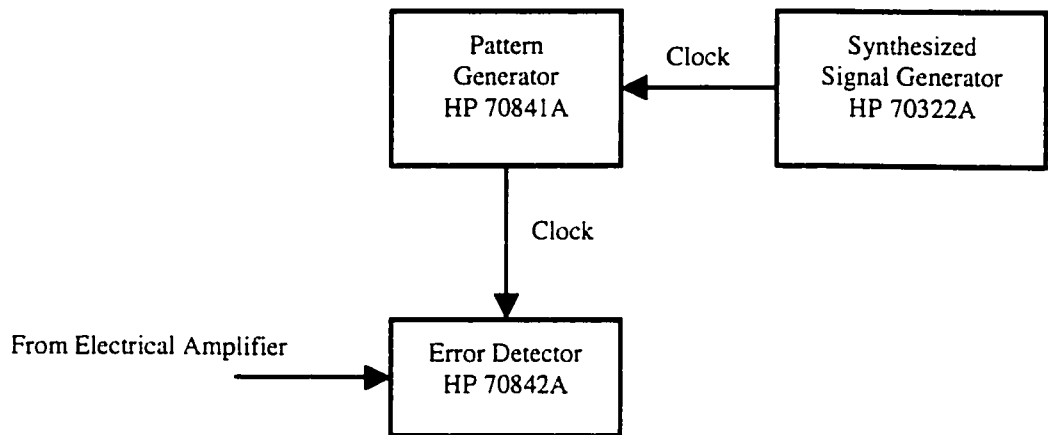


Figure 5.3: Components of the BERT.

The output of the second electrical amplifier is connected to the BERT and the amplified noise is sampled by the error detector. Since the laser power is not modulated, there are no binary digits and clock recovery circuit is not required. Therefore, the clock output of the pattern generator can be connected directly to the error detector and the clock frequency determines the sampling rate. The two-sided electrical bandwidth of the BERT is 7 GHz.

5.2. Threshold Detection of Noise

The following figure is an illustration of the method in which the PDFs are acquired.

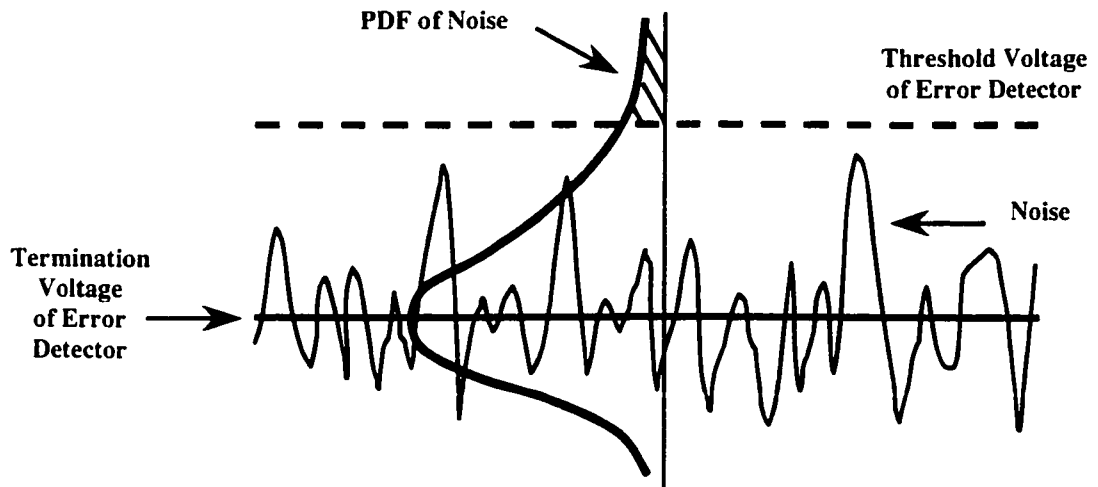


Figure 5.4: Threshold detection of noise.

The noise rides on the DC termination voltage of the error detector and a threshold voltage is applied to detect the noise. The termination voltage can be set to either -2 V or 0 V . The maximum and minimum input voltage of the error detector is 1 V and -4 V respectively. Therefore, a termination voltage of -2 V is used in the experiments since it is closer to the center of the voltages between 1 and -4 V . This ensures that there will be minimal distortion to the PDF measurement. However, there is a 20 mV internal offset in the error detector, thus the actual termination voltage is -1.98 V .

The threshold voltage of the error detector is set to manual so that it can be varied to measure the probability of error, P_e , at different threshold level. In the above figure, the voltage threshold is set above the termination voltage. The shaded area represents the probability of the noise voltage exceeding the threshold voltage. The peak of the PDF is riding on the termination voltage level of the error detector. When the threshold voltage is set higher than the termination voltage, the error detector is instructed to detect all logical zeros. Therefore, when the noise voltage is greater than the threshold voltage, an 'error' will be detected and the shaded area in Figure 5.4 represents the probability of error or BER. When the threshold voltage is moved towards the termination voltage, the shaded area will increase. The relationship between the PDF, $f(x)$, and the probability of error at the threshold voltage V_t can be shown as

$$P_e = \int_{V_t}^{\infty} f(x) dx. \quad (5.1)$$

Hence, the upper part of the PDF can be calculated using the following relation:

$$f(x) = \left| \frac{\partial P_e}{\partial x} \right| \cong \left| \frac{\Delta P_e}{\Delta x} \right|. \quad (5.2)$$

Similarly, when the threshold voltage is set below the termination voltage, the error detector is instructed to detect all logical ones and the lower part of the PDF can be determined using the above relations. However, the integration limits in equation (5.1) will be from $-\infty$ to V_t .

To measure the PDF, the threshold voltage is first set far above the termination voltage and the error detector is set to detect all logical zeros, so that the BER reading is less than 10^{-9} . When the threshold voltage is set, the gating function is enabled to start counting the errors at the sampling intervals. The cumulated error ratio is the ratio of total errors to total samples. The threshold voltage is then gradually decreased, moving towards the termination voltage. The minimum step voltage is 10 mV. After each adjustment, the gating function is restarted to measure the error ratio at the new threshold voltage. As the threshold voltage approaches the termination voltage of -1.98 V, the error ratio increases, since it is more likely that the noise voltage will exceed the threshold voltage. When the measurement at -1.98 V is taken, the threshold voltage is set to a voltage far below the termination voltage and the error detector is set to detect all logical ones, so that the BER reading is again less than 10^{-9} . The threshold voltage is then increased until the threshold voltage reaches -1.98 V again.

The values of the parameters in the PDF measurements are listed in the following table.

Symbol	Description	Value	Unit
λ	Wavelength of laser	1550.92	nm
T_k	Temperature	298	K
G_o	EDFA small signal gain	41.1	dB
\mathfrak{R}	Responsivity of p-i-n diode	0.70	A/W
R_L	Transimpedance of receiver	392	Ω
F	Noise figure of electrical amplifier	7	dB
m_t	Number of polarization mode	2	-
B_{elec}	Two-sided electrical bandwidth (BERT)	7	GHz
G_e	Net electrical gain	variable	dB
B_o	Noise equivalent optical bandwidth	variable	GHz

Table 5.1: Experimental parameters for the PDF measurements.

The electrical gain G_e is the total gain of the two electrical amplifiers minus the loss introduced by the attenuator.

5.3. Experimental Results of PDF Measurements

5.3.1 PDFs with 0.1 nm Fiber Bragg Gratings

FBGs #1 and 2 are used in the experimental setup shown in Figure 5.1. The measured noise equivalent optical bandwidth of cascading the two 0.1 nm FBGs is 16.41 GHz, which gives $M = 4.7$. When no signal power is present, the measured ASE power is -22.75 dBm. The net electrical gain provided by the two electrical amplifiers and the attenuator is 42 dB. The standard deviation of the thermal noise is measured to be 54.413 mV by using the histogram function on the HP 54120B Digitizing Oscilloscope Mainframe. Therefore, the variance of the thermal noise voltage is $2.961 \times 10^{-3} \text{ V}^2$. The measured ASE noise power and the thermal noise voltage variance are used to calculate the theoretical Gaussian and non-Gaussian PDFs for comparison with the experimental result. The Gaussian and non-Gaussian distributions are calculated using expressions (3.81) and (3.55), respectively.

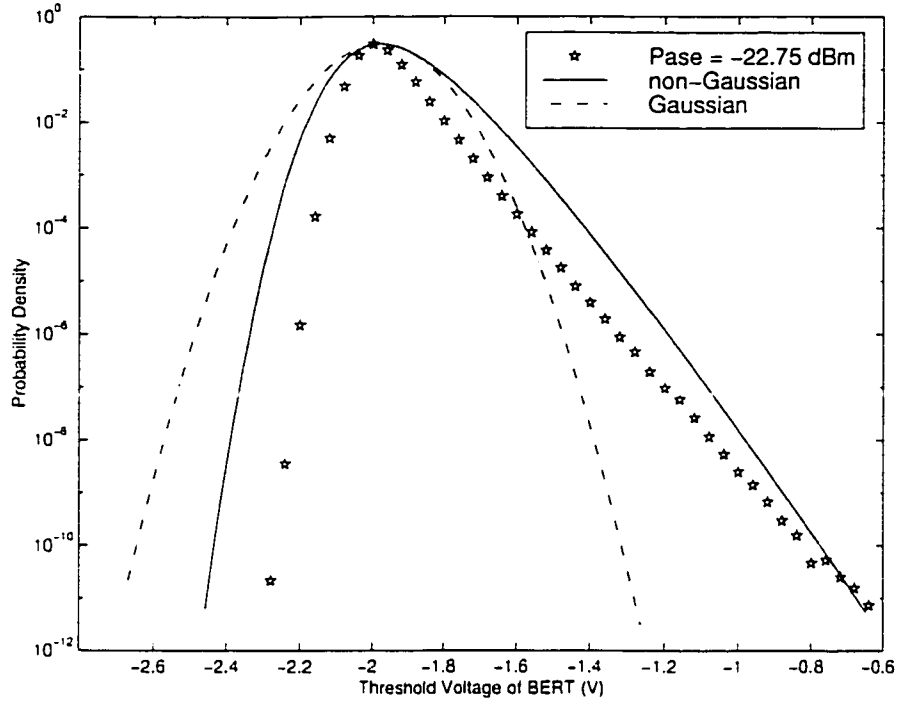


Figure 5.5: PDF of receiver noise for no signal power ($B_o = 16.41$ GHz).

Figure 5.5 shows the PDF of the receiver noise for no optical signal power. The dominant noise component is the spontaneous-spontaneous beat noise. Therefore, it is evident that the PDF for the spontaneous-spontaneous beat noise deviates a lot from the Gaussian distribution. Although the experimental data does not fit the non-Gaussian distribution perfectly, it does follow the general shape of the non-Gaussian PDF.

An input power of -51.5 dBm is used to represent the received power of not perfectly extinct logical zeros. The net electrical gain in both the experiment and simulation is 38 dB. The standard deviation of the thermal noise voltage is measured to be 34.608 mV, so the variance is $1.198 \times 10^{-3} \text{ V}^2$.

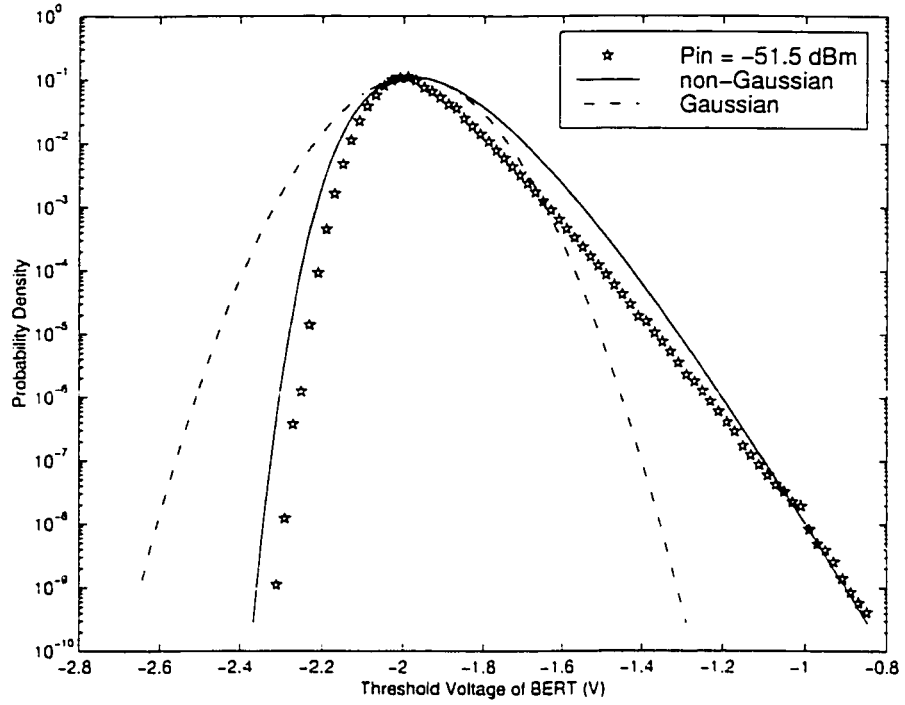


Figure 5.6: PDF of receiver noise for $P_{in} = -51.5$ dBm ($B_o = 16.41$ GHz).

The dominant noise component for the experimental PDF in Figure 5.6 is the spontaneous-spontaneous beat noise since the signal power is very low. The non-Gaussian PDF fits the experimental data reasonably well. The low signal power contributes to a small component of signal-spontaneous beat noise, which has a Gaussian distribution centered at the mean of the signal power. This contributes to the broadening of the experimental PDF around the mean. This phenomenon is clearly visible when comparing Figure 5.6 to Figure 5.5.

An input power of -36.5 dBm is used to represent the received power of logical ones. The net electrical gain in the experiment is 28 dB. The electrical gain used in the theoretical calculations is 27.5 dB. The measured standard deviation of the thermal noise voltage is 11.66 mV, so the variance is $1.360 \times 10^{-4} \text{ V}^2$.

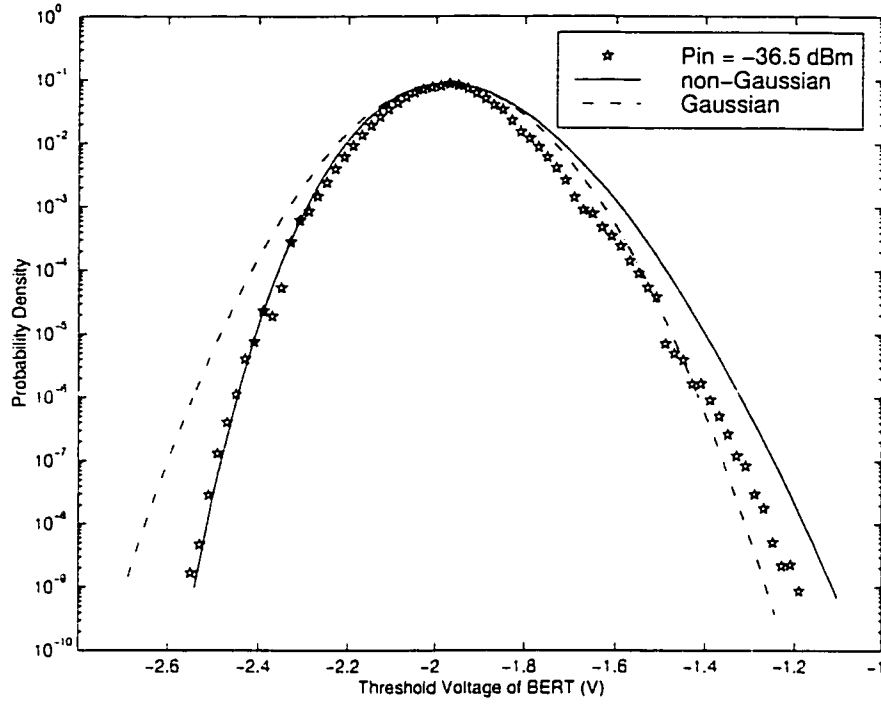


Figure 5.7: PDF of logical ones for $P_{in} = -36.5$ dBm ($B_o = 16.41$ GHz).

For large received power, the dominant noise component is the signal-spontaneous beat noise. Therefore, the difference between the Gaussian and non-Gaussian distribution is less prominent. As a result, the experimental PDF lies in between the Gaussian and non-Gaussian distributions, as shown in Figure 5.7.

5.3.2 PDFs with 0.2 nm Fiber Bragg Gratings

FBGs #3 and 4 are used in the experimental setup shown in Figure 5.1. The measured noise equivalent optical bandwidth for cascading the two 0.2 nm FBGs is 23.17 GHz, which gives $M = 6.6$. When no signal power is present, the measured ASE power is -16.87 dBm. The net electrical gain provided by the two electrical amplifiers and the attenuator is 31 dB. The electrical gain used in the theoretical comparisons is 29.5 dB. The standard deviation of the thermal noise is measured to be 15.846 mV. Therefore, the variance of the thermal noise voltage is $2.511 \times 10^{-4} \text{ V}^2$.

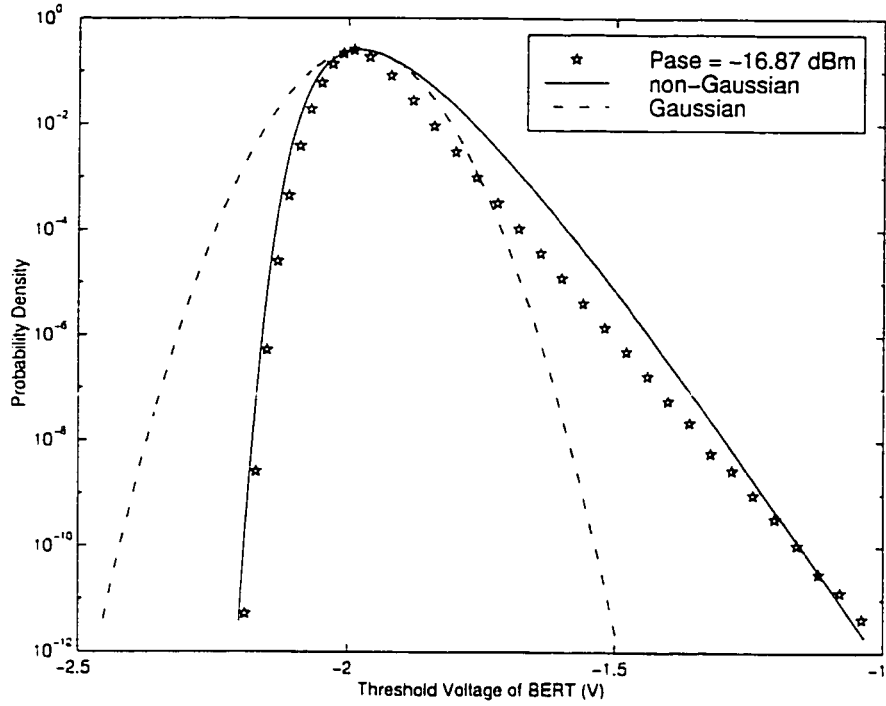


Figure 5.8: PDF of receiver noise for no signal power ($B_o = 23.17$ GHz).

Figure 5.8 shows the PDF of the receiver noise for no optical power. The dominant noise component is the spontaneous-spontaneous beat noise. It is evident that the PDF of the spontaneous-spontaneous beat noise is closer to the shape of the non-Gaussian distribution and deviates a lot from the Gaussian distribution.

An input power of -50.0 dBm is used to represent the received power of not perfectly extinct logical zeros. The net electrical gain in the experiment is 29 dB. The net electrical gain used in the theoretical calculations is 26 dB. The standard deviation of the thermal noise voltage is measured to be 13.662 mV, so the variance is $1.867 \times 10^{-4} \text{ V}^2$.

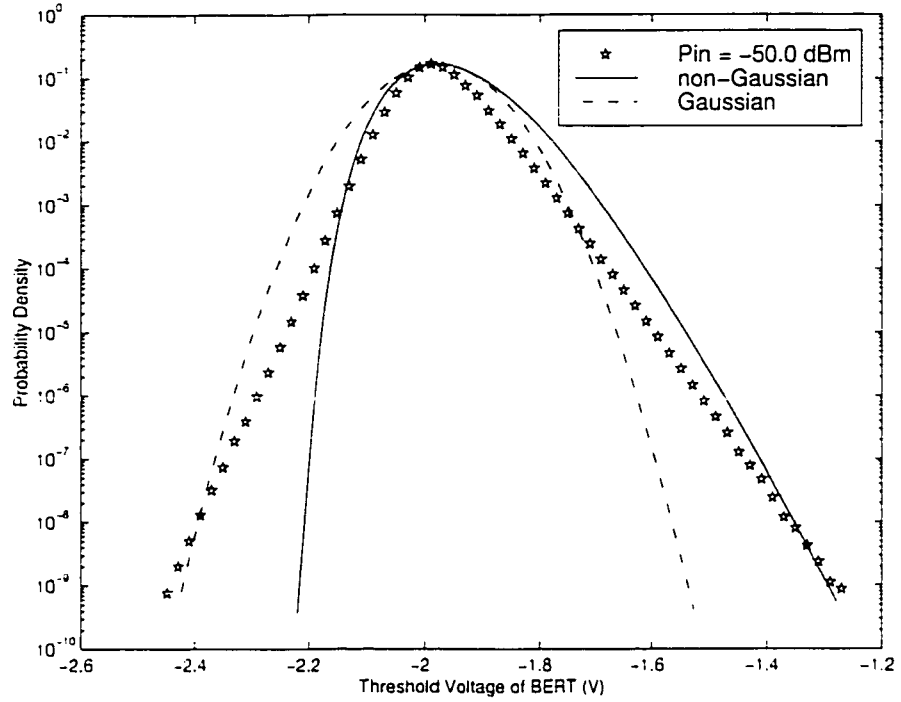


Figure 5.9: PDF of receiver noise for $P_{in} = -50.0$ dBm ($B_o = 23.17$ GHz).

The dominant noise component for the PDF in Figure 5.9 is the spontaneous-spontaneous beat noise since the signal power is very low. The tail on the right side of the experimental PDF is closer to the non-Gaussian PDF. However, the tail on the left side of the experimental PDF has widened and tends towards the Gaussian PDF.

An input power of -35.0 dBm is used to represent the received power of logical ones. The net electrical gain is 23 dB. The electrical gain used in the theoretical calculations is 19.5 dB. The measured standard deviation of the thermal noise voltage is 7.968 mV, so the variance is $6.349 \times 10^{-5} \text{ V}^2$.

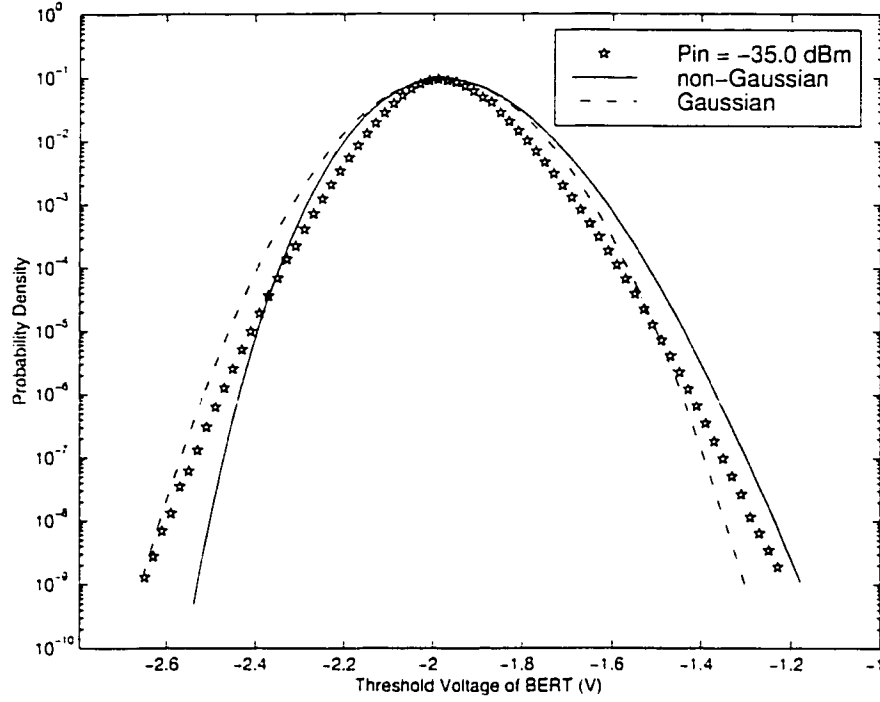


Figure 5.10: PDF of logical ones for $P_{in} = -35.0$ dBm ($B_o = 23.17$ GHz).

Figure 5.10 shows the experimental PDF for logical ones. For large received power, the dominant noise component is the signal-spontaneous beat noise. Therefore, the difference between the Gaussian and non-Gaussian distribution is less prominent. As a result, the experimental PDF lies in-between the Gaussian and non-Gaussian distributions.

5.3.3 PDFs with 0.4 nm Fiber Bragg Gratings

FBGs #5 and 6 are used in the experimental setup shown in Figure 5.1. The measured noise equivalent optical bandwidth for cascading the two 0.4 nm FBGs is 51.08 GHz, which gives $M = 14.6$. When no signal power is present, the measured ASE power is -13.90 dBm. The net electrical gain provided by the two electrical amplifiers and the attenuator is 33 dB. The electrical gain used in the theoretical comparisons is 27.5 dB. The standard deviation of the thermal noise is measured to be 16.362 mV. Therefore, the variance of the thermal noise voltage is $2.677 \times 10^{-4} \text{ V}^2$.

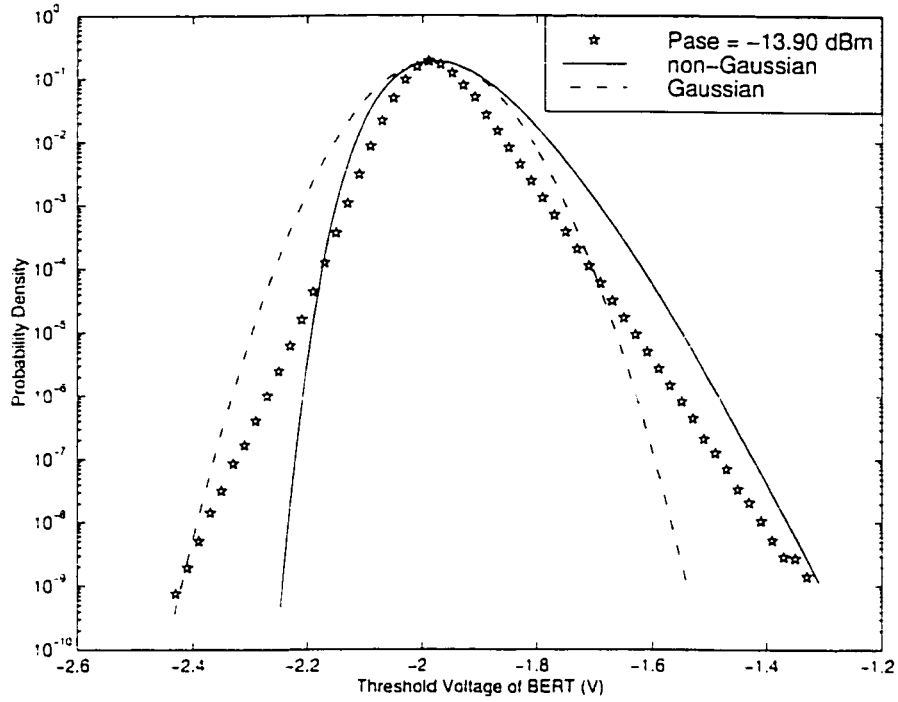


Figure 5.11: PDF of receiver noise for no signal power ($B_o = 51.08$ GHz).

Figure 5.11 shows the PDF of the receiver noise for no optical power. The dominant noise component is spontaneous-spontaneous beat noise. As the optical bandwidth increases, the tail on the left side of the distribution increasingly deviates away from the non-Gaussian PDF.

An input power of -52.5 dBm is used to represent the received power of not perfectly extinct logical zeros. The net electrical gain in the experiment is 30 dB. The net electrical gain used in the theoretical calculations is 24.5 dB. The standard deviation of the thermal noise voltage is measured to be 12.492 mV, so the variance is $1.561 \times 10^{-4} \text{ V}^2$.

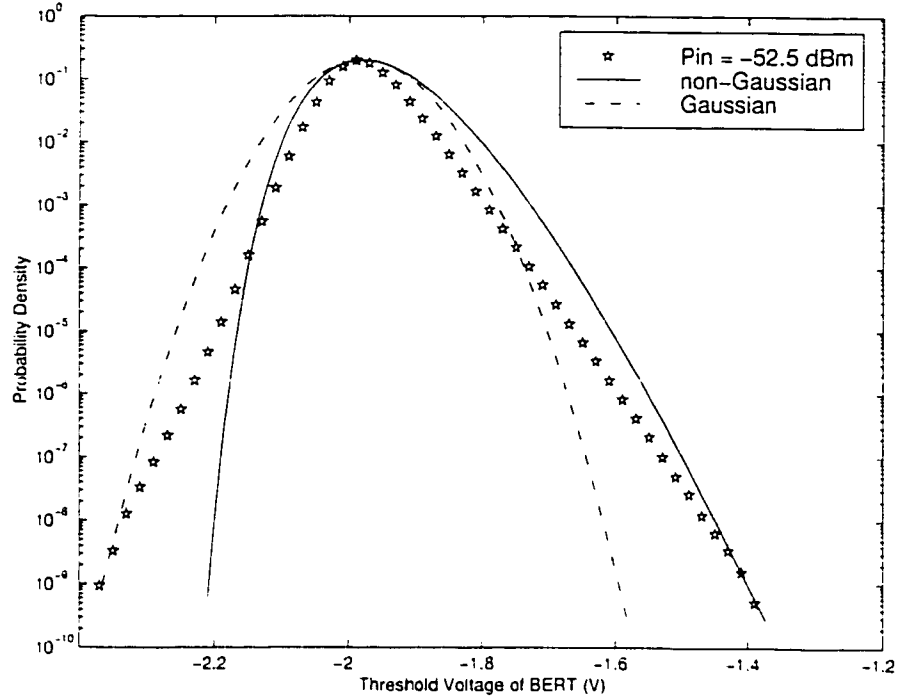


Figure 5.12: PDF of receiver noise for $P_{in} = -52.5$ dBm ($B_o = 51.08$ GHz).

The dominant noise component for the PDF in Figure 5.12 is the spontaneous-spontaneous beat noise since the signal power is very low. As the optical bandwidth increases, the tail on the left side of the distribution increasingly deviates away from the non-Gaussian PDF. Therefore, the experimental data does not fit well with either distribution. However, for PDF of logical zeros, the right tail of the distribution is more important than the left tail since the right tail intersects with the PDF of logical ones, which determines the optimum decision threshold. In this case, the right tail of the experimental PDF still agrees better with the non-Gaussian distribution.

An input power of -37.5 dBm is used to represent the received power of logical ones. The net electrical gain is 24 dB. The electrical gain used in the theoretical comparisons is 19 dB. The measured standard deviation of the thermal noise voltage is 7.595 mV, so the variance is $5.769 \times 10^{-5} \text{ V}^2$.

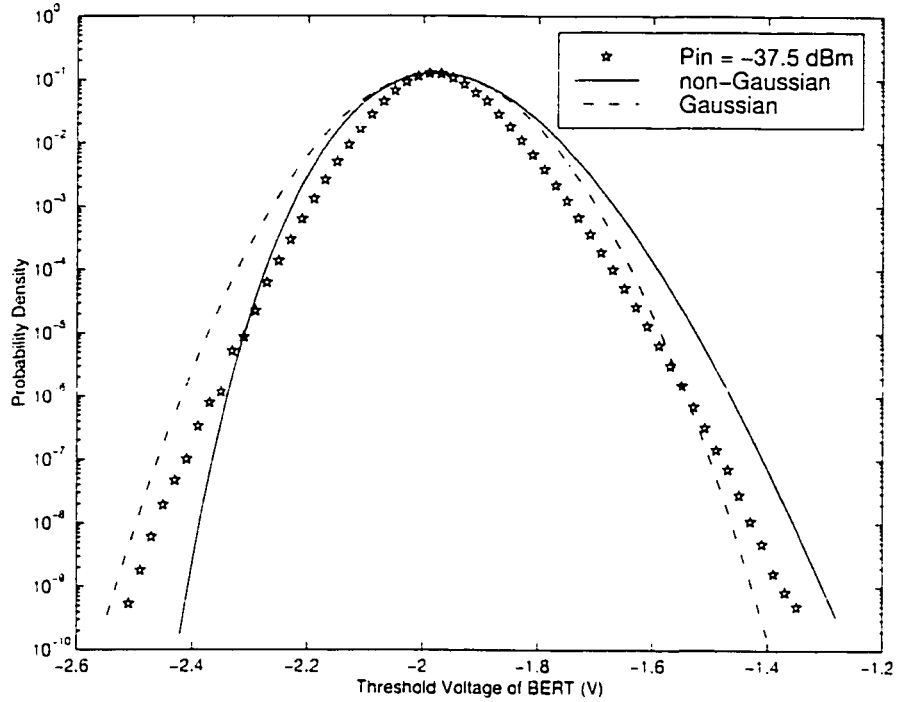


Figure 5.13: PDF of logical ones for $P_{in} = -37.5$ dBm ($B_o = 51.08$ GHz).

The experimental PDF for logical ones shown in Figure 5.13 stays almost the same as the experimental data in Figure 5.7 and Figure 5.10. Since the dominant noise component is the signal-spontaneous beat noise for large received power, the shape of the experimental distribution for logical ones does not change in any significant way as the optical bandwidth increases.

Notice that there is a mismatch between the electrical gain used in the experiments and the simulations. The difference between them increases as the optical bandwidth increases. This could be due to the fact that the frequency dependence of the p-i-n photodiode responsivity and the gain of the electrical amplifier are not accounted for in the theory.

5.4. Optimum Percentage Threshold Measurements

It has been shown in the previous chapter that the optimum percentage thresholds predicted by the non-Gaussian and Gaussian PDFs are very different from each other.

The following experiment is done to investigate the accuracy of the theoretical optimum percentage thresholds with comparison to experimental data.

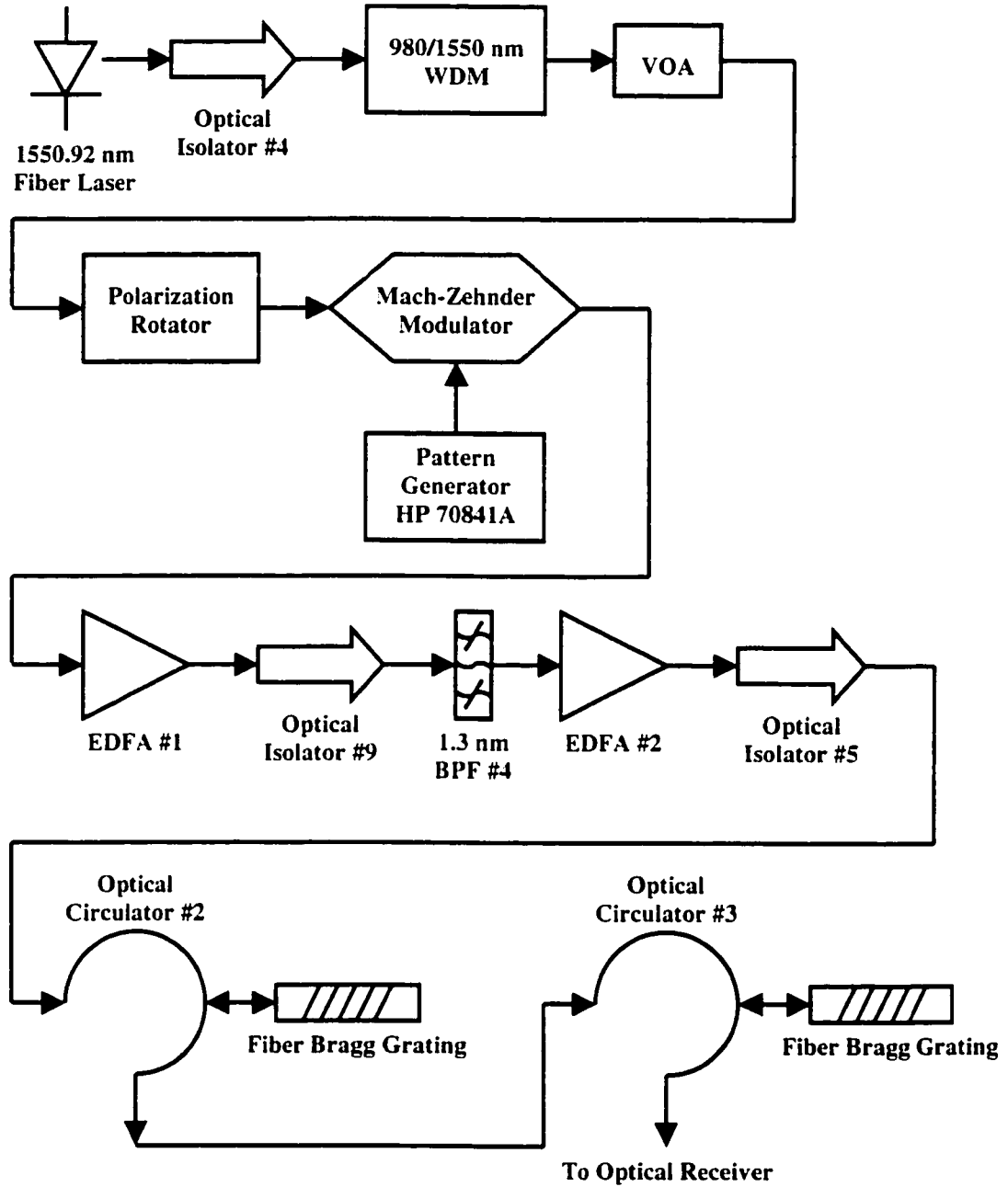


Figure 5.14: Schematic of the optical components for percentage threshold measurements.

The experimental setup for percentage threshold measurement is the same as the PDF measurement with the exception that a polarization rotator and a Mach-Zehnder (MZ) modulator are inserted between the VOA and EDFA #1. The MZ modulator is a

Lucent Technologies Lithium Niobate (LiNbO_3) electro-optic modulator. It is biased at 2.15 V and driven by a 3 GHz 2 V peak-to-peak square wave from the HP 70841A Pattern Generator to generate a binary 1010 sequence for modulating the laser light. The polarization rotator is used to line up the polarization of the laser light with that of the MZ modulator to maximize the extinction ratio.

The extinction ratio is measured as a DC parameter since the optical power meter cannot measure fast varying power. With no modulating signal, the DC bias voltage on the modulator is set to 1.15 V and the measured output power is the power level for logical ones. The DC bias voltage is then set to 3.15 V and the measured output power is the power level for logical zeros. The extinction ratio in the experiment is about -13.5 dB.

The setup of the electrical components and BERT is the same as before which is shown in Figure 5.2 and Figure 5.3. The net electrical gain in this experiment is not important since the optimum thresholds are converted to optimum percentage thresholds. The BERT is instructed to detect an infinite sequence of 1010... and the threshold voltage of the BERT is adjusted until the minimum BER is achieved. The mean values of the logical ones and zeros are measured using the histogram function on the HP 54120B Digitizing Oscilloscope Mainframe. The optimum percentage threshold is calculated using equation (4.1). The values of the parameters in the PDF measurements are listed in the following table.

Symbol	Description	Value	Unit
λ	Wavelength of laser	1550.92	nm
T_k	Temperature	298	K
ε	Extinction ratio	-13.5	dB
G_o	EDFA small signal gain	41.1	dB
\mathfrak{R}	Responsivity of p-i-n diode	0.70	A/W
R_L	Transimpedance of receiver	392	Ω
F	Noise figure of electrical amplifier	7	dB
m_t	Number of polarization mode	2	-
B_{elec}	Two-sided electrical bandwidth	7	GHz
B_o	Noise equivalent optical bandwidth	variable	GHz

Table 5.2: Experimental parameters for optimum percentage threshold measurements.

5.4.1 BER as a Function of Received Power

The BER at different average received power is obtained experimentally and compared with the theoretical curves. The theoretical BER values are calculated using equation (3.89).

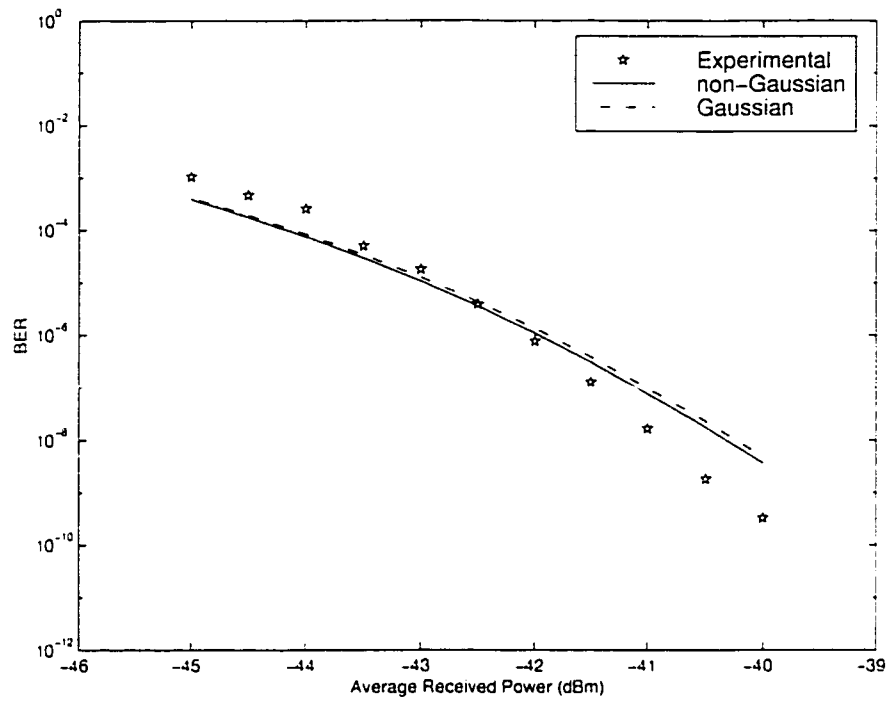


Figure 5.15: BER as a function of received power for $B_0 = 16.41$ GHz.

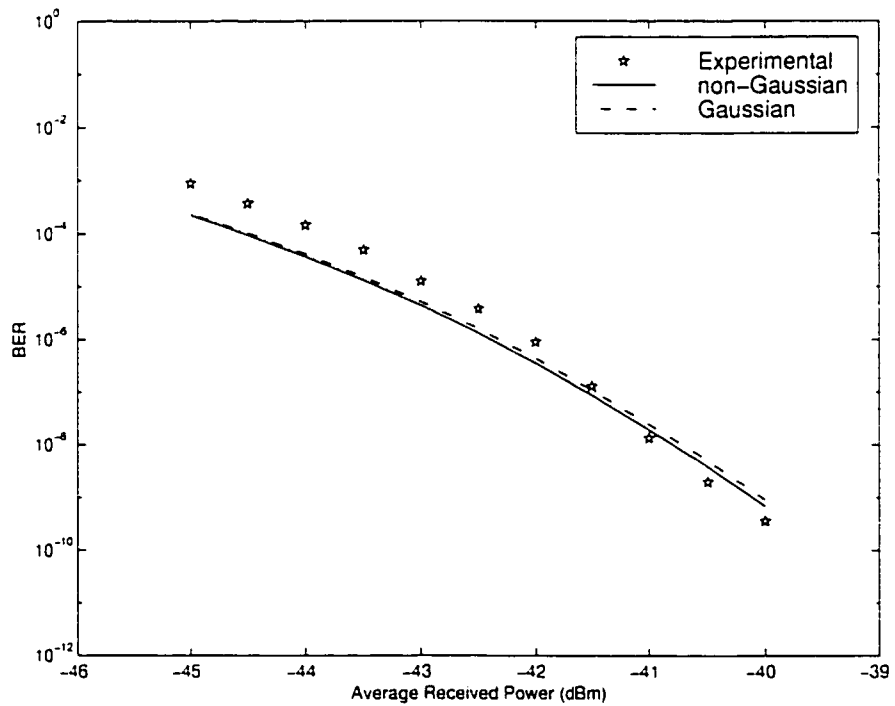


Figure 5.16: BER as a function of received power for $B_0 = 23.17$ GHz.

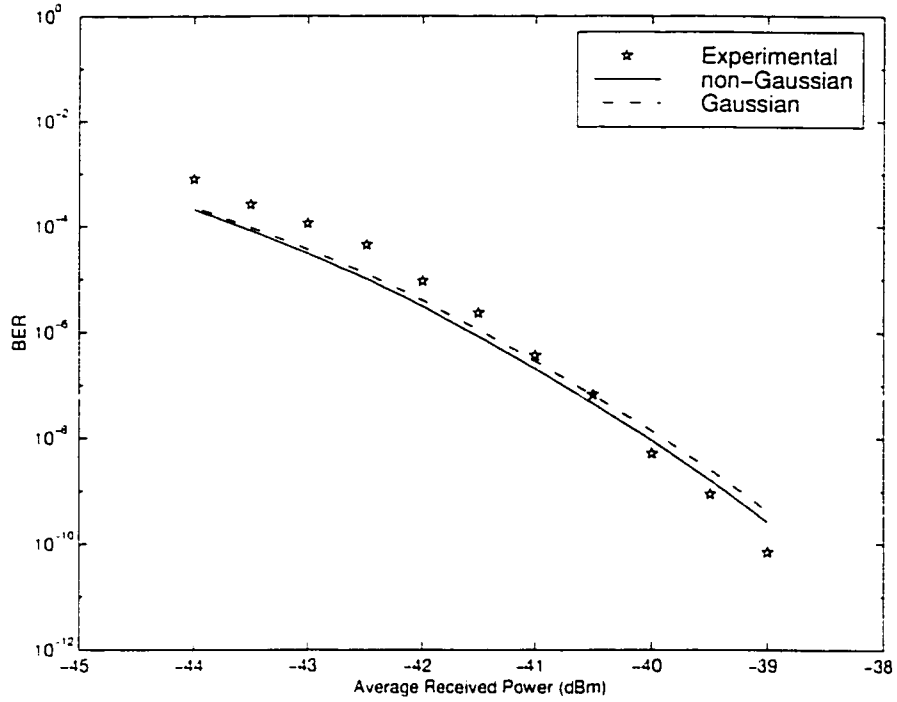


Figure 5.17: BER as a function of received power for $B_0 = 51.08$ GHz.

From Figure 5.15 to Figure 5.17, it can be seen that the experimental BER is close to the values predicted by both Gaussian and non-Gaussian theories. However, for increasing received power, the BER predicted by the Gaussian and non-Gaussian theories is progressively worse than the experimental values.

5.4.2 Optimum Percentage Threshold

The optimum percentage threshold is plotted against the average received power in Figure 5.18 to Figure 5.20. Since the smallest threshold voltage step size of the BERT is 10 mV and the smallest difference between the means of logical ones and zeros is in the order of 300 mV, the 10 mV step size does not provide a fine enough resolution for a smooth experimental curve. Hence, a linear curve is fitted to the experimental data. The theoretical Gaussian and non-Gaussian curves are also calculated for comparison by solving equation (3.92) and using equation (4.1).

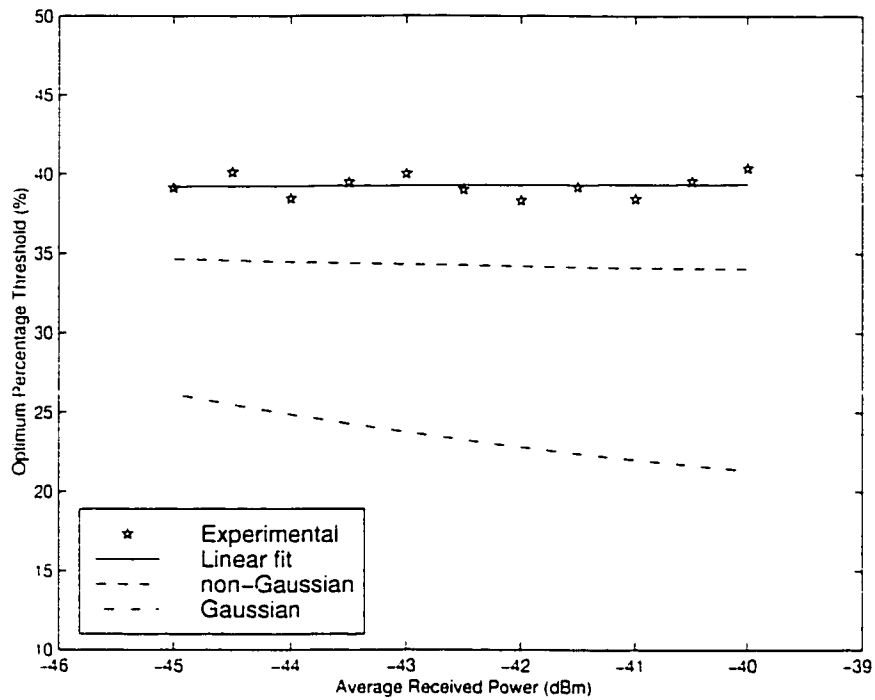


Figure 5.18: Optimum percentage threshold for $B_0 = 16.41$ GHz.

Figure 5.18 shows the optimum percentage threshold for $B_0 = 16.41$ GHz. The difference between the experimental data and the non-Gaussian optimum threshold ranges from 4.6 to 5.3 %, whereas for the Gaussian optimum threshold, the difference ranges from 13 to 18 %.

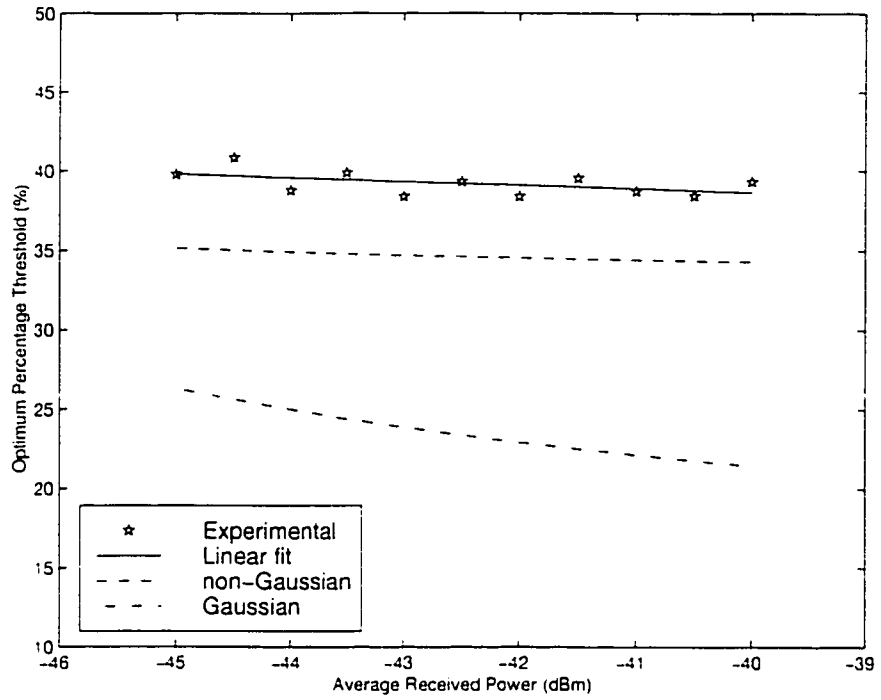


Figure 5.19: Optimum percentage threshold for $B_0 = 23.17$ GHz.

Figure 5.19 shows the optimum percentage threshold for $B_0 = 23.17$ GHz. The difference between the experimental data and the non-Gaussian optimum threshold ranges from 4.4 to 4.7 %, whereas for the Gaussian optimum threshold, the difference ranges from 13.5 to 17.2 %.

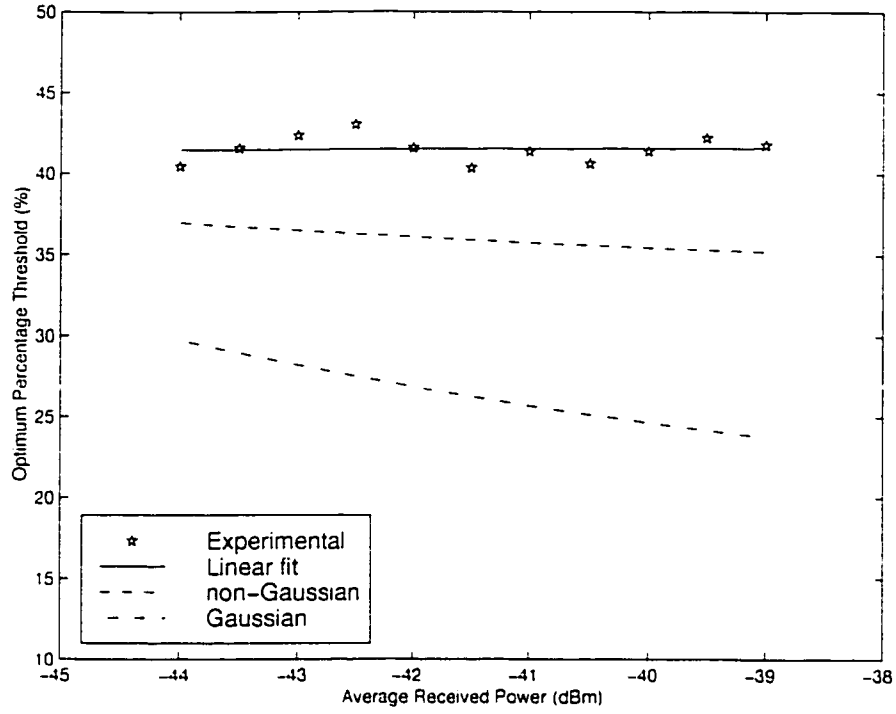


Figure 5.20: Optimum percentage threshold for $B_o = 51.08$ GHz.

Figure 5.20 shows the optimum percentage threshold for $B_o = 51.08$ GHz. The difference between the experimental data and the non-Gaussian optimum threshold ranges from 4.5 to 6.4 %, whereas for the Gaussian optimum threshold, the difference ranges from 11.7 to 17.8 %.

It is clear that the non-Gaussian distribution yielded optimum percentage thresholds which are much closer to the experimental data. The difference is around 5 %. Both the optimum percentage thresholds obtained experimentally and from the non-Gaussian theory stay fairly constant in the range of received power from -39 to -45 dBm. On the other hand, the optimum percentage thresholds predicted by the Gaussian distribution vary over a larger range. The difference between the experimental results and the Gaussian theory lies between 12 and 18 %.

The theoretical curves for BER versus received power are plotted in the following three figures using the optimum percentage thresholds obtained in the experiment. The

purpose of these figures is to compare how well the Gaussian and non-Gaussian theories predict the BER performance when the optimum percentage thresholds are known.

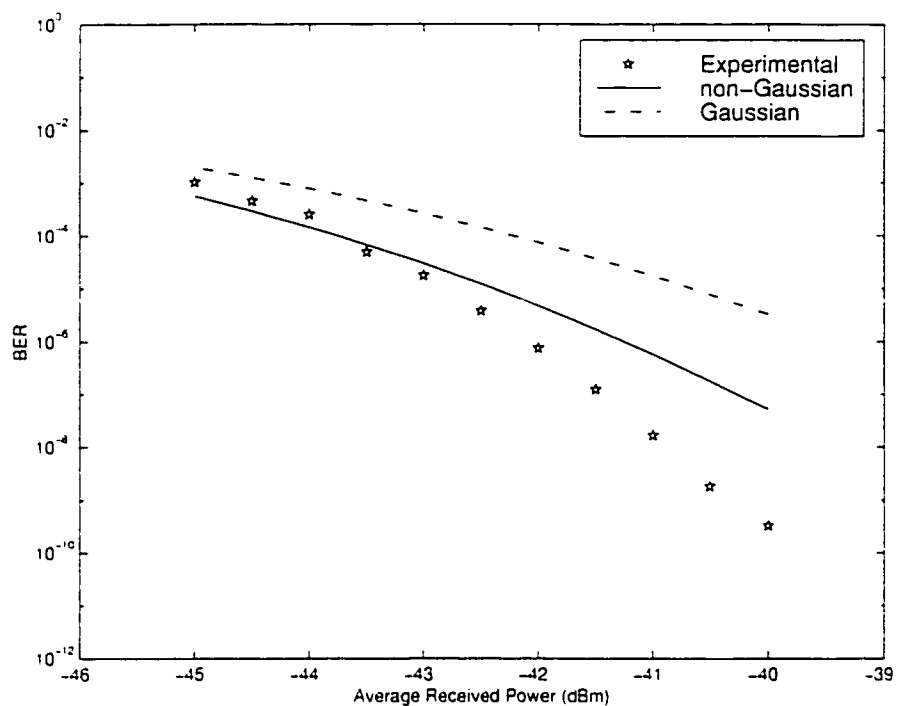


Figure 5.21: BER for $B_0 = 16.41$ GHz.

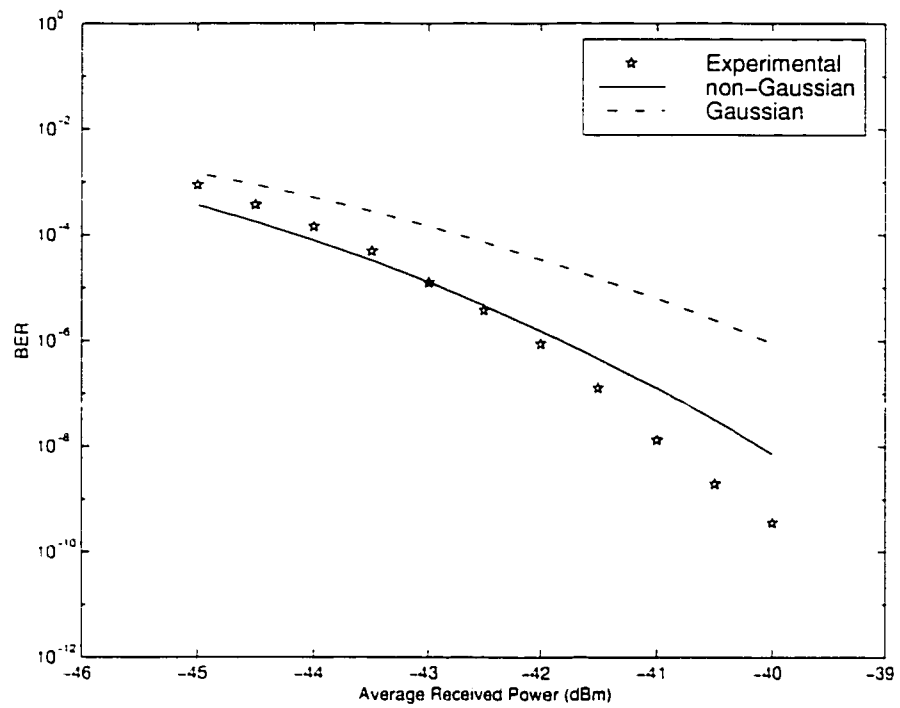


Figure 5.22: BER for $B_0 = 23.17$ GHz.

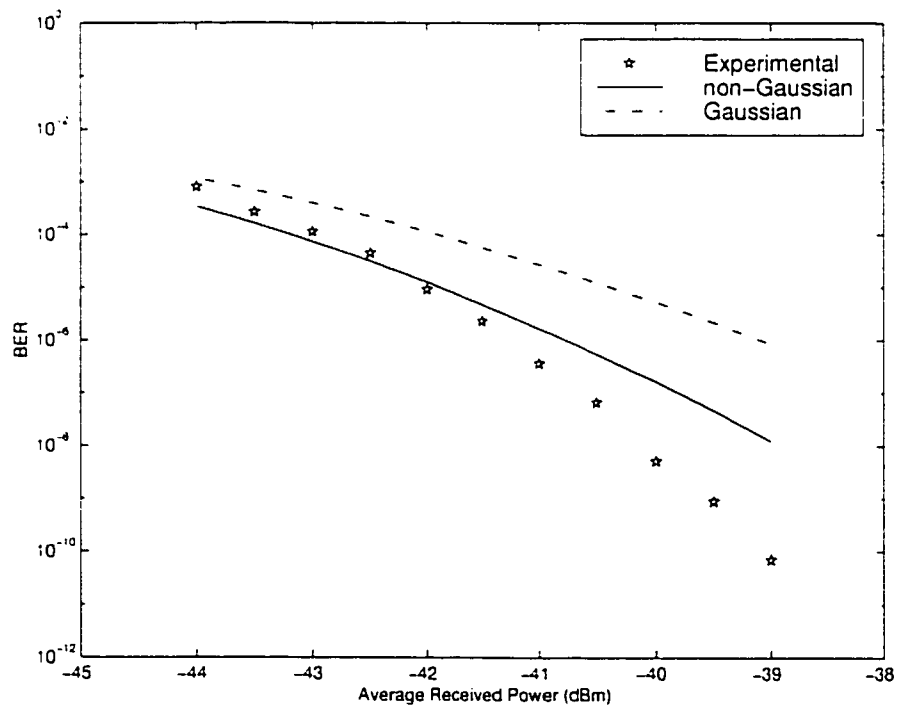


Figure 5.23: BER for $B_0 = 51.08$ GHz.

From Figure 5.21 to Figure 5.23, it can be seen that the BER predicted by the non-Gaussian distribution is closer to the experimental results. However, as the received power increases, both distributions increasingly deviate from the experimental values. Therefore, even when the optimum percentage threshold is known, neither the Gaussian nor the non-Gaussian distribution provides accurate BER analysis.

Chapter 6. Conclusion

In Chapter 2, an overview of the EDFAs and its model has been presented. The gain mechanism in EDFA and the generation of ASE noise are discussed. The various EDFA pumping schemes are presented and their impact on the noise figure is shown. Some recent developments in the area of EDFA gain extension are also presented.

In Chapter 3, the theoretical derivation and analysis of the noise theory proposed by Marcuse is presented. The derivation for the widely used Gaussian approximation is also shown. When the Gaussian thermal and shot noise components are neglected, the theory yields the central chi-square distribution for perfectly extinct logical zeros and non-central chi-square distribution for logical ones. When the ratio of optical to electrical bandwidth decreases, the chi-square distribution will approach the Gaussian distribution. However, when the ratio of optical to electrical bandwidth increases, the noise distribution becomes increasingly non-Gaussian. The theory has been adapted to experimental work by performing current-to-voltage conversion.

In Chapter 4, the simulation results of the PDFs, BER, receiver sensitivity and optimum decision threshold are presented. For logical ones or high received power, the difference between the Gaussian and non-Gaussian distribution is relatively small when compared to the non-Gaussian PDF of logical zeros. This is due to the large signal-spontaneous beat noise component. When the optical bandwidth decreases, the shape of the non-Gaussian distribution for logical ones stays fairly similar. This is because a change in the optical filter bandwidth does not change the signal-spontaneous beat noise provided that all the frequency components of the signal spectrum pass through the optical filter.

For logical zeros, the difference between the Gaussian and non-Gaussian distributions becomes apparent when the system has large EDFA small signal gain and the ratio of optical to electrical bandwidth is small. This is because under these conditions, the ASE generated beat noises are dominant. The simulations show that the

PDFs generated by the Gaussian and non-Gaussian theories are significantly different, with the non-Gaussian PDF tending towards the chi-square distribution. The difference is greater when the optical bandwidth decreases.

For the BER and receiver sensitivity analysis, the difference between the Gaussian and non-Gaussian theories is negligible. This is because the optimum decision threshold has been considered separately for both distributions. The impact of the non-Gaussian distribution on the system shows up in the optimum decision threshold analysis. The optimum percentage decision threshold predicted by the Gaussian distribution is significantly lower than that of the non-Gaussian distribution. The difference increases with decreasing value of M . If the optimum decision threshold is known, the Gaussian and non-Gaussian distribution produce very different results for the BER and sensitivity analysis.

The experimental setups and results have been presented in Chapter 5. The PDFs for logical ones and zeros have been measured experimentally using the threshold noise detection method for different optical bandwidths. For zero or low input signal power as in the case of logical zeros, the dominant noise component is the spontaneous-spontaneous beat noise and the PDF is closer to the non-Gaussian distribution when the optical bandwidth is small. As the optical bandwidth increases, the left tail of the spontaneous-spontaneous beat noise PDF shifts towards the Gaussian distribution. For high input signal power as in the case of logical ones, the dominant noise component is the signal-spontaneous beat noise. The PDF assumes a more Gaussian shape due to the large signal component. The shape of the PDF for logical ones stays fairly constant when the value of M decreases.

There is a discrepancy between the electrical gain used in the experiment and the simulation. The difference between the two cases increases as the optical bandwidth increases. This may be due to the fact that the theory does not account for the frequency dependence of the p-i-n photodiode responsivity and the gain of the electrical amplifier.

The optimum percentage thresholds have been measured for different optical bandwidths. It is evident that the non-Gaussian distribution predicted optimum percentage thresholds which are much closer to the experimental data compared to the Gaussian distribution. BER calculated using the Gaussian and non-Gaussian distributions are very similar but they only provide a loose fit to the experimentally measured BER. However, when the optimum percentage threshold is known, neither the Gaussian nor the non-Gaussian distribution provides accurate BER analysis.

Therefore, the non-Gaussian theory proposed by Marcuse does provide a more accurate prediction of the optimum decision threshold relative to the Gaussian distribution. However, it does not provide an accurate estimation of the BER performance using the known decision threshold.

6.1. Future Work

It is preferable that the effects of ISI and the electrical filter response can be incorporated into future experimental work for a more complete analysis of the ASE noise behavior at detection. For long haul high-speed fiber transmission systems employing EDFAs, high optical power is required to achieve adequate SNR. However, when high signal power travels a very long distance in a fiber, nonlinear interaction between the signal and the fiber can occur. The major nonlinear effects are self-phase modulation, cross-phase modulation, four-wave mixing and stimulated Raman scattering [34]. These effects can severely degrade system performance and their impact on the ASE noise is not well understood. It will be of interest to study the influence of the nonlinear effects on the behavior of the ASE noise since the modern fiber transmission system relies heavily on EDFA.

References

1. J. Freeman, *Theory, Design, and Characterization of Erbium-Doped Fiber Amplifier*, M.Sc. dissertation, Department of Electrical Engineering, University of Alberta, Edmonton, Alberta, 1991.
2. P. C. Becker, N. A. Olsson and J. R. Simpson, *Erbium-Doped Fiber Amplifiers: Fundamentals and Technology*, San Diego: Academic Press, 1999.
3. O. Gautheron, J. B. Leroy and P. Marmier, "32 x 10 Gb/s transmission over 6150 km with a 50 GHz wavelength spacing", *Optical Fiber Communication Conference*, San Diego, 1999.
4. B. Chan, *Statistical Properties of Erbium Doped Fiber Amplifiers*, M.Sc. dissertation, Department of Electrical and Computer Engineering, University of Alberta, Edmonton, Alberta, 1995.
5. P. I. Richards, *Manual of Mathematical Physics*, London: Pergamon Press Ltd., 1959.
6. F. Abramovich and P. Bayvel, "Some statistical remarks on the derivation of BER in amplified optical communication systems", *Transactions on Communications*, vol. 45, no. 9, pp. 1032-1034, 1997.
7. P. Dennery and A. Krzywicki, *Mathematics for Physicists*, New York: Harper & Row, 1967.
8. D. Marcuse, "Derivation of analytical expressions for the bit-error probability in lightwave systems with optical amplifiers", *Journal of Lightwave Technology*, vol. 8, no. 12, pp. 1816-1823, 1990.
9. D. Marcure, "Calculation of bit-error probability for a lightwave system with optical amplifiers and post-detection Gaussian noise", *Journal of Lightwave Technology*, vol. 9, no. 4, pp. 505-513, 1991.
10. W. J. Miniscalco, "Erbium-doped glasses for fiber amplifiers at 1500 nm", *Journal of Lightwave Technology*, vol. 9, no. 2, pp. 234-250, 1991.
11. E. Desurvire, *Erbium-Doped Fiber Amplifier: Principles and Applications*, New York: Wiley, 1994.
12. F. Di Pasquale, G. Grasso, F. Meli, G. Sacchi and S. Turolla, "23 dBm output power Er/Yb co-doped fiber amplifier for WDM signals in the 1575-1605 nm wavelength region", *Optical Fiber Communication Conference*, San Diego, 1999.
13. C. R. Giles and E. Desurvire, "Propagation of signal and noise in concatenated erbium-doped fiber optical amplifiers", *Journal of Lightwave Technology*, vol. 9, no. 2, pp. 147-154, 1991.
14. J. Freeman and J. Conradi, "Gain modulation response of erbium-doped fiber amplifiers", *Photonics Technology Letters*, vol. 5, no. 2, pp. 224-226, 1993.

15. M. Yamada, A. Mori, K. Kobayashi, H. Ono, T. Kanamori, K. Oikawa, Y. Nishida and Y. Ohishi, "Gain-flattened tellurite-based EDFA with a flat amplification bandwidth of 76 nm", *Optical Fiber Communication Conference*, Post Deadline Paper, 1998.
16. J. H. Lee, U. C. Ryu and N. Park, "Improvement of 1.57-1.61 μm band amplification efficiency by recycling wasted backward ASE through the unpumped EDF section", *Optical Fiber Communication Conference*, San Diego, 1999.
17. M. J. Yadlowsky, "Ultra broadband optical amplifiers", *Optical Fiber Communication Conference*, San Diego, 1999.
18. J. Kani, K. Hattori, M. Jinno, S. Aisawa, T. Sakamoto and K. Oguchi, "Trinal-wavelength-band WDM transmission over dispersion-shifted fiber", *Optical Fiber Communication Conference*, San Diego, 1999.
19. A. Zemel and M. Gallant, "Current-voltage characteristics of metalorganic chemical vapor deposition InP/InGaAs p-i-n photodiodes: The influence of finite dimensions and heterointerfaces", *Journal of Applied Physics*, vol. 64, no. 11, pp. 6552-6561, 1988.
20. A. Leon-Garcia, *Probability and Random Processes for Electrical Engineering* 2nd Ed. Reading, Massachusetts: Addison-Wesley, 1994.
21. J. G. Proakis, *Digital Communications* 3rd Ed. New York: McGraw-Hill, 1995.
22. Y. Jaluria, *Computer Methods for Engineering*, Boston: Allyn and Bacon, 1988.
23. N. A. Olsson, "Lightwave systems with optical amplifiers", *Journal of Lightwave Technology*, vol. 7, no. 7, pp. 1071-1082, 1989.
24. L. G. Kazovsky and O. K. Tonguz, "Sensitivity of direct-detection lightwave receivers using optical preamplifiers", *Photonics Technology Letters*, vol.3, no. 1, pp. 53-55, 1991.
25. R. C. Steele, G. R. Walker and N. G. Walker, "Sensitivity of optically preamplified receivers with optical filtering", *Photonics Technology Letters*, vol. 3, no. 6, pp. 545-547, 1991.
26. P. A. Humblet and M. Azizoglu, "On the bit error rate of lightwave systems with optical amplifiers", *Journal of Lightwave Technology*, vol. 9, no. 11, pp. 1576-1582, 1991.
27. L. F. B. Ribeiro, J. R. F. Da Rocha and J. L. Pinto, "Performance evaluation of EDFA preamplified receivers taking into account intersymbol interference", *Journal of Lightwave Technology*, vol. 13, no. 2, pp. 225-232, 1995.
28. Y. Yamamoto, "Noise and error rate performance of semiconductor laser amplifier in PCM-IM optical transmission systems", *Journal of Quantum Electronics*, vol. QE-16, no. 10, pp. 1073-1081, 1980.

29. P. Diamant and M. C. Teich, "Evolution of the statistical properties of photons passed through a traveling-wave laser amplifier", *Journal of Quantum Electronics*, vol. 28, no. 5, pp. 1325-1334, 1992.
30. T. Li and M. C. Teich, "Photon point process for traveling-wave laser amplifiers", *Journal of Quantum Electronics*, vol. 29, no. 9, pp. 2568-2578, 1993.
31. S. S. Walklin, *Multilevel Signaling for Increasing the Capacity of High Speed Optical Communication Systems*, Ph.D. dissertation, Department of Electrical and Computer Engineering, University of Alberta, Edmonton, Alberta, 1997.
32. C. Kan, *Computer Simulation Modules for Modeling the Transmission of Wavelength-Division-Multiplexed Optical Signals in a Single Mode Fiber*, TRILabs, Edmonton, Alberta, 1998.

Appendix A Derivation of the Probability Generating Function

The decision random variable due to the photocurrent is given by

$$y_{ph} = 2K \sum_{v=1}^{v_2} \left[|E_v|^2 + c_{rv}^2 + c_{iv}^2 + 2|E_v|(c_{rv} \cos \theta_v + c_{iv} \sin \theta_v) \right]. \quad (\text{A.1})$$

The PGF is the bilateral Laplace transform of the PDF as given by

$$G_{ph}(s) = \int_{-\infty}^{\infty} f_Y(y_{ph}) e^{-sy_{ph}} dy_{ph} \quad (\text{A.2})$$

$$= \langle \exp(-sy_{ph}) \rangle \quad (\text{A.3})$$

$$= \exp \left(-2Ks \sum_{v=1}^{v_2} |E_v|^2 \right) \prod_{v=1}^{v_2} \left(\exp \left[-2Ks(2|E_v|c_{rv} \cos \theta_v + c_{rv}^2) \right] \right) \cdot \left(\exp \left[-2Ks(2|E_v|c_{iv} \sin \theta_v + c_{iv}^2) \right] \right). \quad (\text{A.4})$$

Since c_{rv} and c_{iv} are Gaussian random variables, the terms containing c_{rv} and c_{iv} can be evaluated using the zero mean Gaussian PDF with variance σ_c^2 :

$$\begin{aligned} & \langle \exp \left[-2Ks(2|E_v|c_{rv} \cos \theta_v + c_{rv}^2) \right] \rangle \\ &= \frac{1}{\sqrt{2\pi\sigma_c^2}} \int_{-\infty}^{\infty} \exp \left(\frac{-c_{rv}^2}{2\sigma_c^2} \right) \exp \left[-2Ks(2|E_v|c_{rv} \cos \theta_v + c_{rv}^2) \right] dc_{rv} \end{aligned} \quad (\text{A.5})$$

$$= \frac{1}{\sqrt{2\pi\sigma_c^2}} \int_{-\infty}^{\infty} \exp \left[\left(\frac{-4K\sigma_c^2 s - 1}{2\sigma_c^2} \right) c_{rv}^2 - 4Ks|E_v|c_{rv} \cos \theta_v \right] dc_{rv} \quad (\text{A.6})$$

$$\begin{aligned} &= \frac{\exp \left(\frac{8K^2\sigma_c^2 s^2 |E_v|^2 \cos^2 \theta_v}{4K\sigma_c^2 s + 1} \right)}{\sqrt{2\pi\sigma_c^2}} \\ & \cdot \int_{-\infty}^{\infty} \exp \left[- \left(\frac{4K\sigma_c^2 s + 1}{2\sigma_c^2} \right) \left(c_{rv} + \frac{4K\sigma_c^2 s |E_v| \cos \theta_v}{4K\sigma_c^2 s + 1} \right)^2 \right] dc_{rv} \end{aligned} \quad (\text{A.7})$$

$$= \frac{1}{\sqrt{4K\sigma_c^2 s + 1}} \exp \left(\frac{8K^2\sigma_c^2 s^2 |E_v|^2 \cos^2 \theta_v}{4K\sigma_c^2 s + 1} \right), \quad (\text{A.8})$$

where

$$\begin{aligned}
& \frac{1}{\sqrt{2\pi\sigma_c^2}} \int_{-\infty}^{\infty} \exp \left[- \left(\frac{4K\sigma_c^2 s + 1}{2\sigma_c^2} \right) \left(c_{rv} + \frac{4K\sigma_c^2 s |E_v| \cos \theta_v}{4K\sigma_c^2 s + 1} \right)^2 \right] dc_{rv} \\
&= \frac{1}{\sqrt{4K\sigma_c^2 s + 1}}
\end{aligned} \tag{A.9}$$

is evaluated using the Gauss integral [7]. Similarly,

$$\begin{aligned}
& \left\langle \exp \left[- 2Ks \left(2|E_v| c_{iv} \sin \theta_v + c_{iv}^2 \right) \right] \right\rangle \\
&= \frac{1}{\sqrt{4K\sigma_c^2 s + 1}} \exp \left(\frac{8K^2 \sigma_c^2 s^2 |E_v|^2 \sin^2 \theta_v}{4K\sigma_c^2 s + 1} \right).
\end{aligned} \tag{A.10}$$

Therefore, the PGF due to the photocurrent can be written as

$$G_{ph}(s) = \frac{1}{(4K\sigma_c^2 s + 1)^M} \exp \left(\frac{-2Ks \sum_{v=1}^{V^2} |E_v|^2}{4K\sigma_c^2 s + 1} \right). \tag{A.11}$$

Appendix B Matlab Programs

B.1. Power of Noise Components

```
% This program calculates all the noise components in the receiver

clear all
q = 1.60e-19;      % electronic charge (C)
extinc = 10^(-20/10); % extinction ratio
probl = .5; % probability of 1
prob0 = 1 - probl; % probability of 0
Nsp = 2; % spontaneous emission factor of EDFA
Go = 10^(35/10); % small signal power gain of EDFA

muin = 1; % EDFA input coupling efficiency
muout = 1; % EDFA output coupling efficiency
L = 1; % transmission efficiency between EDFA & receiver
net_eff = muout*L; % net transmission efficiency
R = 0.83; % responsivity of optical receiver (A/W)

mt = 2; % number of polarization mode
Bo = 20e9; % noise equivalent optical bandwidth (Hz)
Belec = 20e9; % 2 sided electrical bandwidth (Hz)
M = mt*Bo/Belec;

PinavedBm = [-44:-32]; % average input power (dBm)
Pinave = muin.*(10.^(PinavedBm./10)).*1e-3; % average input power (W)
Pinl = Pinave./(probl + prob0*extinc); % power at the EDFA input for 1 (W)
Pin0 = extinc.*Pinl; % power at the EDFA input for 0 (W)

for z = 1:length(PinavedBm)
    var_thermal(z) = thermal_noise(Belec); % variance of thermal noise (A^2)
    G = gain(Go,Pinave(z)); % EDFA gain
    Pout0 = net_eff*G*Pin0(z); % incident power at PIN diode for 0 (W)
    Poutl = net_eff*G*Pinl(z); % incident power at PIN diode for 1 (W)
    Pase = ase_pwr(net_eff,mt,Nsp,G,Bo); % power of amplified spontaneous emission (W)

    I0 = R*Pout0; % signal current for 0 (A)
    I1 = R*Poutl; % signal current for 1 (A)
    Iase = R*Pase; % ASE noise current (A)

    var_sig0_shot(z) = q*I0*Belec; % variance of signal shot noise for 0 (A^2)
    var_sig1_shot(z) = q*I1*Belec; % variance of signal shot noise for 1 (A^2)
    var_sp_shot(z) = q*Iase*Belec; % variance of spontaneous shot noise (A^2)

    % variances of signal-spontaneous beat noises for 0 and 1 (A^2)
    var_sig0_sp(z) = 2*I0*Iase/M;
```

```

var_sig1_sp(z) = 2*I1*Iase/M;

var_sp_sp(z) = (Iase^2)/M;    % variance of spontaneous-spontaneous
beat noise (A^2)
end

colordef none
whitebg('w')
semilogy(PinavedBm,var_sig1_sp,'k^-',PinavedBm,var_sig0_sp,'kv-
',PinavedBm,var_sp_sp,'ks-',PinavedBm,var_thermal,'kp-
',PinavedBm,var_sig1_shot,'k>-',PinavedBm,var_sig0_shot,'k<-
',PinavedBm,var_sp_shot,'ko-')
axis([-50 -32 1e-15 1e-7])
xlabel('Average Received Power (dBm)')
ylabel('Noise Power (A^2)')

legend('signal-spontaneous beat noise for one','signal-spontaneous beat
noise for zero','spontaneous-spontaneous beat noise','thermal
noise','signal shot noise for one','signal shot noise for zero','ASE
shot noise',-1)

```

B.2. Probability Density Functions

% This program calculates the PDF

```

clear all
extinc = 10^(-20/10);    % extinction ratio
prob1 = .5; % probability of 1
prob0 = 1 - prob1;      % probability of 0
Nsp = 2;    % spontaneous emission factor of EDFA
Go = 10^(30/10);    % small signal power gain of EDFA

muin = 1;    % EDFA input coupling efficiency
muout = 1;   % EDFA output coupling efficiency
L = 1;       % transmission efficiency between EDFA & receiver
net_eff = muout*L;    % net transmission efficiency
R = 0.83;    % responsivity of optical receiver (A/W)

mt = 2;      % number of modes
Bo = 20e9;   % optical bandwidth (Hz)
Belec = 20e9;    % 2 sided electrical bandwidth (Hz)
M = mt*Bo/Belec;

var_thermal = thermal_noise(Belec); % variance of thermal noise (A^2)

PinavedBm = -35; % average power at the EDFA input (dBm)
Pinave = muin*(10^(PinavedBm/10))*1e-3; % average input power (W)
Pin1 = Pinave/(prob1 + prob0*extinc); % power at the EDFA input for
1 (W)
Pin0 = extinc*Pin1; % power at the EDFA input for 0 (W)

G = gain(Go,Pinave); % EDFA gain
Pout0 = net_eff*G*Pin0; % incident power at PIN diode for 0 (W)
Pout1 = net_eff*G*Pin1; % incident power at PIN diode for 1 (W)

```

```

Pase = ase_pwr(net_eff,mt,Nsp,G,Bo);      % power of amplified
spontaneous emission (W)

I = [-2e-3:1e-6:6e-3];

for z = 1:length(I)
    [I0,var_shot0] = mean_var(R,Pout0,Pase,Belec); % mean current (A) and
    variance (A^2) for 0
    [I1,var_shot1] = mean_var(R,Pout1,Pase,Belec); % mean current (A) and
    variance (A^2) for 1

    pdf0_c(z) = pdf_chi(M,R,Pase,Pout0,var_thermal,var_shot0,I(z));
    pdf1_c(z) = pdf_chi(M,R,Pase,Pout1,var_thermal,var_shot1,I(z));

    pdf0_g(z) = pdf_gauss(M,R,Pase,Pout0,var_thermal,var_shot0,I0,I(z));
    pdf1_g(z) = pdf_gauss(M,R,Pase,Pout1,var_thermal,var_shot1,I1,I(z));
end

pdf0_c = pdf0_c/sum(pdf0_c);
pdf1_c = pdf1_c/sum(pdf1_c);
pdf0_g = pdf0_g/sum(pdf0_g);
pdf1_g = pdf1_g/sum(pdf1_g);

colordef none
whitebg('w')
semilogy(I,pdf0_c,'k-',I,pdf0_g,'k-.',I,pdf1_c,'k-',I,pdf1_g,'k-.')
axis([-1e-3 1e-1 1])
xlabel('Time Average Current (A)')
ylabel('Probability Density')
legend('non-Gaussian','Gaussian',4)
text(5e-4,2e-2,'one')
text(-1e-4,2e-1,'zero')

```

B.3. Non-Gaussian Probability Density Function

```

function pdf = pdf_chi(M,R,Pase,Pout,var_thermal,var_shot,Id)

% This program calculates the non-Gaussian PDF
% M = ratio of optical to two sided electrical bandwidth
% R = reponsivity of PIN receiver
% Pase = ASE power (W)
% Pout = incident power at detector (W)
% var_thermal = variance of thermal noise (A^2)
% var_shot = variance of shot noise (A^2)
% Id = current (A)

A = R*Pout;
B = (R*Pase)/M;
C = (var_thermal + var_shot)/2;

Gdlc1 = 1; % 1st coefficient for the polynomial G'(u)=0
Gdlc2 = Id*B/(2*C) - 1; % 2nd coefficient for the polynomial G'(u)=0
Gdlc3 = -M*(B^2)/(2*C); % 3rd coefficient for the polynomial G'(u)=0
Gdlc4 = -A*B/(2*C); % 4th coefficient for the polynomial G'(u)=0

```

```

Gd1 = [Gd1c1 Gd1c2 Gd1c3 Gd1c4]; % G'(u)
Gdlroot = roots(Gd1); % solve for roots of G'(u)=0
u = Gdlroot(find(Gdlroot>0)); % find positive roots, the saddle point
Gd2 = (2*A/B)/(u^3) + M/(u^2) + 2*C/(B^2); % G''(u)
G = -A*(u-1)/(B*u) + (C/B^2)*(u-1)^2 + (Id/B)*(u-1) - M*log(u); %
generating function G(u)
pdf = exp(G)/(B*sqrt(2*pi*Gd2)); % probability density function

```

B.4. Gaussian Probability Density Function

```

function pdf_g = pdf_gauss(M,R,Pase,Pout,var_thermal,var_shot,Im,I)

% This program calculates the Gaussian PDF
% M = ratio of optical to two sided electrical bandwidth
% R = reponsivity of PIN receiver
% Pase = ASE power (W)
% Pout = incident power at detector (W)
% var_thermal = variance of thermal noise (A^2)
% var_shot = variance of shot noise (A^2)
% Im = mean current (A)
% I = instantaneous current (A)

var = (((R*Pase)^2) + 2*(R^2)*Pase*Pout)/M + var_thermal + var_shot;
% variance
pdf_g = (1/sqrt(2*pi*var)) * exp(-((I-Im)^2)/(2*var));

```

B.5. Receiver Sensitivity

```

function [sens_c,sens_g] =
sensitivity(M,mt,Bo,Belec,extinc,Nsp,Go,ber,incre_c,incre_g,sens)

% This program calculates the receiver sensitivities for the Gaussian
and non-Gaussian distributions
% M = ratio of optical to electrical bandwidth
% mt = number of polarization modes
% Bo = optical bandwidth (Hz)
% Belec = two sided electrical bandwidth (Hz)
% extinc = extinction ratio
% Nsp = spontaneous emission factor of EDFA
% Go = small signal gain of EDFA
% ber = required BER
% incre_c = multiplication constant for the average input power of the
non-Gaussian distribution
% incre_g = multiplication constant for the average input power of the
Gaussian distribution
% sens = starting point of average EDFA input power (dBm)

probl = .5; % probability of 1
prob0 = 1 - probl; % probability of 0

muin = 1; % EDFA input coupling efficiency
muout = 1; % EDFA output coupling efficiency

```

```

L = 1;          % transmission efficiency between EDFA & receiver
net_eff = muout*L;          % net transmission efficiency
R = 0.83;      % responsivity of optical receiver (A/W)
var_thermal = thermal_noise(Belec); % variance of thermal noise (A^2)

dif = 1e-3; % required minimum percentage difference

sens_c = sens; % sensitivity for non-Gaussian distribution (dBm)
delta = 1; % percentage difference
while abs(delta) > dif,
    Pinave = muin*(10^(sens_c/10))*1e-3; % average input power (W)
    Pinl = Pinave/(probl + prob0*extinc); % power at the EDFA input for
1 (W)
    Pin0 = extinc*Pinl; % power at the EDFA input for 0 (W)

    G = gain(Go,Pinave); % EDFA gain
    Pout0 = net_eff*G*Pin0; % incident power at PIN diode for 0 (W)
    Poutl = net_eff*G*Pinl; % incident power at PIN diode for 1 (W)
    Pase = ase_pwr(net_eff,mt,Nsp,G,Bo); % power of amplified
spontaneous emission (W)

    [I0,var_shot0] = mean_var(R,Pout0,Pase,Belec); % mean current (A) and
variance (A^2) for 0
    [I1,var_shot1] = mean_var(R,Poutl,Pase,Belec); % mean current (A) and
variance (A^2) for 1

    Id =
opt_thres_chi(M,prob0,probl,R,Pase,Pout0,Poutl,I0,I1,var_thermal,var_sh
ot0,var_shot1);
    P0 = prob_err_chi(M,R,Pase,Pout0,var_thermal,var_shot0,Id,0);
    P1 = prob_err_chi(M,R,Pase,Poutl,var_thermal,var_shot1,Id,1);
    ber_c = prob0*P0 + probl*P1; % BER for non-Gaussian distribution
    delta = 1 - ber_c/ber; % percentage difference
    sens_c = sens_c + incre_c*log10(ber_c/ber); % increment sensitivity
for non-Gaussian distribution (dBm)
end

sens_g = sens; % sensitivity for Gaussian distribution (dBm)
delta = 1; % percentage difference
ber_g = 1;
while abs(delta) > dif,
while abs(delta) > dif & ber_g > ber,
    Pinave = muin*(10^(sens_g/10))*1e-3; % average input power (W)
    Pinl = Pinave/(probl + prob0*extinc); % power at the EDFA input for
1 (W)
    Pin0 = extinc*Pinl; % power at the EDFA input for 0 (W)

    G = gain(Go,Pinave); % EDFA gain
    Pout0 = net_eff*G*Pin0; % incident power at PIN diode for 0 (W)
    Poutl = net_eff*G*Pinl; % incident power at PIN diode for 1 (W)
    Pase = ase_pwr(net_eff,mt,Nsp,G,Bo); % power of amplified
spontaneous emission (W)

    [I0,var_shot0] = mean_var(R,Pout0,Pase,Belec); % mean current (A) and
variance (A^2) for 0
    [I1,var_shot1] = mean_var(R,Poutl,Pase,Belec); % mean current (A) and
variance (A^2) for 1

```

```

    Idg =
    opt_thres_chi(M,prob0,prob1,R,Pase,Pout0,Pout1,I0,I1,var_thermal,var_sh
ot0,var_shot1);
    %Idg =
    opt_thres_gauss(M,prob0,prob1,R,Pase,Pout0,Pout1,I0,I1,var_thermal,var_
shot0,var_shot1);
    P0g = prob_err_gauss(M,R,Pase,Pout0,I0,var_thermal,var_shot0,Idg,0);
    P1g = prob_err_gauss(M,R,Pase,Pout1,I1,var_thermal,var_shot1,Idg,1);
    ber_g = prob0*P0g + prob1*P1g;      % BER for Gaussian distribution
    delta = 1 - ber_g/ber; % percentage difference
    sens_g = sens_g + incre_g*log10(ber_g/ber); % increment sensitivity
    for Gaussian distribution (dBm)
end

```

B.6. Non-Gaussian Optimum Decision Threshold

```

function Id =
opt_thres_chi(M,prob0,prob1,R,Pase,Pout0,Pout1,I0,I1,var_thermal,var_sh
ot0,var_shot1)

% This program calculates the non-Gaussian optimum decision threshold
% M = ratio of optical to two sided electrical bandwidth
% prob0 = probability of 0
% prob1 = probability of 1
% R = reponsivity of PIN receiver
% Pase = ASE power (W)
% Pout0 = incident power at detector for 0 (W)
% Pout1 = incident power at detector for 1 (W)
% I0 = current for 0 (A)
% I1 = current for 1 (A)
% var_thermal = variance of thermal noise (A^2)
% var_shot0 = variance of shot noise for 0 (A^2)
% var_shot1 = variance of shot noise for 1 (A^2)

% solve for the optimum decision threshold using the bisection method
Id0 = I0; % current for zero (A)
Id1 = I1; % current for one (A)

eps = 1e-20; % maximum absolute error
Int = Id1 - Id0; % starting interval containing the root
n = ceil(log10(Int/eps)/log10(2) - 1); % number of iterations

A0 = R*Pout0;
B0 = (R*Pase)/M;
C0 = (var_thermal + var_shot0)/2;
G0dlc1 = 1; % 1st coefficient for the polynomial G0'(u)=0
G0dlc3 = -M*(B0^2)/(2*C0); % 3rd coefficient for the polynomial
G0'(u)=0
G0dlc4 = -A0*B0/(2*C0); % 4th coefficient for the polynomial G0'(u)=0

A1 = R*Pout1;
B1 = (R*Pase)/M;
C1 = (var_thermal + var_shot1)/2;

```

```

Gldlc1 = 1; % 1st coefficient for the polynomial G1'(u) = 0
Gldlc3 = -M*(B1^2)/(2*C1); % 3rd coefficient for the polynomial
G1'(u)=0
Gldlc4 = -A1*B1/(2*C1); % 4th coefficient for the polynomial G1'(u)=0

for b = 1:n
    Id = (Id0+Id1)/2;

    G0dlc2 = Id*B0/(2*C0) - 1;
    G0dl = [G0dlc1 G0dlc2 G0dlc3 G0dlc4]; % G0'(u)
    G0dlroot = roots(G0dl); % solve for roots of G0'(u)=0
    u0 = G0dlroot(find(G0dlroot>0)); % find positive roots the saddle
point
    G0d2 = (2*A0/B0)/(u0^3) + M/(u0^2) + 2*C0/(B0^2); % G0''(u)
    G0 = -A0*(u0-1)/(B0*u0) + (C0/B0^2)*(u0-1)^2 + (Id/B0)*(u0-1) -
M*log(u0); % G0(u)
    f0 = exp(G0)/(B0*sqrt(2*pi*G0d2)); % f0

    Gldlc2 = Id*B1/(2*C1) - 1;
    Gldl = [Gldlc1 Gldlc2 Gldlc3 Gldlc4]; % G1'(u)
    Gldlroot = roots(Gldl); % solve for roots of G1'(u)=0
    u1 = Gldlroot(find(Gldlroot>0)); % the saddle point
    Gld2 = (2*A1/B1)/(u1^3) + M/(u1^2) + 2*C1/(B1^2); % G1''(u)
    G1 = -A1*(u1-1)/(B1*u1) + (C1/B1^2)*(u1-1)^2 + (Id/B1)*(u1-1) -
M*log(u1); % G1(u)
    f1 = exp(G1)/(B1*sqrt(2*pi*Gld2)); % f1

    FId = 1 - (f1*probl)/(f0*prob0);

    G0dlc2 = Id0*B0/(2*C0) - 1;
    G0dl = [G0dlc1 G0dlc2 G0dlc3 G0dlc4]; % G0'(u)
    G0dlroot = roots(G0dl); % solve for roots of G0'(u)=0
    u0 = G0dlroot(find(G0dlroot>0)); % the saddle point
    G0d2 = (2*A0/B0)/(u0^3) + M/(u0^2) + 2*C0/(B0^2); % G0''(u)
    G0 = -A0*(u0-1)/(B0*u0) + (C0/B0^2)*(u0-1)^2 + (Id0/B0)*(u0-1) -
M*log(u0); % G0(u)
    f0 = exp(G0)/(B0*sqrt(2*pi*G0d2)); % f0

    Gldlc2 = Id0*B1/(2*C1) - 1;
    Gldl = [Gldlc1 Gldlc2 Gldlc3 Gldlc4]; % G1'(u)
    Gldlroot = roots(Gldl); % solve for roots of G1'(u)=0
    u1 = Gldlroot(find(Gldlroot>0)); % the saddle point
    Gld2 = (2*A1/B1)/(u1^3) + M/(u1^2) + 2*C1/(B1^2); % G1''(u)
    G1 = -A1*(u1-1)/(B1*u1) + (C1/B1^2)*(u1-1)^2 + (Id0/B1)*(u1-1) -
M*log(u1); % G1(u)
    f1 = exp(G1)/(B1*sqrt(2*pi*Gld2)); % f1

    FId0 = 1 - (f1*probl)/(f0*prob0);

    if FId*FId0 < 0
        Id1 = Id;
    else
        Id0 = Id;
    end
end
end

```


B.7. Gaussian Optimum Decision Threshold

```
function Idg =  
opt_thres_gauss(M,prob0,prob1,R,Pase,Pout0,Pout1,I0,I1,var_thermal,var_  
shot0,var_shot1)  
  
% This program calculates the Gaussian optimum decision threshold  
% M = ratio of optical to two sided electrical bandwidth  
% prob0 = probability of 0  
% prob1 = probability of 1  
% R = reponsivity of PIN receiver (A/W)  
% Pase = ASE power (W)  
% Pout0 = incident power at detector for 0 (W)  
% Pout1 = incident power at detector for 1 (W)  
% I0 = current for 0 (A)  
% I1 = current for 1 (A)  
% var_thermal = variance of thermal noise (A^2)  
% var_shot0 = variance of shot noise for 0 (A^2)  
% var_shot1 = variance of shot noise for 1 (A^2)  
  
var0 = (((R*Pase)^2) + 2*(R^2)*Pase*Pout0)/M + var_thermal + var_shot0;  
    % variance of zero  
var1 = (((R*Pase)^2) + 2*(R^2)*Pase*Pout1)/M + var_thermal + var_shot1;  
    % variance of one  
  
A = var1 - var0; % coefficients of prob1*f1-prob0*f0=0  
B = 2*(var0*I1 - var1*I0);  
C = var1*(I0^2) - var0*(I1^2) +  
var1*var0*log(var0*(prob1^2)/(var1*(prob0^2)));  
  
Idgroot = roots([A B C]);  
Idg = Idgroot(find(Idgroot>I0)); % Gaussian approximation of optimum  
threshold  
  
%Idg = (sqrt(var0)*I1 + sqrt(var1)*I0)/(sqrt(var0)+sqrt(var1)); %  
Gaussian approximation of optimum threshold
```

B.8. Non-Gaussian Probability of Error

```
function Pe = prob_err_chi(M,R,Pase,Pout,var_thermal,var_shot,Id,logic)  
  
% This program calculates the non-Gaussian probability of error  
% M = ratio of optical to two sided electrical bandwidth  
% R = reponsivity of PIN receiver  
% Pase = ASE power (W)  
% Pout = incident power at detector (W)  
% var_thermal = variance of thermal noise (A^2)  
% var_shot = variance of shot noise (A^2)  
% Id = optimum decision threshold (A)  
% logic = 0 or 1  
  
A = R*Pout;  
B = (R*Pase)/M;  
C = (var_thermal + var_shot)/2;
```

```

Gdlc1 = 1; % 1st coefficient for the polynomial G'(u)=0
Gdlc2 = Id*B/(2*C) - 1; % 2nd coefficient for the polynomial G'(u)=0
Gdlc3 = -M*(B^2)/(2*C); % 3rd coefficient for the polynomial G'(u)=0
Gdlc4 = -A*B/(2*C); % 4th coefficient for the polynomial G'(u)=0
Gdl = [Gdlc1 Gdlc2 Gdlc3 Gdlc4]; % G'(u)
Gdlroot = roots(Gdl); % solve for roots of G'(u)=0
u = Gdlroot(find(Gdlroot>0)); % find positive roots, the saddle point
Gd2 = (2*A/B)/(u^3) + M/(u^2) + 2*C/(B^2); % G''(u)
G = -A*(u-1)/(B*u) + (C/B^2)*(u-1)^2 + (Id/B)*(u-1) - M*log(u); %
generating function G(u)
f = exp(G)/(B*sqrt(2*pi*Gd2)); % probability density function

S = G + .5*log(Gd2*B); % substitution
Sdlt1 = (2*A/B)*(1-u)/(u^3); % 1st term of S'(u)
Sdlt2 = M*(1-u)/(u^2); % 2nd term of S'(u)
Sdlt3 = (2*C/B^2)*(1-u); % 3rd term of S'(u)
Sdlt4 = -(3*A + M*B*u)/(2*A*u + M*B*(u^2) + 2*C*(u^4)/B); % 4th term
of S'(u)
Sdl = Sdlt1 + Sdlt2 + Sdlt3 + Sdlt4; % S'(u)

if logic == 0
    Pe = exp(S)*(1-exp(-Sdl*u))/(sqrt(2*pi*B)*Sdl); % probability of
error for 0
else
    Pe = exp(S)/(sqrt(2*pi*B)*(-Sdl)); % probability of error for 1
end

```

B.9. Gaussian Probability of Error

```

function Pe =
prob_err_gauss(M,R,Pase,Pout,I,var_thermal,var_shot,Idg,logic)

% This program calculates the Gaussian probability of error
% M = ratio of optical to two sided electrical bandwidth
% R = reponsivity of PIN receiver
% Pase = ASE power (W)
% Pout = incident power at detector (W)
% I = mean current (A)
% var_thermal = variance of thermal noise (A^2)
% var_shot = variance of shot noise (A^2)
% Idg = decision threshold
% logic = logical one or zero

var = (((R*Pase)^2) + 2*(R^2)*Pase*Pout)/M + var_thermal + var_shot;
% variance

if logic == 0
    Pe = .5*erfc((Idg-I)/sqrt(2*var)); % probability of error for logical
zero
else
    Pe = 1 - .5*erfc((Idg-I)/sqrt(2*var)); % probability of error for
logical one
end

```

B.10.EDFA Gain

```
function G = gain(Go,Pinave)

% This program solves for the EDFA gain using the Newton-Raphson method
% Go = EDFA small signal gain
% Pinave = average input power (W)

Psat = 30e-3;      % output saturation power of EDFA (W)
G=Go;
difG = G - Go * exp((1-G)*Pinave/Psat);
difGp = 1 + (Go*Pinave/Psat)*exp((1-G)*Pinave/Psat);
eps = 1e-10;

while difG > eps
    G=G-difG/difGp;
    difG = G - Go * exp((1-G)*Pinave/Psat);
    difGp = 1 + (Go*Pinave/Psat)*exp((1-G)*Pinave/Psat);
end;
```

B.11.ASE Power

```
function Pase = ase_pwr(net_eff,mt,Nsp,G,Bo)

% This program calculates the amplified spontaneous emission power
% net_eff = net transmission efficiency
% mt = number of polarization mode
% Nsp = EDFA spontaneous emission factor
% G = EDFA gain
% Bo = optical bandwidth (Hz)

h = 6.63e-34;      % Planck's constant (Js)
c = 2.998e8;       % speed of light in free space (m/s)
wc = 1550.92e-9;   % wavelength of carrier (m)
fc = c/wc;         % frequency of carrier (Hz)

Pase = net_eff*mt*Nsp*(G-1)*h*fc*Bo;      % power of amplified
spontaneous emission (W)
```

B.12.Variance of Thermal Noise

```
function var_thermal = thermal_noise(Belec)

% This program calculates the variance of thermal noise
% Belec = 2 sided electrical bandwidth (Hz)

k = 1.38e-23;      % Boltzmann's constant (J/K)
T = 273 + 25;     % temperature (K)
F = 10^(7/10);     % noise figure of electrical amplifier
```

```
Rin = 500; % input resistance of electrical amplifier (ohms)
var_thermal = 2*k*T*F*Belec/Rin; % variance of thermal noise (A^2)
```

B.13.Mean and Variance of Shot Noise

```
function [I,var_shot] = mean_var(R,Pout,Pase,Belec)

% This program calculates the mean and variance for the received
optical power
% R = reponsivity of optical receiver (A/W)
% Pout = incident power at PIN diode (W)
% Pase = power of amplified spontaneous emission (W)
% Belec = electrical bandwidth (Hz)

q = 1.60e-19; % electronic charge (C)

I = R*(Pout+Pase); % mean current (A)
var_shot = q*R*(Pout+Pase)*Belec; % variance of shot noise (A^2)
```

Appendix C Characteristics of Optical Components

C.1. IONAS DFB Fiber Laser

DFB fiber lasers are fabricated by introducing a Bragg grating into the core of an erbium doped fiber. Table C.1 shows the characteristics of the IONAS DFB fiber laser.

Parameter	Value
Stability	< ± 0.2 dB (1 hour)
Center Wavelength	1550.92 nm
Linewidth	< 20 kHz
SNR	< 57 dB (0.05 nm resolution)
Temperature Stability	0.0028 nm/K (0 – 70 C)

Table C.1: Specification of the IONAS DFB fiber laser.

C.2. Lucent Mach-Zehnder Modulator

Table C.2 shows the characteristics of the Lucent Mach-Zehnder modulator.

Parameter	Value
Model	X2623C
Serial Number	3023
Wavelength	1550 nm
Bandwidth	10.5 GHz
Switch Voltage (at 1 GHz)	4.45 V
Insertion Loss	3.4 dB
Extinction Ratio	28.2 dB
Impedance	43 Ω
Electrical Return Loss	> 15 dB
Optical Return Loss	> 40 dB

Table C.2: Specification of the Lucent Mach-Zehnder modulator.

C.3. Erbium Doped Fiber Amplifiers

Two EDFAs are used in the experiments and they are referred to as EDFA #1 and EDFA #2. EDFA #1 consists of TRLabs 980 nm EDFA pump laser unit model BFSWA0980SDL1180AB with serial number SP9208, Sifam WDM and 19 m of NOI Er24 erbium doped fiber. EDFA #2 is a fully assembled TRLabs EDFA module with serial number TRL9407-BF450-001. EDFAs can be modeled by three basic parameters: the small signal gain, spontaneous emission power and output saturation power. In the PDF experiments, the EDFAs are cascaded to function as a single EDFA unit. The following figure shows the experimental setup for measuring the cascaded EDFA gain.

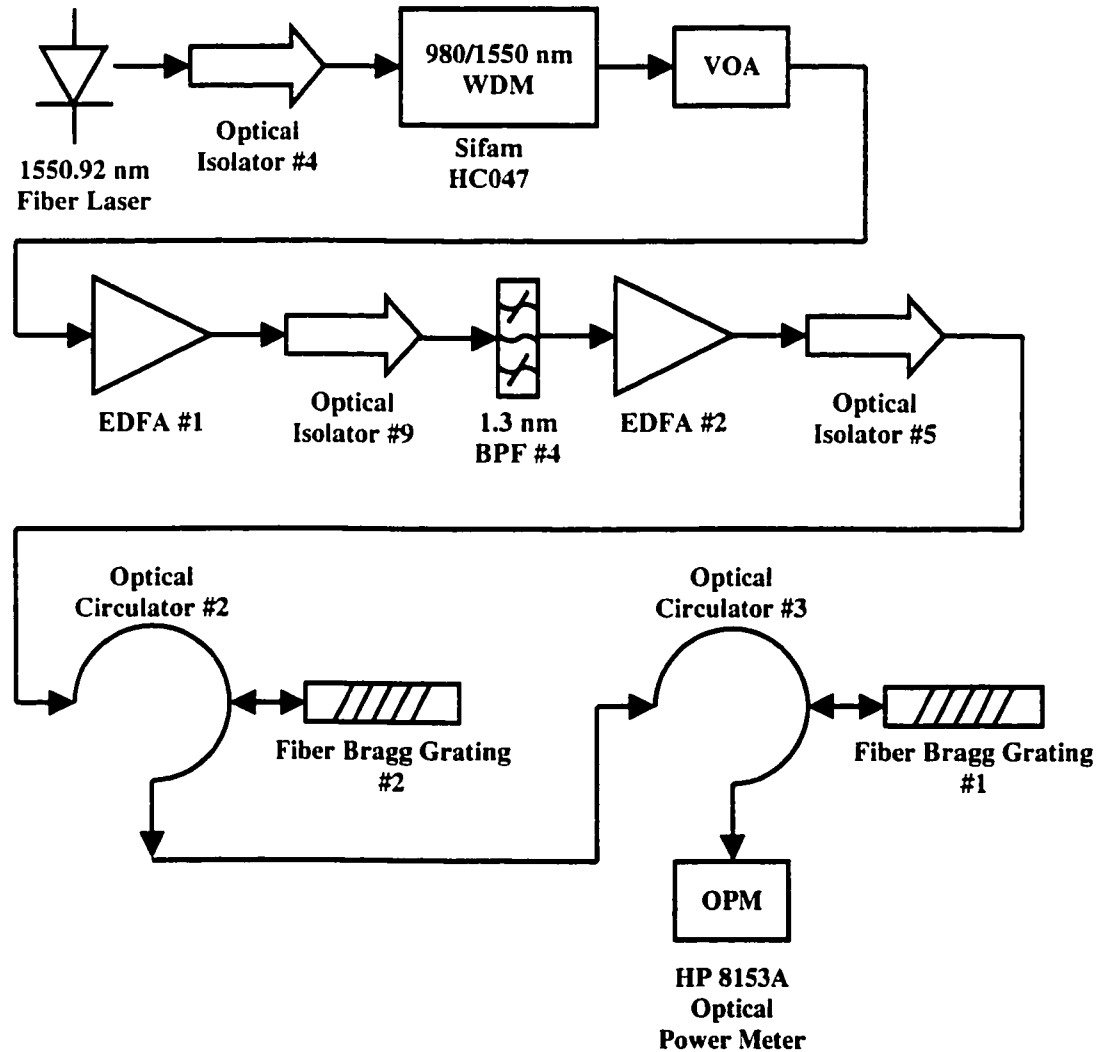


Figure C.1: Experimental setup for EDFA gain measurement.

The input power, P_{in} , is defined as the power at the input of EDFA #1 and the output power, P_{out} , is the power at the output of optical isolator #5. The BPF between the EDFAs is to remove part of the ASE noise so that EDFA #2 will not be saturated. The optical power detected by the OPM is denoted by P'_{out} and the total insertion loss introduced by the optical circulators and FBGs is denoted by IL. Therefore,

$$P_{out} = P'_{out} + IL. \quad (C.1)$$

The output of the EDFA consists of the amplified signal power, P_{sig} , and ASE noise power, P_{ase} . So, P_{out} and P_{sig} can be written as

$$P_{out} = P_{sig} + P_{ase} \quad (C.2)$$

and

$$P_{sig} = GP_{in}, \quad (C.3)$$

where G is the EDFA gain. When the input signal power is sufficiently small, it is assumed that G is equal to the EDFA small signal gain, G_0 . The total EDFA small signal gain is 41 dB. The gain curve is shown in the following plot.

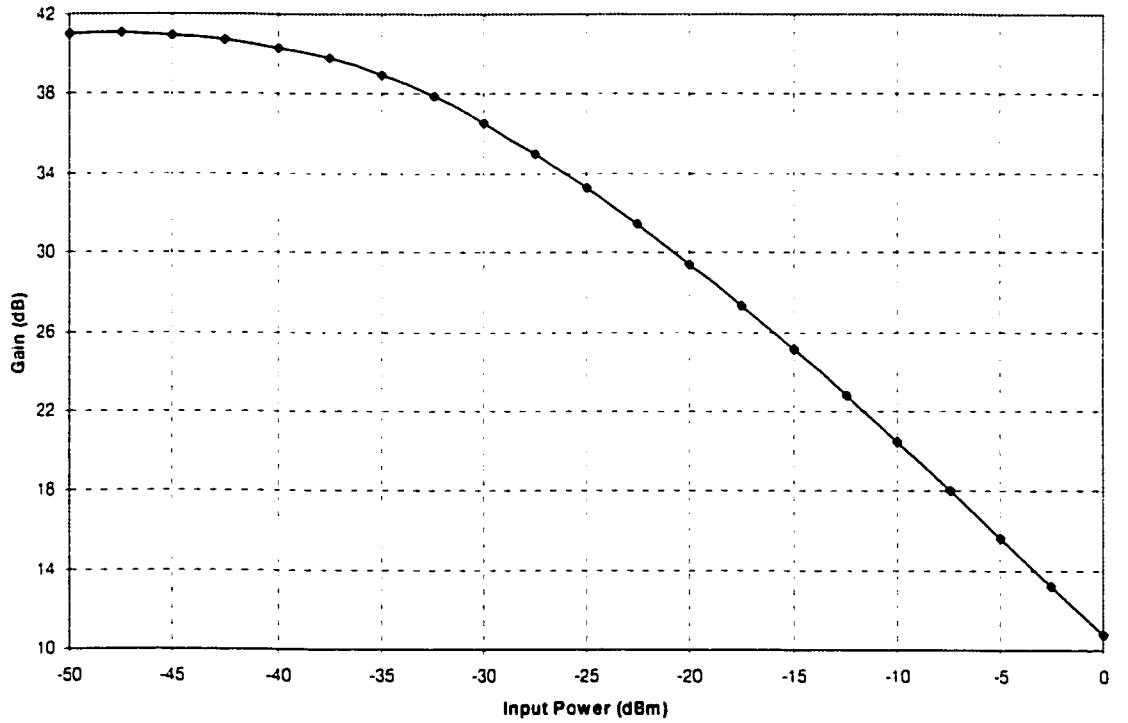


Figure C.2: EDFA gain as a function of input power at 1550.92 nm.

Using equation (2.11), N_{sp} is calculated to be 1.3. From Figure C.2, the output saturation power is determined to be 5 dBm.

C.4. Fiber Bragg Gratings

Fiber Bragg Gratings (FBGs) are wavelength selective reflectors obtained by embedding a Bragg grating in the core of a single-mode fiber. This is done by laterally exposing the core of a single-mode fiber to a periodic pattern of intense ultraviolet (UV) light. The intense UV light exposure produces a structural change in the core material which causes a permanent increase in the refractive index of the core. Therefore, a fixed refractive index modulation according to the exposure pattern is created and it is called a grating. The strength of the change in refractive index along with the grating period and length determine the range of wavelengths that will be reflected, as well as the percentage of reflection. At each modulation period, a fraction of the optical wave is reflected which interferes in a constructive manner. All of the reflected light combines coherently to a single large reflection at a particular wavelength when the grating period is equal to one half the wavelength of the input light. This is the Bragg condition and the wavelength at which this reflection occurs is called the Bragg wavelength. Light signals at wavelengths other than the Bragg wavelength propagate through the grating with negligible attenuation or signal variation.

FBGs show no significant change over time in reflectivity and exhibit well behaved wavelength response to temperature and strain that can be exploited for accurate wavelength tuning. A change in the grating period will result in a change in the reflected wavelength. Therefore, Bragg gratings are susceptible to externally applied thermo-mechanical loads. Temperature change and mechanical strain affect the Bragg response through expansion or contraction of the grating periodicity.

Due to their all fiber construction, FBGs exhibit minimum insertion loss and outstanding long-term stability, all in a small size. Since FBGs come in a wide range of reflectivity, from 1 % to 100 %, spectral bandwidths between 0.1 to 4 nm and central wavelength, they find many applications in fiber optics communication systems. They

make perfect narrowband mirrors for fiber lasers and also used for external cavity semiconductor laser stabilization. The 100% reflective FBG with a flat top response and narrow bandwidth enables ASE suppression at the output of EDFAs and channel selection in DWDM systems.

The center wavelengths of the FBGs that we obtained are not exactly at 1550.92 nm due to manufacturing tolerance. However, the center wavelengths of the gratings can be shifted by changing the temperature. Therefore, each grating is packaged in an aluminum block insulated by styrofoam. The aluminum block is heated by a power transistor or cooled by thermoelectric coolers, depending on the temperature requirement. The temperature of each FBG is measured using a thermistor. According to the manufacturer specification, the FBGs can be temperature tuned over the range of -50°C to 70°C without any change in reflectivity and bandwidth.

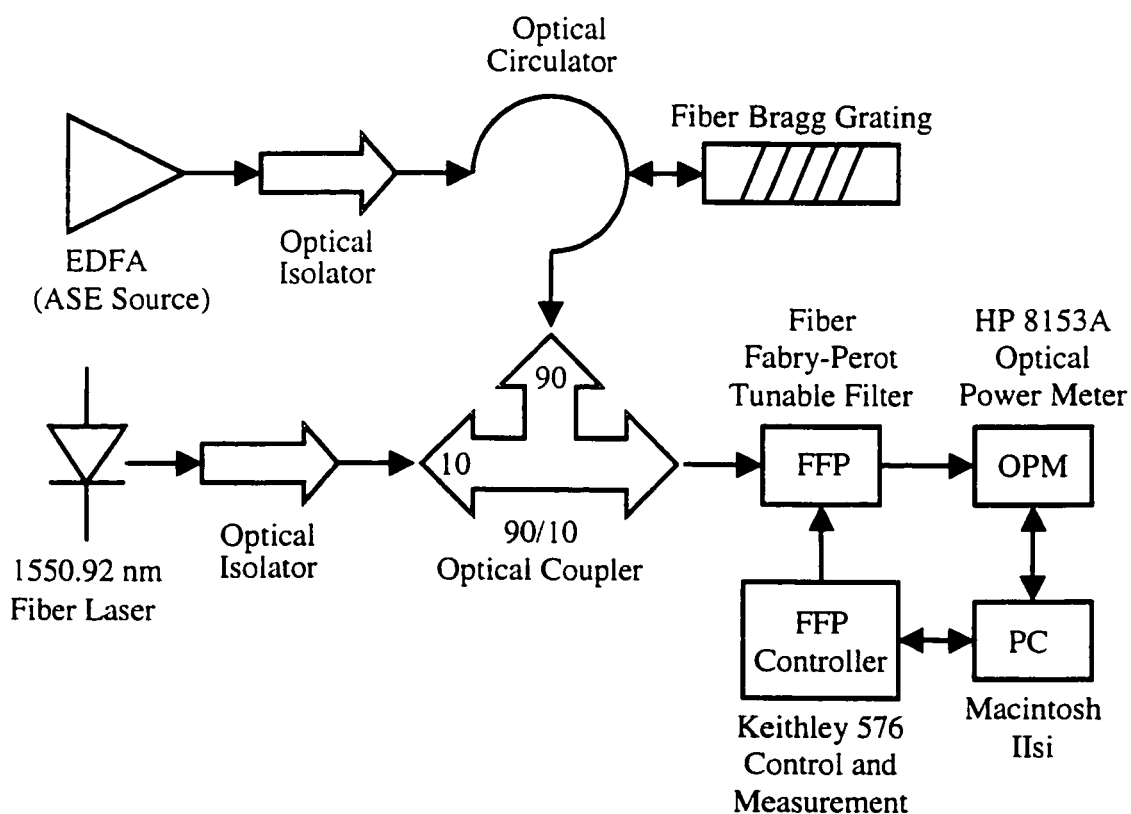


Figure C.3: Experimental setup for measuring the reflection spectra of the FBGs.

ASE generated by an EDFA is coupled to a FBG via an optical circulator. The ASE reflected by the FBG is coupled into the 90% port of an optical coupler. Light from the 1550.92 nm fiber laser is coupled into the 10% port of the optical coupler. The combined output is then scanned using a Fiber Fabry-Perot (FFP) interferometer to obtain the reflection spectrum of the FBGs relative to the center wavelength of the fiber laser.

The following table shows the specification of the individual FBG.

FBG	Serial Number	Center Wavelength @ 25 C (nm)	Maximum Reflectivity	FWHM (nm)
1	BP-G70807-010798-01	1550.72	96.5% (14.6 dB)	0.11
2	BP-G70807-010798-02	1550.60	96.9% (15.1 dB)	0.12
3	BP-G70807-010798-03	1551.11	95.7% (13.6 dB)	0.18
4	BP-G70807-010798-04	1551.02	94.5% (12.6 dB)	0.18
5	BP-G70807-010798-05	1550.92	89.8% (9.9 dB)	0.42
6	BP-G70807-010798-06	1550.95	93.6% (12.0 dB)	0.46

Table C.3: Characteristics of the FBGs.

The following table shows the measured bandwidths of the FBGs.

FBG	3 dB Bandwidth (nm)	3 dB Bandwidth (GHz)	Noise Equivalent Bandwidth (GHz)
1	0.12	14.97	20.41
2	0.12	14.97	20.94
3	0.18	22.45	27.90
4	0.18	22.45	28.52
1 and 2	0.11	13.72	16.41
3 and 4	0.16	19.96	23.17
5 and 6	0.36	44.90	51.08

Table C.4: Measured bandwidth of the FBGs.

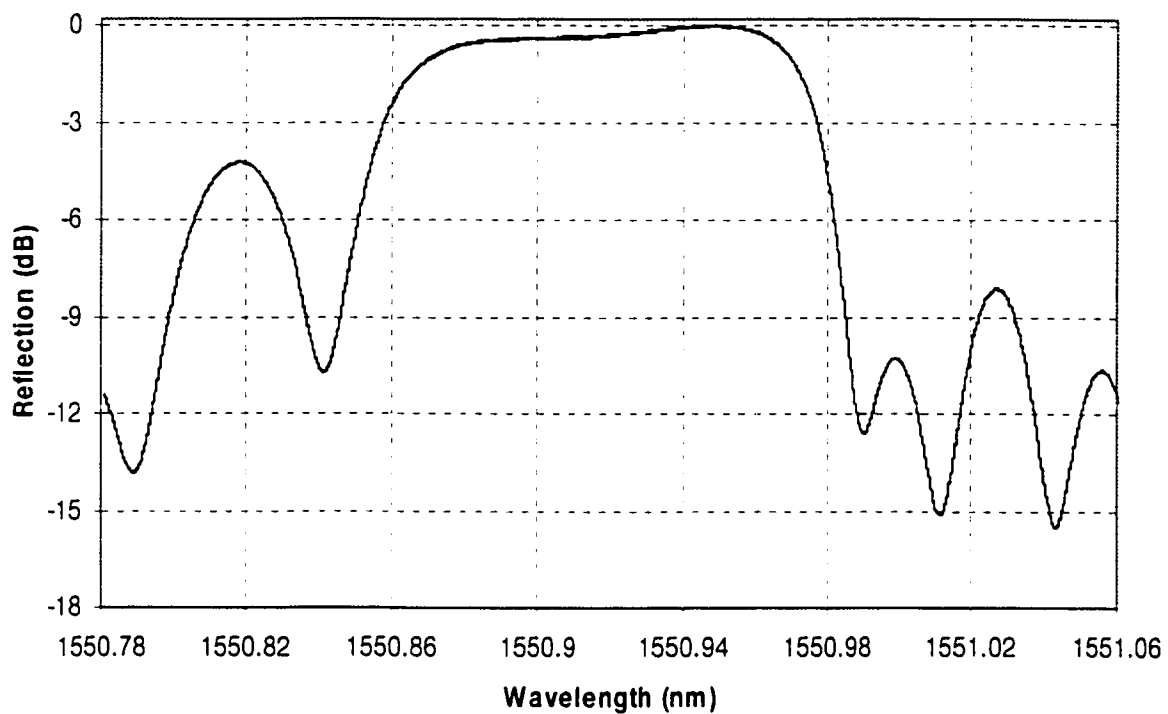


Figure C.4: Reflection spectrum of FBG #1.

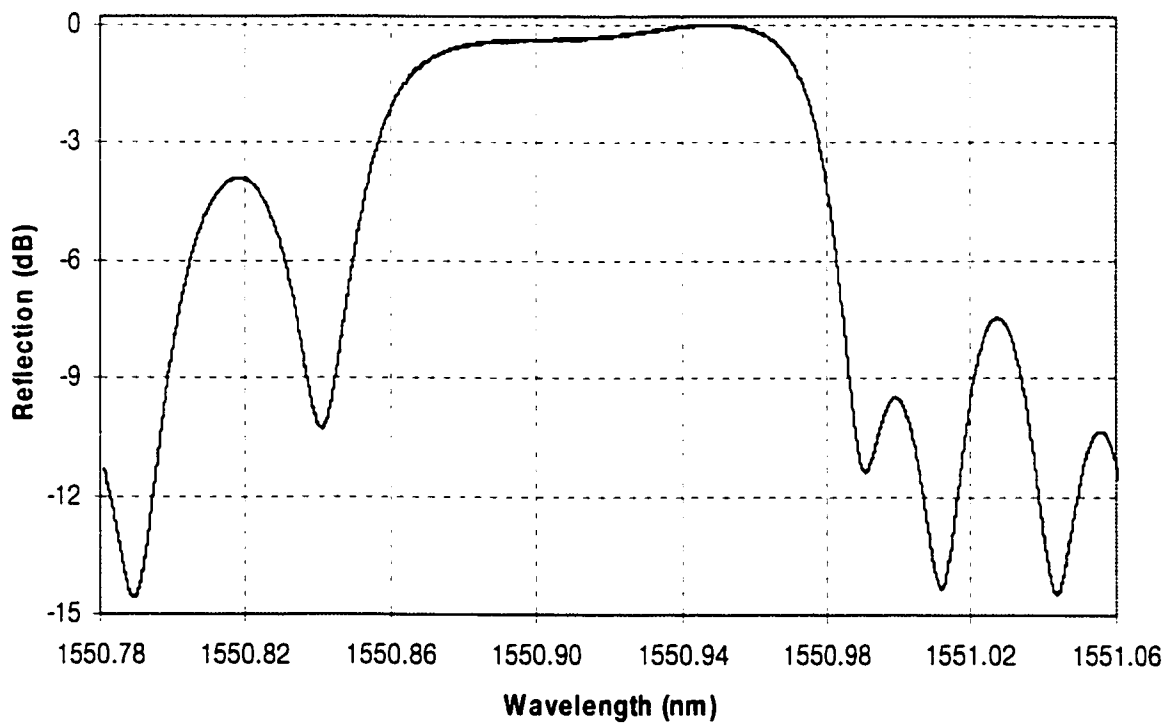


Figure C.5: Reflection spectrum of FBG #2.

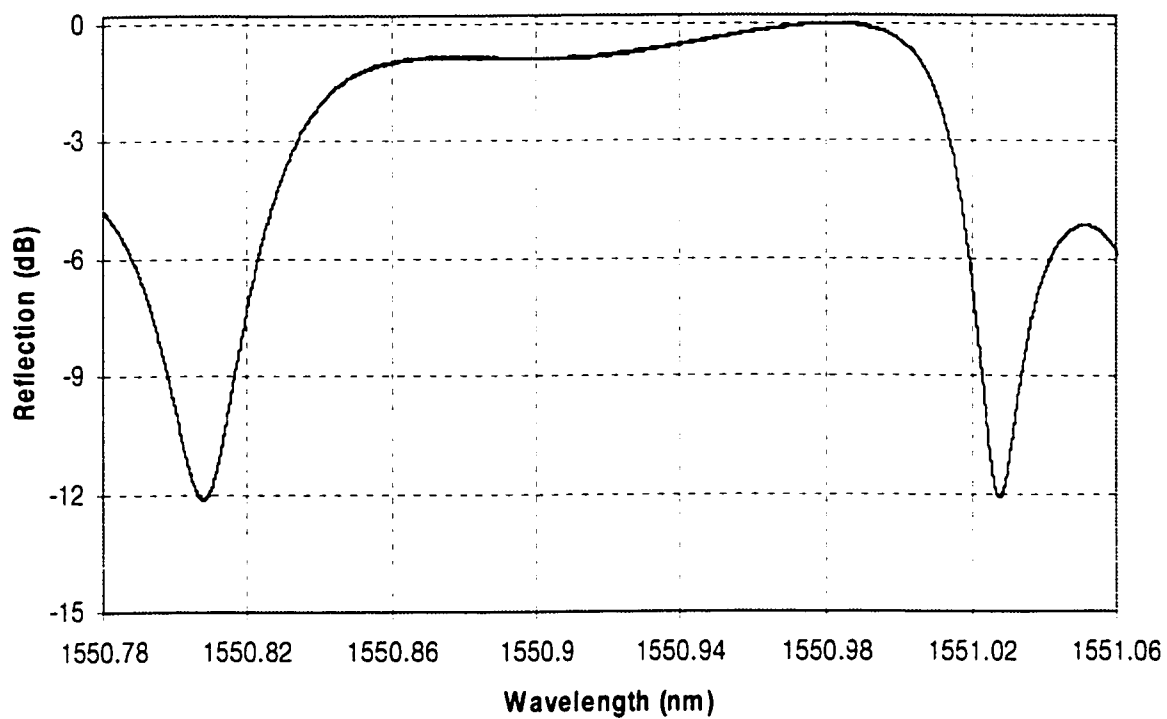


Figure C.6: Reflection spectrum of FBG #3.

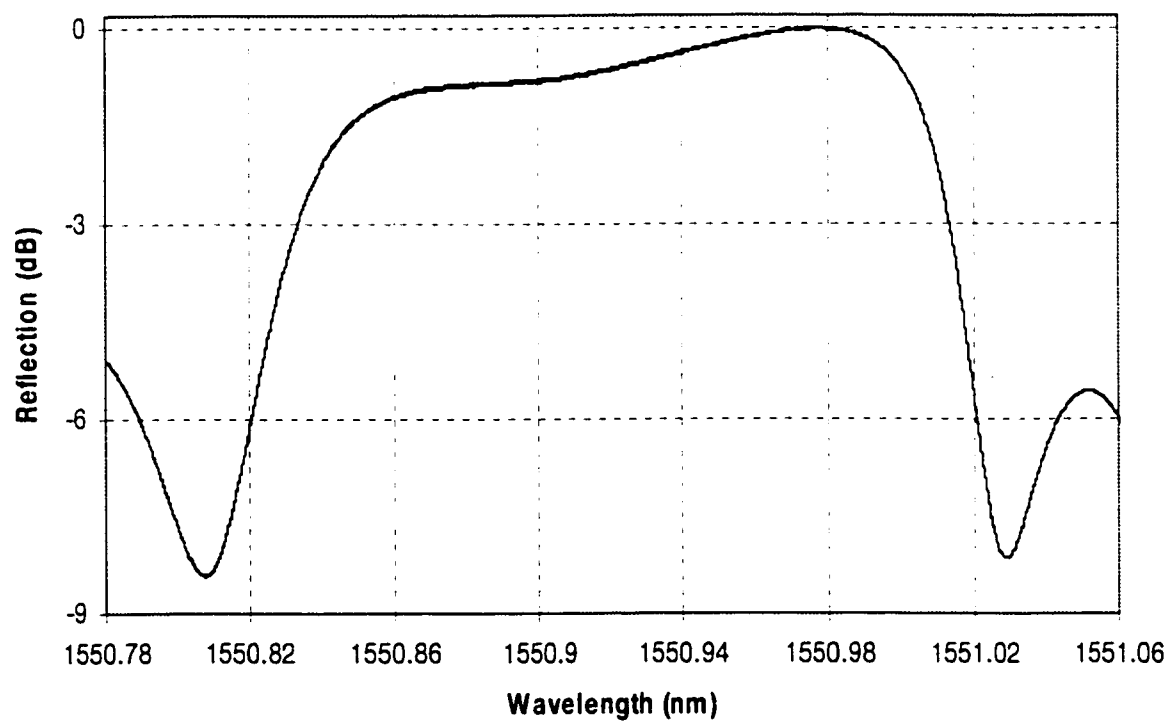


Figure C.7: Reflection spectrum of FBG #4.

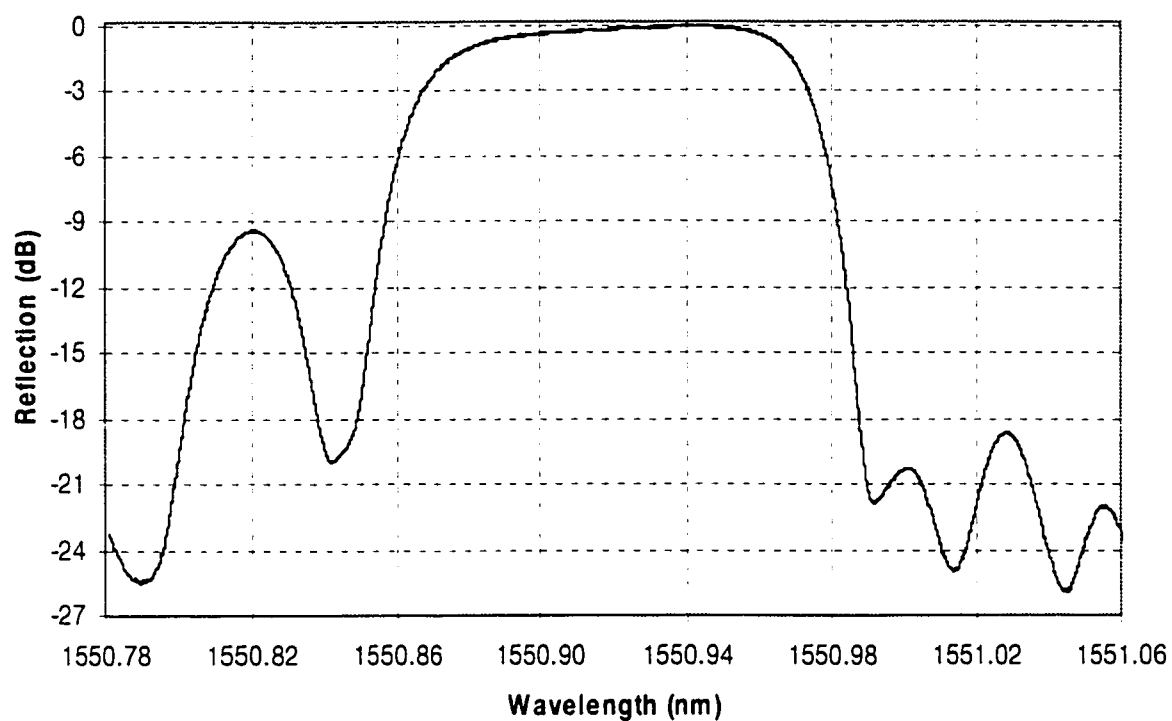


Figure C.8: Reflection spectrum of cascaded FBG #1 and 2.

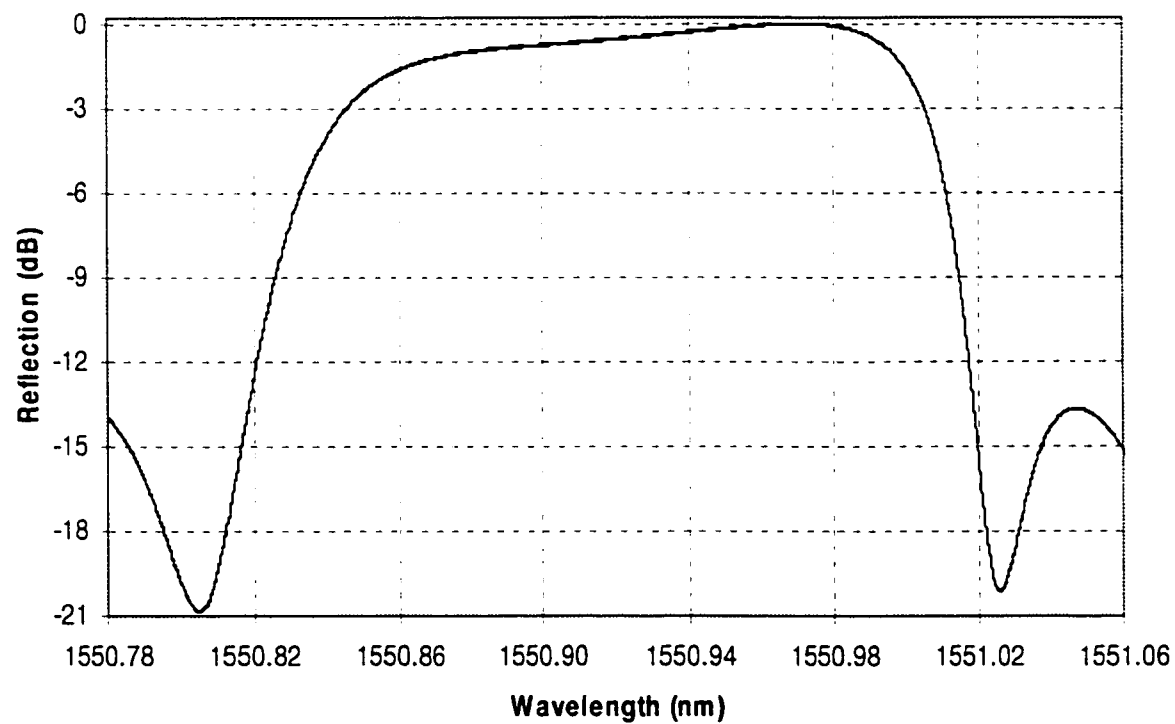


Figure C.9: Reflection spectrum of cascaded FBG #3 and 4.

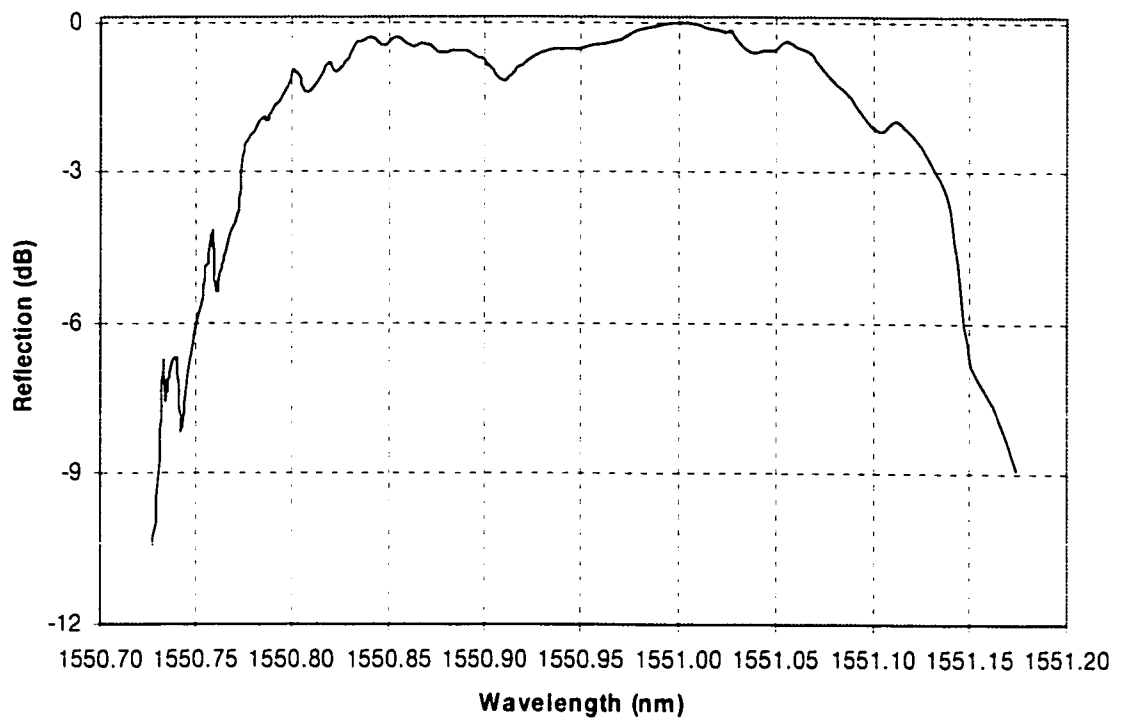


Figure C.10: Reflection spectrum of cascaded FBG #5 and 6.

The reflection spectrum of cascaded FBG #5 and 6 are scanned using the setup in Figure C.3 with an additional optical circulator and 0.1 nm FBG due to the FFP free spectral range of only 40 GHz.

C.5. Optical Isolators

Table C.5 shows the insertion losses of the optical isolators at a wavelength of 1550.92 nm.

Number	Insertion Loss (dB)
2	2.16
3	1.07
4	1.00
5	0.54
6	0.97
7	1.08
9	0.60
10	0.61

Table C.5: Insertion losses of optical isolators.

C.6. Optical Circulators

Table C.6 to Table C.8 show the identifications and characteristics of the optical circulators. All measurements are made at a wavelength of 1550.92 nm.

Parameter	Value
Manufacturer	OFR
Model	OC-IR2-3
Number	0204888
Port 1 to Port 2 Insertion Loss	1.82 dB
Port 2 to Port 3 Insertion Loss	2.84 dB
Port 1 to Port 3 Isolation	46 dB
Port 2 to Port 1 Isolation	40 dB

Table C.6: Characteristics of optical circulator #1.

Parameter	Value
Manufacturer	OFR
Model	OC-IR2-3
Number	0204889
Port 1 to Port 2 Insertion Loss	1.30 dB
Port 2 to port 3 Insertion Loss	1.04 dB
Port 1 to port 3 Isolation	34 dB

Table C.7: Characteristics of optical circulator #2.

Parameter	Value
Manufacturer	Kaifa
Model	CIR5
Serial Number	C0030
Port 1 to Port 2 Insertion Loss	0.68 dB
Port 2 to Port 3 Insertion Loss	0.58 dB
Port 1 to Port 3 Isolation	60 dB
Port 2 to Port 1 Isolation	60 dB

Table C.8: Characteristics of optical circulator #3.

Appendix D Characteristics of Electrical Components

D.1. Nortel 10 Gb/s Optical Receiver

The conversion gain of the optical receiver is measured using the following experimental setup. The modulation frequency provided by the signal generator is 1 GHz with 1 dBm power. The MZ modulator is biased at 2.25 V.

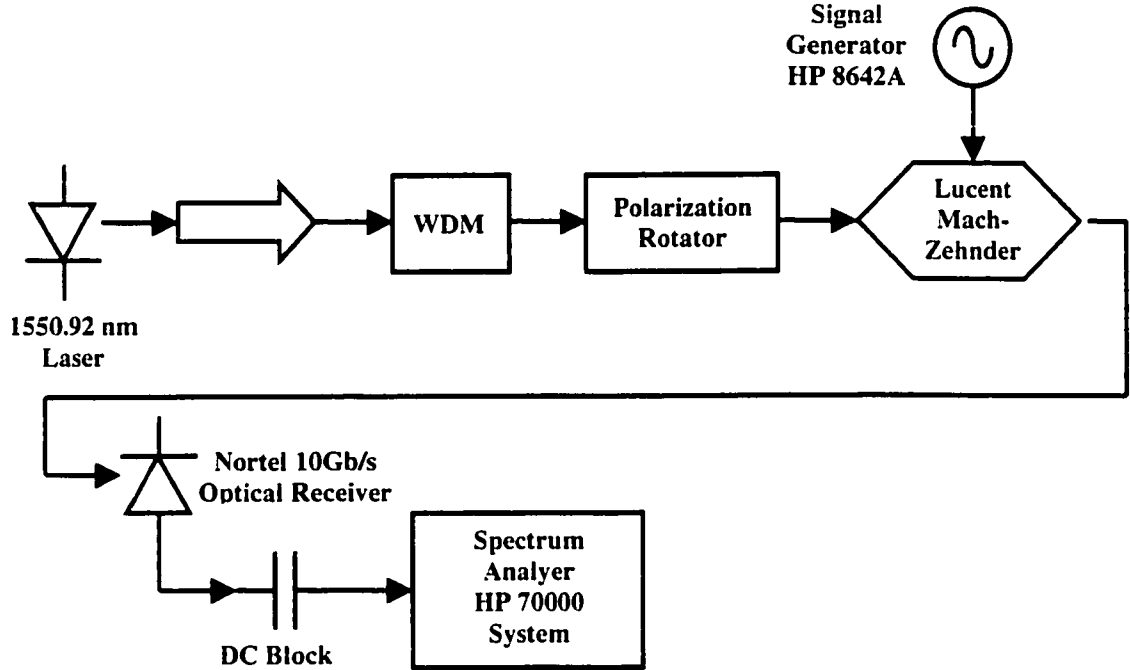


Figure D.1: Experimental setup for conversion gain measurement.

The conversion gain of the Nortel receiver is measured to be 274.33 V/W for a wavelength of 1550.92 nm. The responsivity of the Nortel receiver is 0.70 [31]; thus the transimpedance gain of the Nortel receiver is calculated to be 392 Ω . This value is much lower than the typical value of 500 Ω in the published specification.

D.2. B&H Electrical Amplifiers

Table D.1 shows the specification of the B&H electrical amplifiers.

Parameter	Value
Model	AC260XYH24ELL9P1
Frequency response	2 MHz – 26 GHz
Gain	23 dB typical
1 dB compression output	24 dBm
Noise figure	7 dB

Table D.1: Specification of the B&H electrical amplifiers.

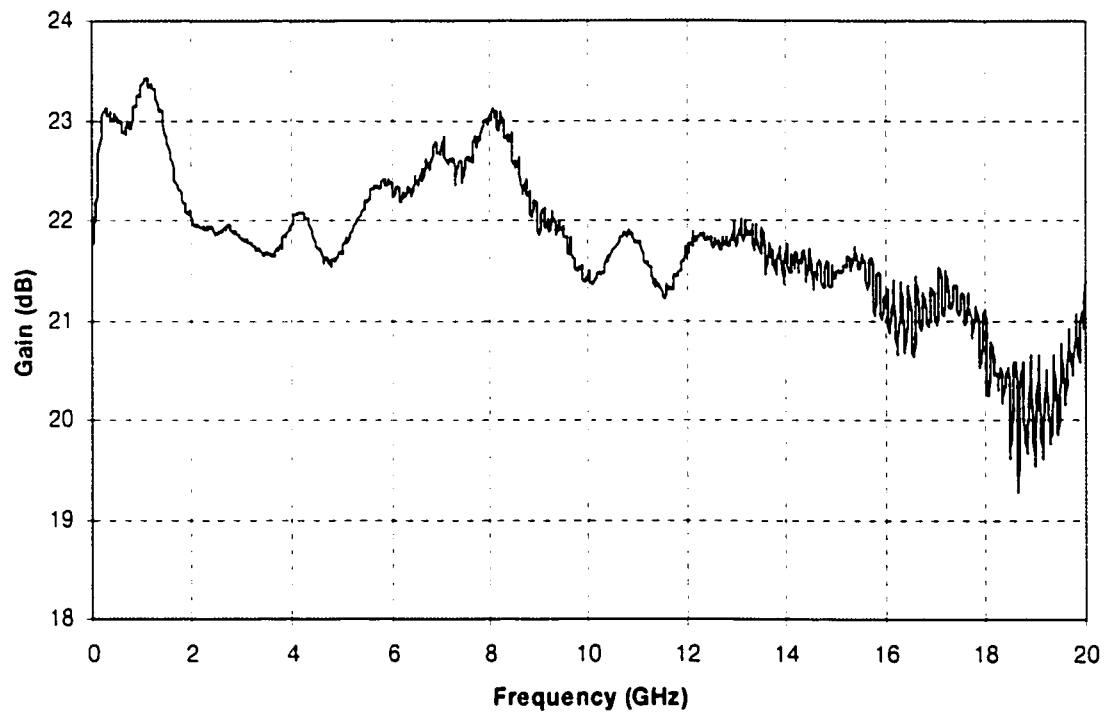


Figure D.2: Frequency response of amplifier with serial number 6235.

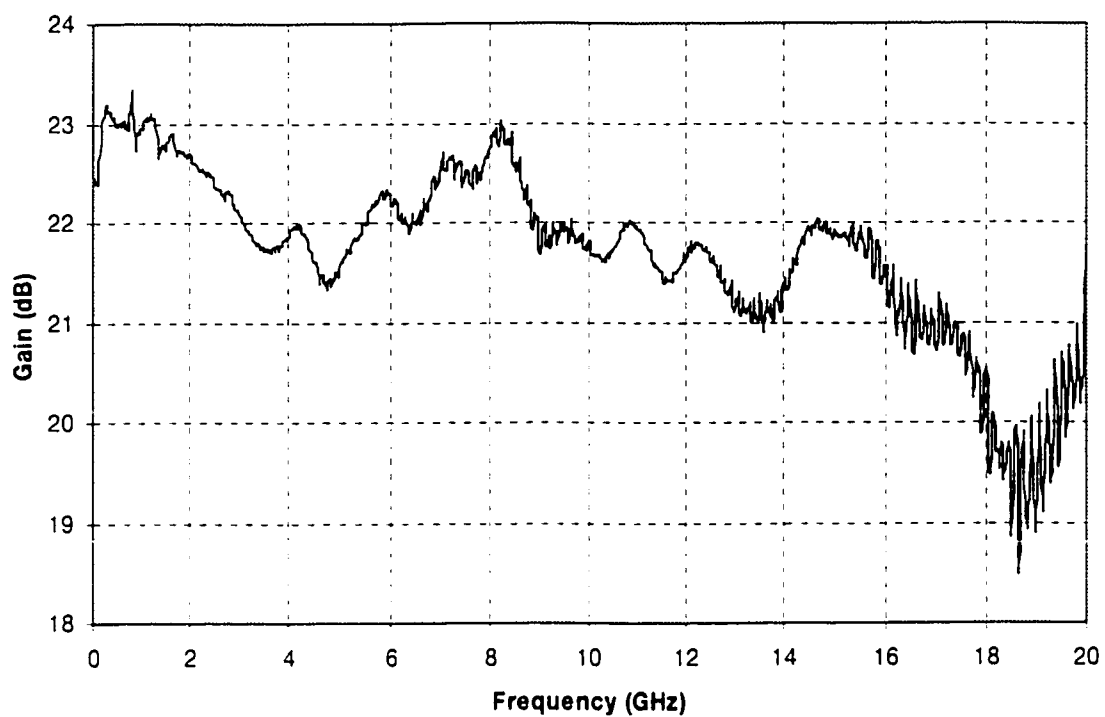


Figure D.3: Frequency response of amplifier with serial number 7693.